MicroGC: Of Detectors and their Integration

Shree Narayanan Sreedharan Nair

Dissertation submitted to the faculty of the Virginia Polytechnic Institute and State University in partial fulfillment of the requirements for the degree of

Doctor of Philosophy

In

Electrical and Computer Engineering

Masoud Agah, Chair

Luke F. Lester

John R. Morris

Leyla Nazhandali

Gary W. Rice

26 March, 2014

Blacksburg, VA

Keywords: micro gas chromatography, gas detector, thermal conductivity, ionization

MicroGC: Of Detectors and their Integration

Shree Narayanan Sreedharan Nair

Gaseous phase is a critical state of matter around us. It mediates between the solid crust on earth and inter-stellar vacuum. Apart from the atmosphere surrounding us where compounds are present, natively, in a gaseous phase, they are also trapped within soil and dissolved in oceanic water. Further, those that are less volatile do enter the gaseous phase at high temperatures. It is this gaseous phase that we inhale every second. It is thus critical that we possess the tools to analyze a mixture of gaseous compounds. One such method is to separate the components in time and then identify, primarily based on the retention times, also known as gas chromatography.

This research focuses on the development of gas detectors and their integration, in different styles, primarily for gas chromatography. Utilizing fabrication techniques used in semiconductor industry and exploiting scaling laws we investigate the ability to improve on conventional gas separation and identification techniques. Specifically, we have provided a new spin to the age-old thermal conductivity detector enabling its monolithic integration with a separation column. A reference-less, two-port integration architecture and a one-of-its-kind released resistor on glass are some of its salient features. The operation of this integrated device with a preconcentrator and in a matrix array was investigated. The more unique contribution of this research lies in the innovative discharge ionization detector. An ultra-low power, sensitive, easy to fabricate detector, it requires more investigation for a thorough understanding and will likely mature to replace the thermal conductivity detector, as the detector of choice for universal detection, in time to come.

To my family

Acknowledgements

I thank my advisor Dr. Masoud Agah for handing me this wonderful opportunity to research in his lab. He has invested a lot of time from the beginning, not just guiding the research, but also advising on nitty gritties. It has been a wonderful experience to travel half way around the globe (like many others), learn to adapt, and attempt to excel. I am thankful for the many wonderful opportunities I have been presented with, inside and outside the lab.

My PhD advisory committee - Dr. Luke Lester, Dr. John Morris, Dr. Leyla Nazhandali, and Dr. Gary Rice - have been really great to work with. They have provided a good balance of advising and autonomy. In particular Dr. Rice has had to bear the brunt of my ignorance in chemistry and special requests. I have had the opportunity to interact with a lot of faculty over these seven years in graduate school. Some of the insights they have provided, I am sure, will help me analyze a problem more effectively in future.

Current members and alumni in VTMEMS lab deserve praise that go beyond words that can be documented.

Mr. Don Leber has been of great help during my entire stay, sharing information on all aspects. Without his help, the probe station to anodic bonder conversion would have been a mess! Dr. Bob Geil at UNC-CH, Mr. Marcio Cerullo at NCState, and Mr. Guy Lavellee and Dr. Shane Miller at Penn State have been of great help. There is something about cleanroom managers that makes them very kind and I needed loads of it.

Along the way, I have had the chance to meet some wonderful set of folks, not just in Blacksburg. Some of them have taken the initiative to get in touch with me and continued to do so even when I have cocooned out. Seven years in graduate school is a long time. I wished my PhD meant to me something. It is impossible to document the support I received but I am glad to have had their unstinted support and trust, all through, when I needed it.

Finally, my parents and my sister deserve all credits for me having reached this milestone. From having encouraged and motivated me for a doctoral degree, to supporting me all the way through, and correcting my mistakes, I have had the best!

Attribution

Several colleagues aided in the writing and research behind four of my chapters presented in this dissertation. Few colleagues contributed with their technical expertise in three of the chapters. A brief description of their contributions is included here.

Chapter 2: A 2-port monolithic integration of a thermal conductivity detector with a separation column for gas chromatography

Chapter 2 was submitted to *IEEE Sensors Journal.* © 2012 IEEE. Reprinted, with permission, from *Shree Narayanan, Bassam Alfeeli, and Masoud Agah*, "Two-Port Static Coated Micro Gas Chromatography Column with an Embedded Thermal Conductivity Detector," *Sensors Journal, IEEE,* vol. 12, no. 6, pp. 1893-1900, 2012.

Bassam Alfeeli, PhD, (Electrical Engineering Department, Virginia Tech), is currently a Scientific Consultant and Program Manager at the Kuwait Foundation for the Advancement of Sciences. Dr. Alfeeli was a coauthor on this paper, supported with the coating of the column, SEM imaging of the coated film, and testing of the column.

Masoud Agah, PhD, (Electrical Engineering Department, Virginia Tech), is currently an Associate Professor at Virginia Tech. Dr. Agah was a co-author on this paper, principal investigator for the grants supporting this research, and contributed editorial comments.

Chapter 3: A means to suspend a microfabricated resistor on glass and anodic bond it to silicon for a thermal conductivity detector

Chapter 3 was submitted to *IEEE JMEMS.* © 2012 IEEE. Reprinted, with permission, from *Shree Narayanan and Masoud Agah*, "Fabrication and Characterization of a Suspended TCD Integrated with a Gas Separation Column," *J. Microelectromech. Syst.*, vol. 22, no. 5, pp. 1166-1173, 2013.

Masoud Agah, PhD, (Electrical Engineering Department, Virginia Tech), is currently an Associate Professor at Virginia Tech. Dr. Agah was a co-author on this paper, principal investigator for the grants supporting this research, and contributed editorial comments.

Chapter 4: Loading of a preconcentrator from a microfabricated purge device and subsequent gas analysis using an integrated column, for water monitoring

Muhammad Akbar, (Electrical Engineering Department, Virginia Tech), is currently pursuing his doctoral degree at Virginia Tech. Mr. Akbar was the lead author on this chapter, contributed with his expertise on the design, fabrication, test and operation of the microfabricated purge device, and subsequent loading of the preconcentrator.

Masoud Agah, PhD, (Electrical Engineering Department, Virginia Tech), is currently an Associate Professor at Virginia Tech. Dr. Agah was a co-author on this chapter, principal investigator for the grants supporting this research, and contributed editorial comments.

Chapter 5: Operation of multiple integrated columns in an array for polarity and temperature tuned multidimensional analysis and detection

Apoorva Garg, (Electrical Engineering Department, Virginia Tech), is currently pursuing his Master's degree at Virginia Tech. Mr. Garg was a coauthor on this chapter, contributed with his expertise by providing the circuits for the PCBs and editorial comments.

Masoud Agah, PhD, (Electrical Engineering Department, Virginia Tech), is currently an Associate Professor at Virginia Tech. Dr. Agah was a co-author on this chapter, principal investigator for the grants supporting this research, and contributed editorial comments.

Chapter 6: Conceptualization, fabrication and testing of a helium discharge detector

Chapter 6 was submitted to *Microchimica Acta*

Gary Rice, PhD, (Chemistry Department, College of William and Mary), is currently an Associate Professor and former Chair of the Department of Chemistry at College of William and Mary. Dr. Rice was a coauthor on this paper, and contributed with related technical expertise and editorial comments.

Masoud Agah, PhD, (Electrical Engineering Department, Virginia Tech), is currently an Associate Professor at Virginia Tech. Dr. Agah was a co-author on this paper, principal investigator for the grants supporting this research, and contributed editorial comments.

Chapter 7: An empirical optimization of the helium discharge detector

Gary Rice, PhD, (Chemistry Department, College of William and Mary), is currently an Associate Professor and former Chair of the Department of Chemistry at College of William and Mary. Dr. Rice was a coauthor on this chapter, and contributed with related technical expertise and editorial comments.

Masoud Agah, PhD, (Electrical Engineering Department, Virginia Tech), is currently an Associate Professor at Virginia Tech. Dr. Agah was a co-author on this chapter, principal investigator for the grants supporting this research, and contributed editorial comments.

Table of Contents

List of Figures

List of Tables

1

Introduction

Gas chromatography (GC) is a premier analytical technique used to analyze the composition of a mixture of gases. By separating the components, over time, GC finds applications in diverse fields such as space and fossil fuel exploration, food and water quality monitoring, air monitoring at workplace and terrestrial environment, and testing of electrical equipment such as power transformers [1-5].

MicroGC is the art and science of developing miniaturized systems for gas chromatography. This aims to address the need for portable, hand-held systems, very much unlike conventional GC equipment. Such systems enable remote, onsite measurement which otherwise would require continuous manual involvement resulting in sampling errors, raising questions about the integrity. Some salient features of miniaturized GC systems are low-power, light-weight, short analysis times, and reduced consumable usage. At the micro-level, the presence of additional physical phenomenon also lets us harness new means to separate and detect gases efficiently.

A μGC system is characterized by three components as shown in Figure 1-1. The preconcentrator (μPC), at the inlet, serves as a chemical amplifier. It is typically realized as a "bed" coated with a suitable adsorbent that collects the analytes of interest from the sample mixture [6-8]. After a specified time, the preconcentrator is thermal spiked to release a sharp plug of collected analytes. This plug is released into the separation column in a stream of carrier gas. The separation column is realized as a microfluidic "channel". The channel's inner surface is coated with a stationary phase [9-12]. Different analytes in the plug interact to a different extent. The retardation effectively separates the analytes into individual distinct plugs that elute out of the column at different instants of time. The separated plugs flow into the detector, where they are detected, one at a time. Typically, detectors used in μGC system can provide only the retention time of the analyte plug. By characterizing the μGC system for known compounds, one

can map the time of the unknown plug to a known compound. The following chapters deal with development of micro gas detectors and their integration with micro separation columns (μSC) on a single substrate.

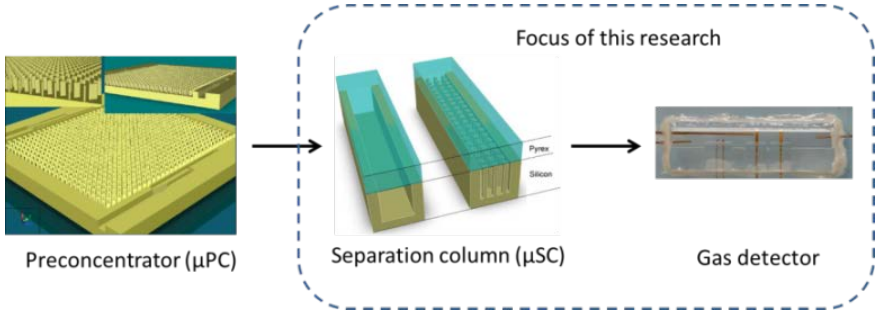

Figure 1-1: A typical GC system showing its core components – a preconcentrator, separation column and a gas detector [13, 14].

The first μGC system came into being, when in a seminal 1979 paper, Terry et. al. presented the results of a silicon micromachined μSC [15]. Temperature is an important parameter in GC and the ability to change temperature quickly makes silicon a very good candidate. A glass lid made of Pyrex or Borofloat seals the channel tight since they can be anodically bonded. Anodic bonding is a method wherein the cationic impurities of a specially made glass wafer drift at a high temperature and voltage so as to cause the permanent bonding of the silicon and glass at the interface. Such open channels coated on its inner surface are referred to as capillary GC as opposed to channels that are packed with coated particles, called packed column GC. The absence of a preconcentrator and non-optimal coating of the stationary phase left huge room for improvements. In addition, a thermal conductivity detector (TCD) was miniaturized by fabricating thin film nickel resistors on a Pyrex diaphragm and mechanically clamped on the backside of the device. TCDs are non-selective, non-destructive detectors that are easy to fabricate and use. However, their inherent sensitivity is limited to the 10-100 ppm range, at best. The need for better μSCs led to the fabrication of shallow and wide channels in [16] and circular cross section channels in [17-19].

In the late 90s, researchers at Sandia Labs embarked on a program focusing on gas detectors leading to the development of handheld gas systems [20]. Developments in silicon micromachining such as deep reactive ion-etching techniques enabled high-aspect ratio channels in a compact area, resulting in good separation performance. Thin diaphragm based surface micromachined μPCs were demonstrated which helps to reduce the detection limit expected of the detector [21, 22]. The development of surface acoustic wave (SAW) sensors marked the beginning of a race in micro gas detectors [23]. A microplasma based on a DC discharge was used to detect 800ppb of hexane with just 9mW of power dissipation [24]. Sorption of analytes on specific polymers, coated across an electrode gap, change the electrical properties resulting in

chemiresistive and chemicapacitive detectors [25]. Arrays of such sensors coated with different polymers introduce specificity and provide for multi-dimensional detection.

The dominant gas detector used in conventional GC is a flame ionization detector (FID) which operates by measuring the current from pyrolysis of the analyte. The hydrogen flame used in an FID makes it more sensitive to hydrocarbons and provides limits of detection in the ppb range. Attempts have been made to obtain a similar detector based on catalytic combustion [26]. Independent efforts have also focused on a structural miniaturization of an FID using a three wafer stack [27]. However, material degradation in the combustor case and reduced ionizing power of a micro flame in the latter greatly restrict the application of a μFID. Notable other micro detectors include the MagFPW, metal oxide resistors, micro-nitrogen phosphorous detector, micro-thermionic ionization detector and nanoelectromechanical mass sensors [28, 29].

Meanwhile, continued interest in μTCDs has seen investigations to optimize the performance. All of this research was focused entirely on an insulator diaphragm bulk-etched on a silicon substrate, similar to the pioneering paper by Terry [30-40]. A TCD consists of a heated resistor in the path of a carrier gas stream. Typically the carrier is helium due to its high thermal conductivity. When an analyte plug crosses the heater, the thermal conductivity drops sharply, resulting in a rise in the temperature of the heater. This difference in the temperature is filtered by a differential measurement against a reference channel of helium. This minimizes noise from ambient fluctuations.

It should also be noted that integration of gas detectors has focused to a great extent on hybrid integrations. In one case, where a μTCD was monolithically integrated with a μSC, the two were cascaded, ignoring the possibility of further improvement by embedding [41]. In Chapter 2, we focus on integrating the brain and heart of a GC system in a monolithic process flow. The reference channel for the μTCD is avoided altogether by placing the reference resistor close to the inlet. This reduces the number of fluidic ports from four to two, apart from avoiding helium consumption on the reference channel. Further, we have also demonstrated the ability to extract the signal from a μTCD, when the column is thermostatted, for the first time. Monolithic integration overcomes the issue of “cold spots” in a hybrid integration wherein, the lower temperature of the interconnecting capillaries result in a drop in separation efficiency.

Improvements in architecture presented in Chapter 2, notwithstanding, our focus turned towards isolating the resistor from the substrate for better sensitivity. Bulk etched μTCD versions, seen in the literature was not an option since it results in the creation of wide channels unsuited for capillary GC [41]. Packing such a wide column results in very high operating pressures, unsuited for portable systems. Hence, a first-of-its-kind process was developed to surface micromachine and release the μTCD resistors on glass, as presented in Chapter 3. Further, the process is still compatible for anodic bonding to a μSC etched on silicon, and create

a tight seal. The decoupled process flow enables flexible processing of the silicon to fabricate current state-of-the-art semipacked and multi-capillary columns with nanostructured stationary phases. The improvement in sensitivity from 5000ppm to 200ppm demonstrates the validity of this claim.

The integrated column, developed in the previous two chapters, has two critical parameters. The first is its detection limit. TCDs have inherent poor detection limits. Primarily they are sensitive to temperature. Further, being a bulk detection mechanism, they also respond to changes in the carrier gas properties. A straightforward approach to improve the detection limit would be to concentrate the sample with a preconcentrator, right before the separation column. This approach is investigated in Chapter 4 wherein a previously developed micro-preconcentrator precedes the integrated device in a hybrid fashion. Preconcentrators, as previously described, are thermally responsive devices and interact with the thermally sensitive TCDs. The means to detect a compound in such a noisy environment is the prime focus of this chapter. In addition, an application for such a configuration in monitoring volatile organic compounds trapped in water is demonstrated. This required the modification of the TCD process flow to prevent interaction with moisture from the sample.

The second aspect of concern of the integrated column is its peak capacity. The separation efficiency of a separation column is defined by a plate number. The plate number is higher for a better column that results in a narrower peak at the same retention time. Given the numerous known volatile organic compounds, a practical column with a finite plate number requires impractical lengths of the separation column to be able to differentiate the entire list. However, utilizing multiple columns with different stationary phase selectivity, one can get closer to the ideal separation abilities. The monolithic integration of the separation column and the thermal conductivity detector developed in Chapter 1 and 2, were motivated by this need. Arrays of such integrated devices operated in a matrix, coated differently and operating at different column temperatures can increase peak capacity. Distinct from multi-chromatography and multi-dimensional GC, the ability to miniaturize and batch fabricate detectors with separation columns gives a multi-dimensional analysis and separation ability to such a technique. Specifically, we explore the ability to separate a wide range of boiling points and identify them precisely, within a minute.

A μTCD, despite its simplicity, is still found wanting in terms of limit of detection. Apart from its temperature dependence, the power consumption of a μTCD is also prohibitive in power-starved environments. A suitable alternative is to utilize the ionization effect of a helium microdischarge. It is known that photons from the discharge can ionize analytes without fragmenting them [42]. These ionized analytes are sensed for picoamperes of current. This detector, a μHe-DID, is universal and non-destructive, like the μTCD. However, it is more sensitive than a μTCD (50ppm) while consuming only 1.4mW of power making it suitable for

handheld applications. Chapter 6 discusses the fabrication and working of such a proof-of-concept detector.

As is expected of every proof-of-concept device, Chapter 7 is a detailed analysis of the effect of the electrode placement and electrode voltages in the discharge detector. The effect of design parameters – discharge to bias electrode distance, bias electrode to collector electrode distance –, and operating parameters – discharge voltage and bias voltage – are parametrically studied to obtain insights into the operation of the renamed discharge ionization detector (DID). It is hypothesized that the means of analyte ionization is not restricted to photons and metastable helium atoms from the discharge but also charged flux that flows from the discharge. The method is elaborated based on the experimental results. A 24-hour continuous operation is also presented without any visible deterioration. The limit of detection is also improved to 60pg at a power consumption of 3.3mW.

Finally, Chapter 8 will conclude by summarizing the accomplishments, listing the next set of improvements that are being proposed.

REFERENCES

[1] G. Monti, *et al.*, "Monitoring Food Quality by Microfluidic Electrophoresis, Gas Chromatography, and Mass Spectrometry Techniques: Effects of Aquaculture on the Sea Bass (Dicentrarchus labrax)," *Anal. Chem.*, vol. 77, no. 8, pp. 2587-2594, 2005.

[2] D. Puente, *et al.*, "Thermal conductivity microsensor for determining the Methane Number of natural gas," *Sens. Actuators B Chem*, vol. 110, no. 2, pp. 181-189, 2005.

[3] R. W. Cernosek, *et al.*, "Micro-analytical systems for national security applications," in *Proc. SPIE-Micro (MEMS) and Nanotechnologies for Space Applications*, Orlando (Kissimmee), FL, USA 2006, p. 622306.

[4] A. D. Radadia, *et al.*, "Micromachined GC Columns for Fast Separation of Organophosphonate and Organosulfur Compounds," *Anal. Chem.*, vol. 80, no. 11, pp. 4087-4094, 2008.

[5] D. Nielsen, *Practical handbook of environmental site characterization and ground-water monitoring*: CRC press, 2006.

[6] M. Akbar, *et al.*, "Improved performance of micro-fabricated preconcentrators using silica nanoparticles as a surface template," *Journal of Chromatography A*, vol. 1322, no. 0, pp. 1-7, 2013.

[7] M. Akbar, *et al.*, "A Microfabricated Propofol Trap for Breath-Based Anesthesia Depth Monitoring," *J. Microelectromech. Syst.*, vol. PP, no. 99, pp. 1-9, 2012.

[8] M. Akbar, *et al.*, "A cascaded micro preconcentration approach for extraction of volatile organic compounds in water," in *Sensors, 2012 IEEE*, 2012, pp. 1-4.

[9] H. Shakeel, *et al.*, "Self-Patterned Gold-Electroplated Multicapillary Gas Separation Columns With MPG Stationary Phases," *J. Microelectromech. Syst.*, vol. 22, no. 1, pp. 62-70, Feb. 2013.

[10] H. Shakeel, *et al.*, "First reconfigurable MEMS separation columns for micro gas chromatography," in *Micro Electro Mechanical Systems (MEMS), 2012 IEEE 25th International Conference on*, 2012, pp. 823-826.

[11] H. Shakeel, *et al.*, "Semipacked separation columns with monolayer protected gold stationary phases for microgas chromatography," in *Sensors, 2012 IEEE*, 2012, pp. 1-4.

[12] D. Wang, *et al.*, "Highly Stable Surface Functionalization of Microgas Chromatography Columns Using Layer-by-Layer Self-Assembly of Silica Nanoparticles," *Analytical Chemistry, [online early access]*, Jul. 27 2013 2013.

[13] B. Alfeeli, *et al.*, "MEMS-based multi-inlet/outlet preconcentrator coated by inkjet printing of polymer adsorbents," *Sens. Actuators B Chem*, vol. 133, no. 1, pp. 24-32, 2008.

[14] S. Ali, *et al.*, "MEMS-based semi-packed gas chromatography columns," *Sens. Actuators B Chem*, vol. 141, no. 1, pp. 309-315, 2009.

[15] S. C. Terry, *et al.*, "A gas chromatographic air analyzer fabricated on a silicon wafer," *Electron Devices, IEEE Transactions on*, vol. 26, no. 12, pp. 1880-1886, 1979.

[16] R. R. Reston, *et al.*, "Silicon-micromachined gas chromatography system used to separate and detect ammonia and nitrogen dioxide. I. Design, fabrication, and integration of the gas chromatography system," *J. Microelectromech. Syst.*, vol. 3, no. 4, pp. 134-146, 1994.
[17] C. M. Yu, *High performance hand-held gas chromatograph*, 1998.
[18] G. E. Spangler, "Height Equivalent to a Theoretical Plate Theory for Rectangular GC Columns," *Anal. Chem.*, vol. 70, no. 22, pp. 4805-4816, 1998.
[19] G. E. Spangler, "Relationships for modeling the performance of rectangular gas chromatographic columns," *Journal of Microcolumn Separations*, vol. 13, no. 7, pp. 285-292, 2001.
[20] R. Manginell, *et al.*, "Advancements in the Monolithically-Integrated MicroChemLab," in *Proceedings of the m-TAS 2004 Workshop*, Malmo, Sweden, 2004, pp. 61-63.
[21] R. P. Manginell, *et al.*, "Mass-Sensitive Microfabricated Chemical Preconcentrator," *J. Microelectromech. Syst.*, vol. 17, no. 6, pp. 1396-1407, 2008.
[22] B. Alfeeli, *et al.*, "MEMS-Based Selective Preconcentration of Trace Level Breath Analytes," *IEEE Sensors J.*, vol. 9, no. 9, 2009.
[23] S. J. Martin, *et al.*, "Gas sensing with acoustic devices," in *Ultrasonics Symposium, 1996. Proceedings., 1996 IEEE*, 1996, pp. 423-434 vol.1.
[24] J. C. T. Eijkel, *et al.*, "A dc Microplasma on a Chip Employed as an Optical Emission Detector for Gas Chromatography," *Anal. Chem.*, vol. 72, no. 11, pp. 2547-2552, 2000.
[25] Q.-Y. Cai, *et al.*, "Dual-Chemiresistor GC Detector Employing Monolayer-Protected Metal Nanocluster Interfaces," *Anal. Chem.*, vol. 74, no. 14, pp. 3533-3539, 2002/07/01 2002.
[26] M. Moorman, *et al.*, "Microcombustor array and micro-flame ionization detector for hydrocarbon detection," in *Proc. SPIE—MEMS Components and Applications for Industry, Automobiles, Aerospace, and Communication II,*, San Jose, CA, USA, 2003, pp. 40-50.
[27] W. J. Kuipers, *et al.*, "A planar micro-flame ionization detector with an integrated guard electrode," *J. Micromech. Microeng*, vol. 18, no. 6, p. 064015, 2008.
[28] J. J. Whiting, *et al.*, "High-speed two-dimensional gas chromatography using microfabricated GC columns combined with nanoelectromechanical mass sensors," in *TRANSDUCERS*, 2009, pp. 1666-1669.
[29] S. Bedair, *et al.*, "CMOS MEMS oscillator for gas chemical detection," in *Proceedings of IEEE Sensors*, 2004, pp. 955-958.
[30] M. Gajda, *et al.*, "Applications of thermal silicon sensors on membranes," *Sens. Actuators A Phy*, vol. 49, no. 1-2, pp. 1-9, 1995.
[31] M. Kimura, *et al.*, "Application of the air-bridge microheater to gas detection," *Sens. Actuators B Chem*, vol. 25, no. 1-3, pp. 857-860, 1995.
[32] Y. Huang, *et al.*, "The effects of forced convection on the power dissipation of constant-temperature thermal conductivity sensors," *Journal of heat transfer*, vol. 119, p. 30, 1997.
[33] S. Sorge, *et al.*, "Fully integrated thermal conductivity sensor for gas chromatography without dead volume," *Sens. Actuators A Phy*, vol. 63, no. 3, pp. 191-195, 1997.
[34] K. Chen, *et al.*, "Thermal analysis and simulation of the microchannel flow in miniature thermal conductivity detectors," *Sens. Actuators A Phy*, vol. 79, no. 3, pp. 211-218, Feb. 2000.
[35] I. Simon, *et al.*, "Thermal and gas-sensing properties of a micromachined thermal conductivity sensor for the detection of hydrogen in automotive applications," *Sens. Actuators A Phy*, vol. 97, pp. 104-108, 2002.
[36] Y. Wu, *et al.*, "Fabrication and characterization of thermal conductivity detectors (TCDs) of different flow channel and heater designs," *Sens. Actuators A Phy*, vol. 100, no. 1, pp. 37-45, 2002.
[37] J. Lysko, *et al.*, "Silicon thermal conductivity detector (TCD) with the Pt resistors," in *Proc. SPIE 5124, Optoelectronic and Electronic Sensors*, 2003, p. 258.
[38] S. Showalter, *et al.*, "Design and Testing of a Micro Thermal Conductivity Detector (TCD) System," SAND2003-0954, Sandia National Labs., Albuquerque, NM (US);2003.
[39] A. Gutierrez, "New Thermal Conductivity Microsensor to measure the methane number of natural gas," in *23rd World Gas Conference*, Amsterdam, 2006.
[40] B. Kaanta, *et al.*, "High sensitivity micro-thermal conductivity detector for gas chromatography," in *22nd IEEE International Conference on Micro Electro Mechanical Systems (MEMS '09)*, Sorrento, Italy, 2009, pp. 264-267.
[41] B. Kaanta, *et al.*, "A monolithically fabricated gas chromatography separation column with an integrated high sensitivity thermal conductivity detector," *J. Micromech. Microeng*, vol. 20, no. 5, p. 055016, 2010.
[42] W. Wentworth, *et al.*, "Pulsed discharge helium ionization detector," *Chromatographia*, vol. 34, no. 5, pp. 219-225, 1992.

2

Monolithic Integrated Separation Column with a Thermal Conductivity Detector

Shree Narayanan, Bassam Alfeeli, and Masoud Agah

The continuous development of micro gas chromatography systems (μGCs) is driven by their important application as a handheld analytical instrument in homeland security, medical diagnostics, food quality monitoring, and environmental monitoring among others [1-6]. In all these cases, the gas sample to be analyzed can be complex in composition. For instance, a sample of breath mixture can contain as many as 1200 volatile organic compounds (VOCs) [7]. Such complex mixtures of VOCs are analyzed by chromatographic methods such as gas chromatography. This analytical technique relies on the separation of gases based on their relative sorption levels to a stationary phase coating and is a premier analytical technique [8].

Advantages of μGC technology include lower cost due to batch fabrication techniques, decreased device dimensions for field testing, lower power consumptions, shorter analysis times, and the possibility of introducing innovative designs and architectures which are otherwise difficult to realize in traditional GCs[7, 9-11]. However, this emerging technology has limited separation efficiency and sample capacity owing to its relatively small size. Improvement in performance is anticipated as the technology matures.

The main components of a GC system are the separation column, the heart of the system, and the gas detector. Considerable research effort has been directed towards the development of columns. Semi-packed [10], multi-capillary [9], chemical vapor deposition (CVD)-sealed [12], Lithographie, Galvanoformung, Abformung (LIGA)-based [13], parylene coated [14, 15] columns among others are examples of microcolumns developed by the utilization of microelectromechanical systems (MEMS) technology. Miniaturized gas detectors have also been the subject of research for many years. Examples include thermal conductivity detectors (TCD)

[16, 17], flame ionization detectors (FID) [18-20], surface acoustic wave (SAW) resonators [21, 22], and chemiresistor arrays [23, 24].

To date, μGC development has been focusing on the realization of the individual components of the system. However, integration of the various components is a critical yet under-explored aspect. Hybrid integrations of separation columns and detectors have been reported using SAW, TCD, and chemiresistors. Of significance are the Sandia National Laboratories' μChem Lab and the University of Michigan's SPRION and ORION designs [2, 25]. Hybrid integration, though, is saddled with cold-spot efficiency reduction as well as increased cost and maintenance when compared to monolithic integration [22]. Such integration requires judicious selection of the detector and column configurations to keep the cost of fabrication down to a minimum while not sacrificing the performance.

TCDs, among different detector types, are easy to construct and are universal detectors unlike most other detectors used in GC such as electron capture detectors (ECD) and Nitrogen Phosphorous detectors (NPDs), which can detect only specific classes of compounds. In this chapter, TCDs are used to readily sense the separated volatile organic compounds (VOCs) as they exit the column. Detection of gases down to ppb levels has been reported earlier using micromachined TCDs [26, 27]. It is noteworthy that TCD was employed in the first microfabricated (hybrid) GC implementation in 1979 [28]. This chapter discusses the theory, fabrication, and the experimental results of a new microchip comprising a separation column and a TCD having only two fluidic ports. In addition, the chip has heaters and sensors for temperature programming which is essential for general separation optimization.

2.1 Theory

2.1.1 Separation column

The separation column is an etched channel in the substrate whose inner wall is coated with a stationary phase such as polydimethylsiloxane. Different molecules in a sample mixture injected into the carrier gas stream interact to different extents with the stationary phase, and hence, travel with different velocities and get separated. The separation efficiency of a column can be quantified by the height-equivalent-to-a-theoretical-plate (H) that needs to be minimized. There are three contributing factors as defined in [29]

$$H = A + \frac{B}{u} + Cu \qquad \textbf{2-1}$$

Here, u denotes the average linear gas velocity while, the coefficients A, B and C take into account the eddy-diffusion, longitudinal molecular diffusion and mass transfer in the stationary liquid phase in order. The constant term, which represents the contribution of eddy diffusion to band broadening, is absent in the case of capillary columns but non-zero for packed columns

[29-31]. The pressure drop across a packed structure can also be prohibitive for μGC applications. This provides motivation for using open columns over packed columns for monolithic integration.

2.1.2 Thermal Conductivity Detector

In a TCD, a resistive heater is placed in the path of the carrier gas of higher thermal conductivity compared to the volatile compounds that are analyzed. Under normal conditions, the high thermal conductivity of the carrier gas results in a lower resistance compared to when the separated volatile compounds pass over the heater [16, 32]. In theory, this technique can be employed to detect any compound that has a different thermal conductivity from that of the carrier gas. However, to detect a difference that is larger than the background noise, helium, with a thermal conductivity of 0.1513W/(m.K) is used as the carrier gas in TCDs. This is because its thermal conductivity is an order of magnitude greater than that of the organic compounds analyzed in gas chromatography. Figure 2-1 shows a plot of the simulated temperature of the heater with $3x10^6$ W/m^2 heat flux as the thermal conductivity of the gas varies between 0.030-0.222 W/(m.K). These values correspond to acetone and helium, respectively, at 500K [33]. For a thermal coefficient of resistance (TCR) of 1700 ppm/˚C, this translates to a 5% change in the normalized resistance.

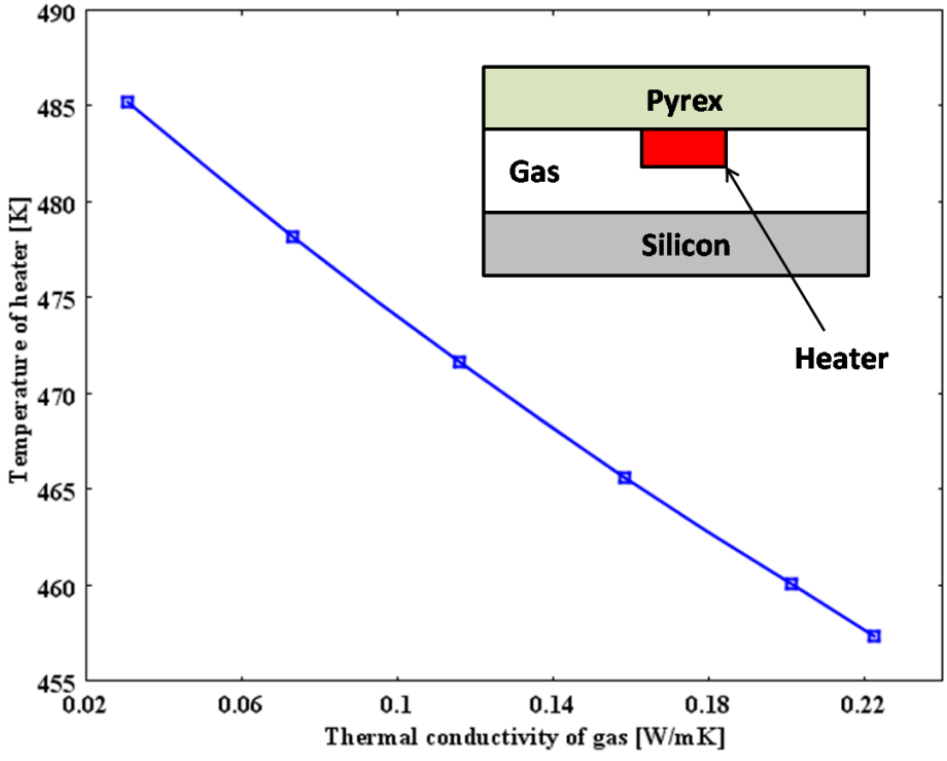

Figure 2-1: A simulated plot of the temperature of a resistive heater in contact with Pyrex on one side and separated from silicon on the other side by a gas. A representation of the 2D model with heater used for the simulation is shown in the inset, top right.

TCDs are a promising candidate for monolithic integration due to their simple fabrication process flow, universal detection, and non-destructive nature. To ensure that conduction dominates over convection as the main mode of heat transport, fluid flow velocity needs to be low enough to keep the Peclet number (Pe) lower than 0.1 [34].

$$Pe = \frac{\rho C_p U L}{k_t} \qquad \textbf{2-2}$$

Here, ρ is the density, C_p is the specific heat, U is the velocity, L is the characteristic length, and k_t is the thermal conductivity of the carrier. It should be noted that the sensitivity of the TCD can be improved by reducing the conductive paths from the heater through isolating it from the surroundings [35].

In order to filter out the fluctuations due to external heat (ambient) and the fluctuations in the carrier gas flow velocity, a differential measurement against a reference heater placed in a parallel carrier flow channel gives the signal due to the detected component only. This method of detection has been widely reported. However, our monolithic integration adopts a unique approach (presented in the next section) to avoid the reference channel.

2.1.3 Monolithic Integration

Integration of a TCD with a separation column was recently reported by cascading the two (similar to a hybrid integration) [36]. In a marked improvement, we have embedded the TCD within the separation column as shown in Figure 2-2. This was made possible by placing the reference detector close to the inlet. As the sample is injected, it first comes in contact with the inlet detector. Thereafter, the inlet detector is exposed only to the carrier gas and hence acts as the reference detector after the sample passes that point. The sample of gas undergoes separation within the column, thereby generating a signal for every component as it passes over the output detector. A differential measurement against the reference detector cancels variations generated due to ambient fluctuations. It should be noted that at the low operating pressures, the flow velocity experienced by both resistors would have a finite but minimal difference. Furthermore, the number of fluidic ports is reduced to just 2 when compared to 4 in all previously reported results. This reduces the overall size of the chip as well as the number of macro-to-micro fluidic interfaces, thereby enhancing the overall reliability of the device for field-use applications.

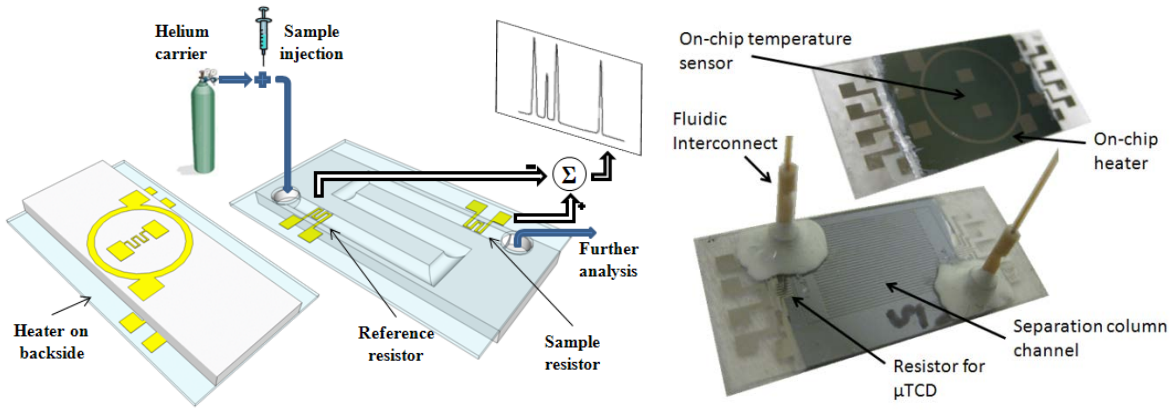

(a) (b)

Figure 2-2: (a) is a representation of the operation of a μGC chip. The unique positioning of the reference resistor close to the inlet reduces the number of ports to 2. (b) shows our packaged μGC chip with just 2 fluidic ports.

2.1.4 Temperature programming for high-speed analysis

The time taken for a component to elute is given by the expression [37]

$$t_R = (L/u) * (k+1) \qquad \textbf{2-3}$$

Here, u is the average carrier gas velocity and L is the column length. k is the retention factor of the respective component and is given by the expression

$$log(k) = A/T_c + B \qquad \textbf{2-4}$$

where A and B are empirical constants and T_c is the absolute column temperature. Increasing the temperature reduces the retention factor, thereby decreasing the elution time. To enable faster analysis at elevated temperatures, an on-chip heater and sensor were introduced on the backside of the device. In a previous work on silicon-glass columns [3], a resistive heater was placed at the midpoint of each edge of the chip to ensure a uniform temperature. This approach requires eight bond pads. We have opted for a circular heater with just two bond pads. Our first-order Finite element simulation results in Figure 2-3, performed in COMSOL, show that this design exhibits a lower temperature gradient across the device when compared to the previously reported configuration. The simulated model consisted of a 2cm x 2.5cm x 500μm silicon chip placed at the center of a 3cm x 3.5cm x 2.5mm enclosure filled with nitrogen. The walls of the enclosure were constrained at 300K. For the original case, four 1mm x 1mm titanium thin films placed at the midpoint of each edge, as shown in Figure 2-3, served as the heaters. On the other hand, the heater in our case was represented by a circular thin film with an outer radius of 0.9cm and a width of 100μm. The surfaces of these thin films in contact with the silicon substrate are

maintained at 423K and are comparable in both cases. The presence of greater symmetry gives a more uniform temperature profile in our case when compared to having four distinct resistors.

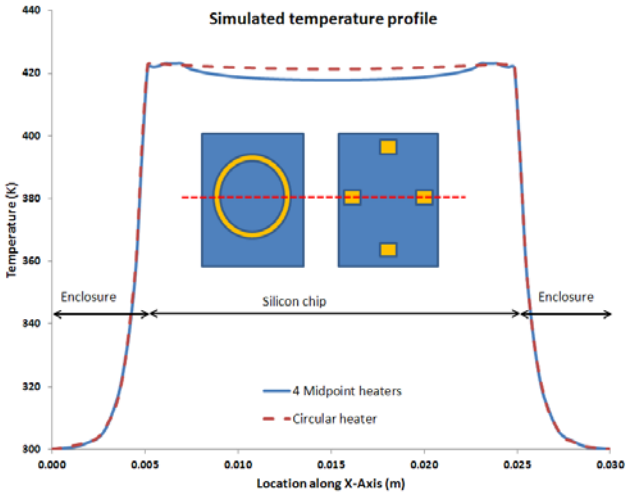

Figure 2-3: Comparison of the simulated temperature distribution along the chip (red color dashed line) for two different heater designs. Our design (to the left) shows lesser gradient.

2.2 Fabrication

The μGC chip was realized by bonding two separately processed wafers (silicon and Pyrex), as shown in Figure 2-4. Pyrex served as an insulating substrate for the μTCD elements and being transparent, it made it possible to observe the fluid in the channel while coating. The microfluidic structures were implemented on a 4" p-type <100> oriented double-side polished silicon of 0-100 ohm-cm resistivity. The TCD elements were fabricated by utilizing a lift-off process of a 300Å/1000Å Ti/Pt stack in a KJL PVD-250 e-beam evaporator. The metal pattern can be divided into 3 sections. The resistive elements within the channel, interconnect that takes the connection out of the silicon area, and the bond pads.

Apart from the separation channel and the port regions, silicon needs to be etched under the metal pattern to ensure proper bonding to the Pyrex and to avoid metal-silicon contacts. The three different sections of metal require three different etch depths. The column depth is aligned with the actual resistive element and is an important parameter influencing the separation efficiency. The second depth (minimum) allows the insulation of interconnects from silicon and thus is aligned with interconnects. This was obtained by 2μmx2μm squares spaced 4μm apart. On the other hand, an 800μm diameter open area resulted in the third depth (maximum) corresponding to the inlets and outlets as well as the bond pad regions. The alignment of the etch depths against the detector elements can be observed in the final integrated cross-section in Figure 2-4(e). To etch silicon to three different depths and to minimize the required processing steps, we utilized reactive ion etch lag in isotropic silicon etching and its dependence to the

geometrical patterns of the photomask layout as previously published by our group [38, 39]. The etch depth was shown to be modeled by a modified Langmuir equation

$$Depth = \exp\left(\frac{\alpha\beta F^{\gamma}}{1+\beta F^{\gamma}}\right) \qquad \textbf{2-5}$$

where α, β, γ and F are empirically obtained values

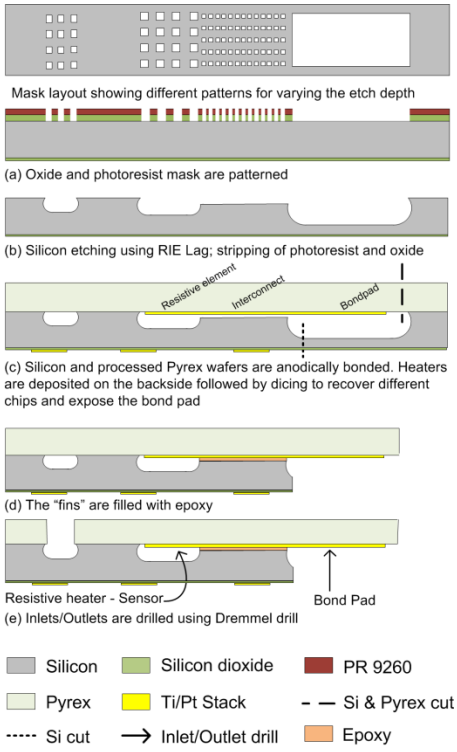

Figure 2-4: Fabrication process (not to scale) shows the silicon etch step in (a) and (b) followed by bonding with the Pyrex wafer with detectors and backside heater/sensor deposition in (c). Finally (d) and (e) show the packaging steps.

In this technique, differently sized holes (squares) spaced close to each other experience different local etch rates since etching species are depleted to different extents and reach different etch depths with different concentration. This is shown on the mask layout at the top of Figure 2-4. Both the size of the opening holes and their spacing can be used as design parameters on the layout to achieve three-dimensional profiles in silicon using a single-mask, single-etch process.

The fabrication process of the silicon wafer began by growing a 5000Å-thick thermal oxide layer. The oxide on the backside is used as an electrical insulation layer at a later stage. The oxide on the front side is patterned with a 7μm thick spun AZ9260 photoresist mask. Next, without removing the photoresist, silicon was etched isotropically using a SF_6 plasma in a deep reactive ion etcher (DRIE) with RIE-lag enhanced parameters. A recipe with an SF_6 flow rate of 400sccm, coil power of 2200W, platen power of 50W, chamber pressure of 0.11mbar, and platen temperature of 20°C was employed for a total of 40 minutes. Further characterization

information regarding this process, published by our group in [38, 39], indicates less than 10% prediction error in the width and height. Figure 2-5 displays the scanning electron microscopy (SEM) images of the three different depths achieved in a single-etch process for three different parts of the μGC chip. The tunnel for the metal interconnects is about 105μm-wide and 16μm-deep. The cavity underneath the bond pads is about 200μm-deep and the semi-circular column is about 75μm-deep and 140μm-wide. After removing the oxide layer in buffered oxide etchant (BOE), the silicon and Pyrex wafers were aligned in a probe station modified to serve as an anodic bonder at 300˚C in air. Following bonding, the backside of silicon was patterned and a Ti/Pt stack with 300Å /1200Å in thickness was deposited, similar to the previous lift-off step.

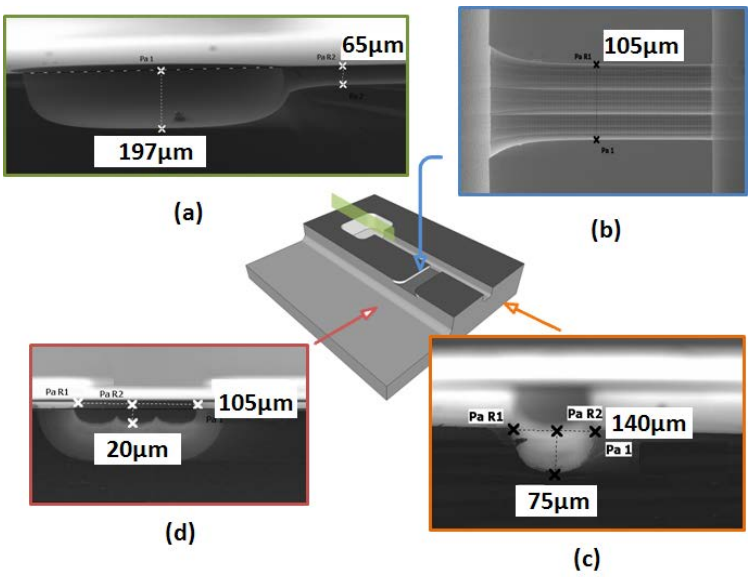

Figure 2-5: Multiple channel depths utilizing RIE-Lag to achieve multiple etch depths and minimize the dead-volume. (b), (c) and (d) show the SEM images of the resulting etch from three different directions while (a) is a SEM of the cross section.

The stack was then diced to release the individual devices and to provide access to the bond pads on the Pyrex substrate. Epoxy was used to fill the 16μm gap between interconnects and silicon to prevent leakage of gases. Holes were drilled through Pyrex using a Dremmel drill for the fluidic ports. A manually assembled connector out of stepped polyethyl ether ketone (PEEK) tubes was used to slide the deactivated fused silica tubing into the drilled hole.

2.3 Experiments and results

2.3.1 Standalone μTCD

To verify the suitability of our fabrication and packaging method, a standalone μTCD was fabricated using two channels having a depth of 70μm, width of 140μm, and length of 2.5cm. The final device is shown in Figure 2-6(a). The standalone μTCD, as can be seen, has 4 fluidic ports and two fluidic channels, one of which acts as the reference. The resistors of the detector were

characterized to obtain the temperature-voltage applied relation. A typical temperature-resistance-voltage map is presented in Figure 2-6(b). The resistor was placed in an environmental chamber and its resistance was measured against a set temperature. The measured data was fit to a straight line and extrapolated to obtain the plot with the (red) square marker. Next, the current through the resistor was measured against an applied voltage. From this measurement, the resistance against applied voltage plot - with (blue) triangle marker - was obtained. The resistance varied with applied voltage due to Joule heating.

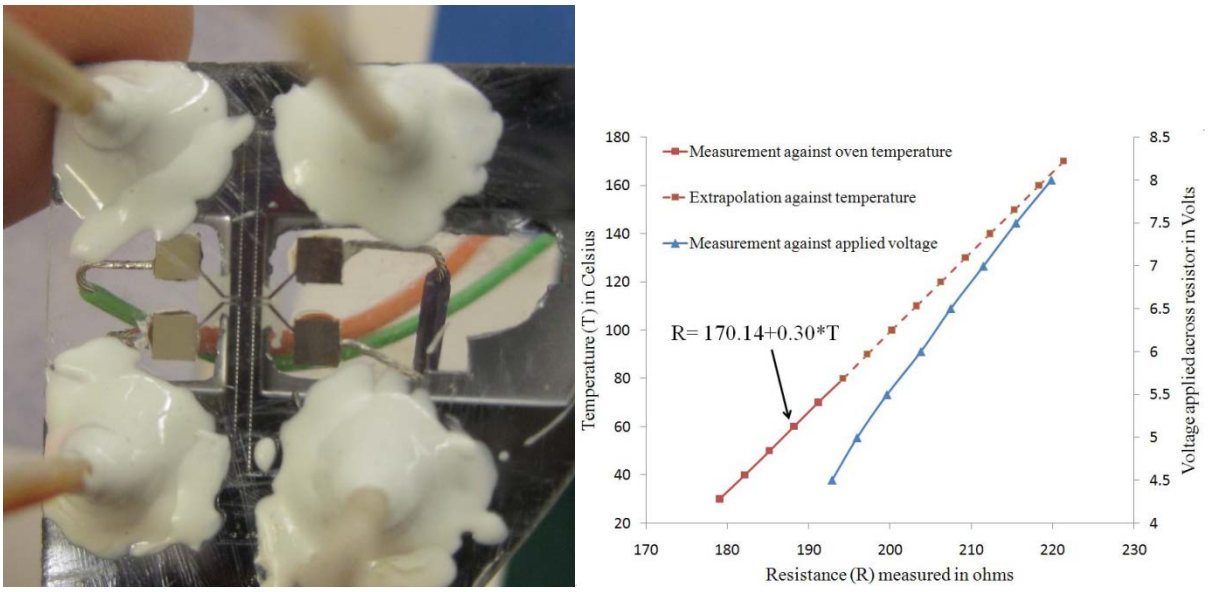

(a) (b)

Figure 2-6: (a) shows an image of a packaged standalone μTCD suitable for hybrid integration. The 4 fluidic ports and two channels are shown. (b) is a Voltage-Resistance-Temperature map for a typical resistor. The line with the square marker is a plot of the resistance against the resistor's temperature. While the solid line is the measured value, the dashed line is the extrapolation assuming a linear variation. The line with the triangle marker is a plot of the applied voltage against the resistance which varies due to Joule heating.

A 10m-long, 250μm-I.D. commercial column with polydimethylsiloxane coating (Restek Cat#13320) preceded the standalone μTCD. For verification purposes, the outlet of the sample channel was connected to a commercial FID. This made the μTCD in series with the FID. The injector of an HP 5890 maintained at 280˚C was used to split-inject the sample into the column. A current source was used to drive 22mA current through a series combination of the two resistors while a LabVIEW program measured the voltages across the two resistors of the μTCD. The difference in the voltages was calculated in LabVIEW and plotted. A sample mixture of 8 components including 1-propanol, dichloromethane, n-pentane, n-hexane, n-heptane, 1,2-dichloroethane, benzene, and toluene was injected in the column. Figure 2-7 shows the response of the standalone μTCD, in the top half, and compares it with that of the FID, in the lower half. The result, confirmed by the FID signal, clearly indicated that the μTCD is capable of detecting the separated compounds. In Figure 2-7, the retention time of the components as detected by the

FID is slightly longer than the ones obtained by the μTCD mainly due to the ~20cm-long capillary tube that connects the FID to TCD. The shape of the peaks as observed by both detectors closely match. The reason that the peak heights are different in the two cases is that in FID, the peak is determined by the extent to which the carbon atoms can be ionized. For TCD, however, it depends on the compound's thermal conductivity and its concentration.

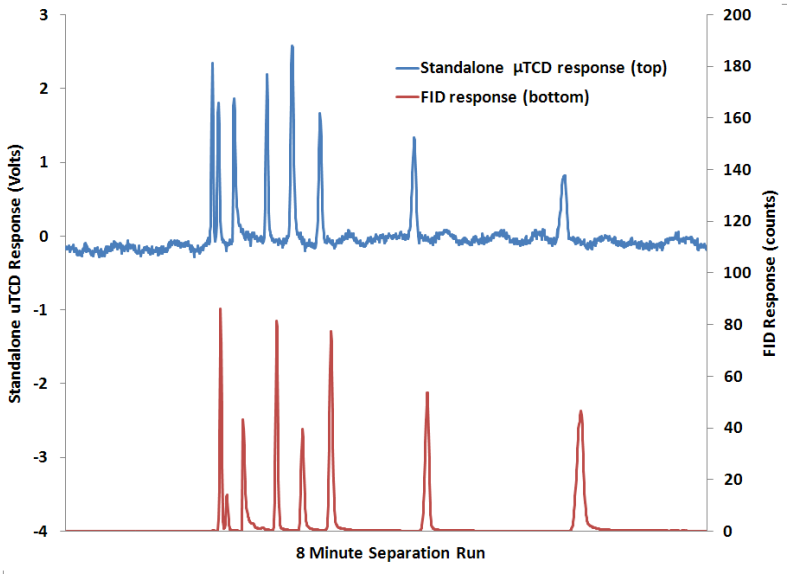

Figure 2-7: Comparison of the separation of an 8-component mixture -1-Propanol, dichloromethane, n-pentane, n-hexane, n-heptane, 1,2-dichloroethane, benzene, and toluene, in order from left to right - as detected by FID and the standalone μTCD

2.3.2 Thermostatted μGC chip

A 120μm-wide, 50cm-long column with a 300Å/1000Å Ti/Pt stack for the TCD on Pyrex was fabricated according to the process described earlier. The packaged device was previously shown in Figure 2-2. In comparison with Figure 2-6(a), this device has just one channel and two fluidic ports. The device was static coated with polydimethylsiloxane by filling it with a solution of 10mg/ml OV-1 in pentane, followed by carefully sealing one end with wax and pulling a vacuum at the open end. This procedure leaves a thin layer of polydimethylsiloxane coating on the walls [40]. An SEM image of the stationary phase coating is shown in Figure 2-8(a). The rounded cross section due to isotropic etching has been speculated to perform better due to reduced pooling effects [41]. Pooling refers to the sagging of the stationary phase around sharp corners commonly seen in rectangular MEMS columns. The temperature of the device was controlled by the feedback circuit shown in Figure 2-8(b). The comparator operates in a pulse-width modulated mode to maintain the same voltage across the sensor resistor and the trimpot by switching the heater resistor on and off. The voltage across the trimpot, therefore, corresponds

to the temperature of the column. By varying this resistance and hence the voltage across the trimpot, the column temperature can be varied.

The device was connected to an HP5890 injector with helium as the carrier gas. The inlet pressure was set to 4psi at 280°C. The detector resistors, maintained at 170°C, were connected in a Wheatstone bridge configuration. A LabVIEW program measured the differential voltage across the bridge. It should be noted that the presence of the resistive detectors raised the temperature of the device to 60˚C.

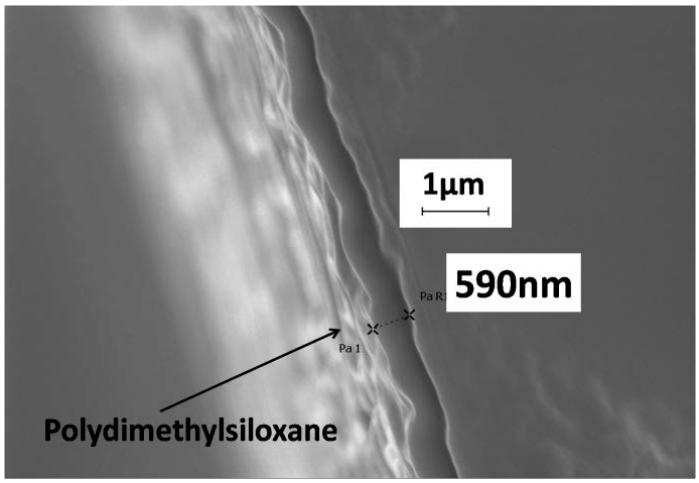

(a)

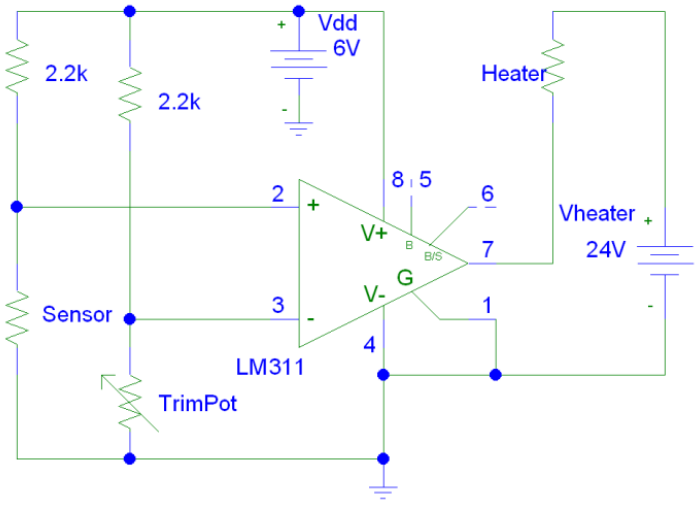

(b)

Figure 2-8: (a) is an SEM of the polydimethylsiloxane coating on the interior wall of the channel. (b) is the feedback circuitry to maintain the temperature of the device at a given setpoint. The voltage across the trimpot defines the setpoint temperature.

First, separation was performed at 60°C in the absence of thermostatting using a 200nl sample (4-component mixture of n-octane, n-nonane, n-decane and n-undecane). The μGC chip response is shown in blue color, on the top half of Figure 2-9. The initial negative dip corresponds to the sample mixture passing under the reference detector. At this stage, the signal detector experiences carrier gas and hence is constant. This results in a negative voltage output. As the sample mixture moves through the column, it is separated over time. As the individual components pass under the sample detector, the reference detector experiences the carrier gas and hence results in positive peaks corresponding to each eluted compound. To demonstrate the benefit of thermostating in reducing analysis time, the thermostatting circuit was switched on and the setpoint was set to 75˚C. The corresponding chromatogram to the same injection is shown in red color on the lower half of Figure 2-9. It should be noted that for a 15˚C device temperature rise, we observe halving of the retention time for the eluted components [30].

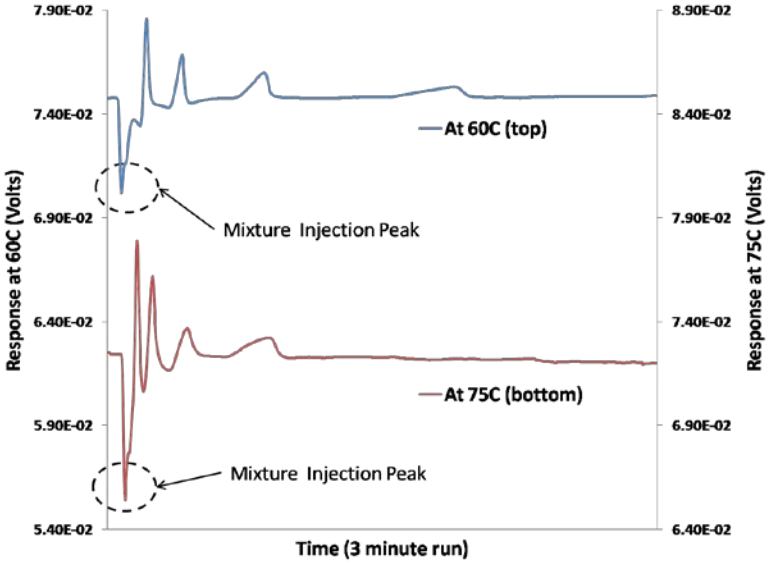

Figure 2-9: μGC response, with the on-chip heater deactivated is shown on top. The plot in the lower half is in the presence of thermostatting to raise the temperature of the device to 75˚C.

2.4 Inference

By embedding the reference resistor of the μTCD close to the inlet of the separation column, a novel monolithic integration has been established with reduced number of fluidic ports. Achieving this in one single etch step required an in-house developed RIE-Lag process which has also been employed to fabricate a standalone μTCD. In addition, the chip has been thermostatted and the μTCD signal, which is temperature dependent, has been recovered even in the presence of the additional heat source (thermostatting). The detector response can be significantly improved by under-etching the substrate below the resistor and by leaving it suspended [35]. For a given detector temperature, this will reduce the TCD power consumption and consequently, decreases the column temperature below 60˚C due to the TCD operation.

REFERENCES

[1] R. Manginell, *et al.*, "Advancements in the Monolithically-Integrated MicroChemLab," in *Proceedings of the m-TAS 2004 Workshop*, Malmo, Sweden, 2004, pp. 61-63.

[2] S. K. Kim, *et al.*, "Prototype micro gas chromatograph for breath biomarkers of respiratory disease," in *Solid-State Sensors, Actuators and Microsystems Conference. TRANSDUCERS. International*, 2009, pp. 128-131.

[3] M. Agah, *et al.*, "High-performance temperature-programmed microfabricated gas chromatography columns," *J. Microelectromech. Syst.*, vol. 14, no. 5, pp. 1039-1050, 2005.

[4] A. D. Radadia, *et al.*, "Micromachined GC Columns for Fast Separation of Organophosphonate and Organosulfur Compounds," *Anal. Chem.*, vol. 80, no. 11, pp. 4087-4094, 2008.

[5] A. Bhushan, *et al.*, "Fabrication of micro-gas chromatograph columns for fast chromatography," *Microsyst. Technol.*, vol. 13, no. 3, pp. 361-368, 2006.

[6] Q. Zhong, *et al.*, "Characterization of a high-performance portable GC with a chemiresistor array detector," *The Analyst*, vol. 134, no. 2, pp. 283-293, 2009.

[7] B. Alfeeli, *et al.*, "MEMS-Based Selective Preconcentration of Trace Level Breath Analytes," *IEEE Sensors J.*, vol. 9, no. 9, 2009.

[8] F. L. Dorman, *et al.*, "Gas Chromatography," *Anal. Chem.*, vol. 82, no. 12, pp. 4775-4785, 2010/06/15 2010.

[9] M. A. Zareian-Jahromi, *et al.*, "Design, Modeling, and Fabrication of MEMS-Based Multicapillary Gas Chromatographic Columns," *J. Microelectromech. Syst.*, vol. 18, no. 1, pp. 28-37, 2009.

[10] S. Ali, *et al.*, "MEMS-based semi-packed gas chromatography columns," *Sens. Actuators B Chem*, vol. 141, no. 1, pp. 309-315, 2009.

[11] B. Alfeeli, *et al.*, "Low pressure drop micro preconcentrators with cobweb Tenax-TA film for analysis of human breath," in *Micro Electro Mechanical Systems (MEMS), 2011 IEEE 24th International Conference on*, 2011, pp. 916-919.

[12] M. Agah, *et al.*, "Low-Mass PECVD Oxynitride Gas Chromatographic Columns," *J. Microelectromech. Syst.*, vol. 16, no. 4, pp. 853-860, 2007.

[13] A. Bhushan, *et al.*, "Fabrication and Preliminary Results for LiGA Fabricated Nickel Micro Gas Chromatograph Columns," *J. Microelectromech. Syst.*, vol. 16, no. 2, pp. 383-393, 2007.

[14] H.-S. Noh, *et al.*, "Parylene gas chromatographic column for rapid thermal cycling," *J. Microelectromech. Syst.*, vol. 11, no. 6, pp. 718-725, 2002.

[15] T. Nakai, *et al.*, "Amorphous Parylene Stationary Phase for Microfabricated Gas Chromatographic Columns," in *uTAS*, Jeju, Korea, 2009.

[16] R. Pecsar, *et al.*, "Performance of a reduced volume thermal conductivity detector," *Anal. Chem.*, vol. 45, no. 13, pp. 2191-2198, 1973.

[17] S. Sorge, *et al.*, "Fully integrated thermal conductivity sensor for gas chromatography without dead volume," *Sens. Actuators A Phy*, vol. 63, no. 3, pp. 191-195, 1997.

[18] S. Zimmermann, *et al.*, "Micro flame ionization detector and micro flame spectrometer," *Sensors & Actuators: B. Chemical*, vol. 63, no. 3, pp. 159-166, 2000.

[19] W. J. Kuipers, *et al.*, "A planar micro-flame ionization detector with an integrated guard electrode," *J. Micromech. Microeng*, vol. 18, no. 6, p. 064015, 2008.

[20] M. Moorman, *et al.*, "Microcombustor array and micro-flame ionization detector for hydrocarbon detection," in *Proc. SPIE—MEMS Components and Applications for Industry, Automobiles, Aerospace, and Communication II*,, San Jose, CA, USA, 2003, pp. 40-50.

[21] S. J. Martin, *et al.*, "Gas sensing with acoustic devices," in *Ultrasonics Symposium, 1996. Proceedings., 1996 IEEE*, 1996, pp. 423-434 vol.1.

[22] P. R. Lewis, *et al.*, "Recent advancements in the gas-phase MicroChemLab," *Sensors Journal, IEEE*, vol. 6, no. 3, pp. 784-795, 2006.

[23] S. Bedair, *et al.*, "CMOS MEMS oscillator for gas chemical detection," in *Proceedings of IEEE Sensors*, 2004, pp. 955-958.

[24] J. J. Whiting, *et al.*, "High-speed two-dimensional gas chromatography using microfabricated GC columns combined with nanoelectromechanical mass sensors," in *TRANSDUCERS*, 2009, pp. 1666-1669.

[25] R. W. Cernosek, *et al.*, "Micro-analytical systems for national security applications," in *Proc. SPIE-Micro (MEMS) and Nanotechnologies for Space Applications*, Orlando (Kissimmee), FL, USA 2006, p. 622306.

[26] S. Showalter, *et al.*, "Design and Testing of a Micro Thermal Conductivity Detector (TCD) System," SAND2003-0954, Sandia National Labs., Albuquerque, NM (US);2003.

[27] B. Kaanta, *et al.*, "High sensitivity micro-thermal conductivity detector for gas chromatography," in *22nd IEEE International Conference on Micro Electro Mechanical Systems (MEMS '09)*, Sorrento, Italy, 2009, pp. 264-267.

[28] S. C. Terry, *et al.*, "A gas chromatographic air analyzer fabricated on a silicon wafer," *Electron Devices, IEEE Transactions on*, vol. 26, no. 12, pp. 1880-1886, 1979.

[29] J. J. van Deemter, *et al.*, "Longitudinal diffusion and resistance to mass transfer as causes of nonideality in chromatography," *Chemical Engineering Science*, vol. 5, no. 6, pp. 271-289, 1956.

[30] R. Grob, *et al.*, *Modern practice of gas chromatography*: Wiley-IEEE, 2004.

[31] G. E. Spangler, "Relationships for modeling the performance of rectangular gas chromatographic columns," *Journal of Microcolumn Separations*, vol. 13, no. 7, pp. 285-292, 2001.

[32] K. Chen, *et al.*, "Thermal analysis and simulation of the microchannel flow in miniature thermal conductivity detectors," *Sens. Actuators A Phy*, vol. 79, no. 3, pp. 211-218, Feb. 2000.
[33] D. Lide, *CRC handbook of chemistry and physics: a ready-reference book of chemical and physical data*: CRC Pr I Llc, 2004.
[34] W. Kays, *et al.*, *Convective Heat and Mass Transfer*, 4th International Edition ed.: McGraw-Hill, 2005.
[35] D. Cruz, *et al.*, "Microfabricated thermal conductivity detector for the micro-ChemLab™," *Sens. Actuators B Chem*, vol. 121, no. 2, pp. 414-422, 2007.
[36] B. Kaanta, *et al.*, "A monolithically fabricated gas chromatography separation column with an integrated high sensitivity thermal conductivity detector," *J. Micromech. Microeng*, vol. 20, no. 5, p. 055016, 2010.
[37] H. McNair, *et al.*, *Basic gas chromatography*: Wiley-Interscience, 1997.
[38] K. Gantz, *et al.*, "Development of a comprehensive model for RIE-lag-based three-dimensional microchannel fabrication," *J. Micromech. Microeng*, vol. 18, no. 2, p. 025003, 2008.
[39] P. Zellner, *et al.*, "A fabrication technology for three-dimensional micro total analysis systems," *J. Micromech. Microeng*, vol. 20, p. 045013, 2010.
[40] S. Reidy, *et al.*, "High-Performance, Static-Coated Silicon Microfabricated Columns for Gas Chromatography," *Anal. Chem.*, vol. 78, no. 8, pp. 2623-2630, 2006.
[41] J. C. Giddings, "Liquid Distribution on Gas Chromatographic Support. Relationship to Plate Height," *Anal. Chem.*, vol. 34, no. 4, pp. 458-465, 1962.

3

Fabrication and Characterization of a Released TCD on Glass for Increased Sensitivity

Shree Narayanan and Masoud Agah

In spite of its introduction in 1979, the field of micro gas chromatography (μGC) continues to excite interest among researchers due to its application across diverse fields such as homeland security, food and environment monitoring, dissolved gas analysis, and space exploration [1-7]. Traditional gas chromatography involves the use of bulky, power-hungry equipment confined to laboratories which process samples brought from the field. A commercially available portable GC system employing a silicon micromachined injector and a micro-thermal conductivity detector (μTCD) can take a volume footprint of 28cm x 15cm x 30cm [8]. Yet, the system weighs 11 pounds and upwards depending on the configuration. Such systems employ traditional capillary tube columns whose temperature control setup (oven) and associated battery requirements can dominate the weight of the entire system. This makes it unwieldy for field use where the need is to obtain a quick analysis while consuming low power.

Extensive research into micro gas chromatography has been documented. In particular there is a tremendous focus on hybrid integration of silicon micromachined separation columns, detectors and pre-concentrators [9-14]. Silicon based separation columns are remarkable for their low power consumption to heat up; an important requirement in GC [15-17]. However, the performance of hybrid μGC systems is limited by the presence of cold spots. This refers to the relatively lower temperature in interconnecting capillary tubes since the separation column is heated by chip-scale contact heaters. Efforts to circumvent this issue include the use of a manifold to heat the capillary tubes, utilizing very short interconnecting capillary tubes or direct

chip-to-chip connects [18, 19]. While the former increases power consumption, the latter introduce a weak point in the mechanical reliability of the device.

Monolithic integration which involves fabricating various components on the same die, eliminating cold spots and reducing cost due to batch fabrication, has received limited attention [20, 21]. TCDs, in literature, are bulk-silicon etch released to increase sensitivity [22-27]. However, integrating them with a separation column can result in an under-etch from the release step causing a very wide channel. Such wide channels are suitable only for packed columns as presented in [28]. Wide channels decrease the efficiency of open tubular columns [29]. Further, packed columns require high inlet pressures (40-50psi), which is less desirable for portable applications. It should be noted that field tests require analysis of small sample quantities and less consumable gases, which is better served by open tubular columns. Thus, a technique to obtain high sensitivity of a TCD without losing out on other performance characteristics is necessary. Previously, we have reported a static coated open tubular separation column monolithically integrated with a thermal conductivity detector (TCD) in a unique 2-port 2-mask scheme (as shown in Figure 3-1) [30]. In addition, we presented the ability to thermostat the separation column at elevated temperatures while recovering the signal from the monolithically integrated TCD. This TCD was, however, anchored to the substrate and characterized by a poor sensitivity.

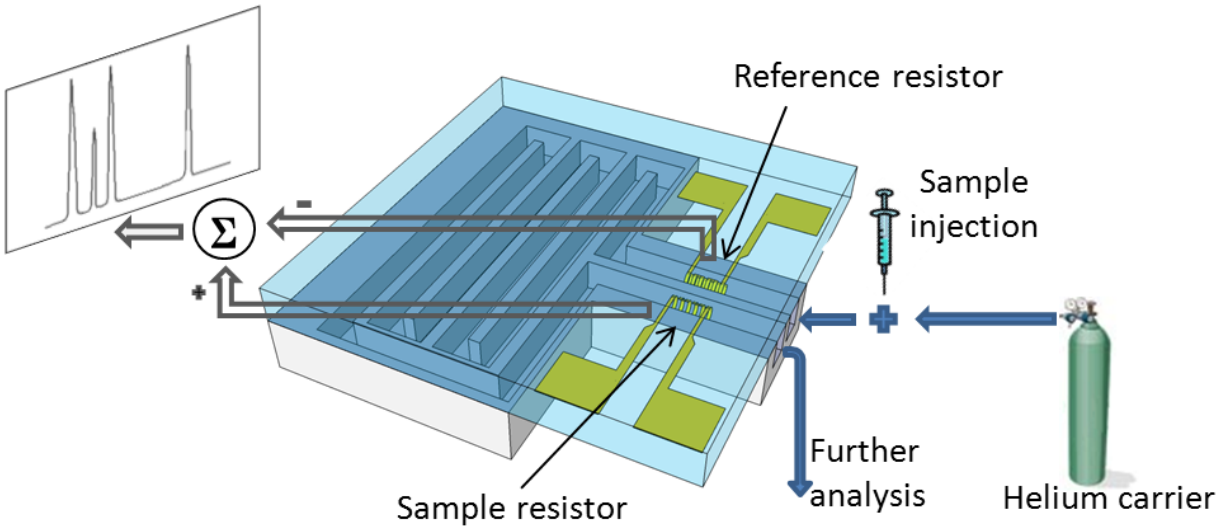

Figure 3-1: A conceptual realization of released resistors suspended inside microfluidic channels to serve as a TCD

In this chapter, we present an improved high performance thermal conductivity detector (TCD) monolithically integrated with a separation column for micro gas chromatography. Clearly distinct from prior literature, the released resistors for the detector are fabricated on glass using a dry release process, allowing the silicon to be independently fabricated and yet anodically bonded to the glass. The thermal isolation of the active element provides for reduced power

consumption, quicker time response and improved sensitivity without compromising on fabrication flexibility [31].

3.1 Theory

3.1.1 GC System

A gas chromatography system consists of three main components – preconcentrator, separation column, and gas detector. Typically cascaded in order, a carrier gas flowing through the system serves to transport the analytes from one component to the next. A preconcentrator connected to the inlet performs the task of adsorbing analytes of interest from a dilute sample over time, say 10 minutes [32, 33]. A sharp heat pulse applied to the preconcentrator force exits the analytes through the outlet in one narrow plug (less than 2 seconds), thereby concentrating the original sample above the detection limit of the detector. The narrow plug exits the preconcentrator to enter the separation column, which is the heart of the system.

A separation column consists of a fluidic channel coated or packed with a stationary phase. Different compounds interact with the stationary phase to a different extent and hence are retained differently. Thus, every analyte travels at different velocity and elutes out of the separation column at different instants of time. These separated plugs of elutants are detected by, one among many, gas detectors.

Microfabrication provides for the development of innovative structures such as semi-packed, multi-capillary separation columns, which extend the operating range of the system [34-40]. The smaller dimensions provide faster thermal response, reduced power consumption and consumable gases, and enable the analysis of smaller analyte quantity.

3.1.2 Thermal Conductivity Detector

We have chosen a thermal conductivity detector (TCD) from an array of gas detectors owing to its universality in detection, independence from make-up/auxiliary gases and robustness [41-47]. A TCD operates on the principle that a temperature of a resistive heater in a fluid is determined by the rate at which heat is dissipated from the heater through the fluid [48]. This heat transfer mode is conduction dominated at low fluid velocities and hence, a measure of thermal conductivity of the fluid. Helium with an order of magnitude higher thermal conductivity (0.142 W/(m.K)) compared to other analytes is the preferred carrier gas to operate a TCD. In the absence of an analyte, this high thermal conductivity results in a lower resistor temperature. However, in the presence of an eluted analyte from the separation column, the temperature increases. This temperature translates to a resistance, which is measured against a reference resistor not exposed to the analyte but only the carrier gas.

3.1.3 Thermal Modeling of TCD

The performance of TCD is well documented in the literature [48-51].The transient temperature profile of an object immersed in a fluid can be treated as a lumped circuit depending on Biot number (*Bi*). In the case of a thin film silicon dioxide resistor with internal heat generation suspended in a fluidic channel, the Biot number is defined as the ratio of the thermal conductance of the fluid to the thermal conductance of the resistor itself. When Bi<0.1, the temperature drop is primarily in the fluid and the resistor can be represented by a single time varying temperature that is spatially uniform across the resistor.

$$Bi = \frac{hL_{solid}}{k_{solid}} = \frac{324*1\times10^{-6}}{1.4} = 2.3 \times 10^{-4} \qquad \textbf{3-1}$$

Here, 'h' is the equivalent heat transfer co-efficient obtained by dividing the temperature difference into the surface heat flux from the heater, expressed in (W/(m^2.K)). The thermal time constant for a single lump is a product of the thermal resistance offered by the fluid-solid interface $\left({}^{1}/_{hA_{eff}}\right)$ and the heat capacity of the resistor(ρcV). Here, A_{eff}, ρ, c and V are the wetted surface area, density, heat capacity and volume, respectively, of the resistor.

3.2 Analysis by finite element simulation

3.2.1 Simulation setup

The effect of suspending the resistor on power consumption and time constant was studied by performing 3D Finite element simulation of heat transfer on representative models in COMSOL.

The anchored device model consists of a 2μm thick oxide film resting on a 700μm thick Borofloat (Schott, NY) substrate. A 500μm wide and deep channel etched in a 750μm thick silicon serves as the cavity to seat the heater in. This cavity is filled with nitrogen. The model, with the heater highlighted, is shown in Figure 3-2(a). The serpentine portion of the heater (highlighted in Figure 3-2) is the source of constant volumetric heat flux whereas the exterior surfaces of the device are held at 273K. The leads are in contact with silicon, ignoring the thin layer of epoxy in our packaged device. The released device model is similar to the anchored device. However, the serpentine portion of the heater, highlighted in Figure 3-2(b), is in contact with the Borofloat substrate only at the point of contact with the leads and otherwise suspended in the nitrogen filled cavity. The shape of the suspended portion is not coil shaped for ease of simulation.

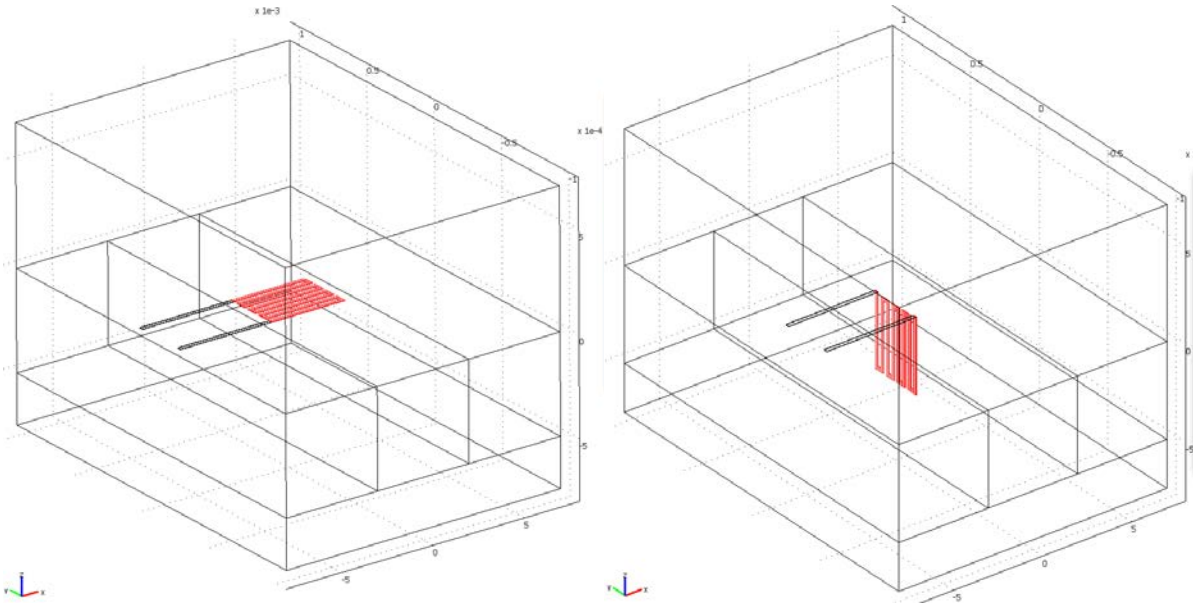

(a) (b)

Figure 3-2: Model of the (a) anchored and (b) released device with the heaters highlighted

There is no fluid flow in the channel, to parallel with the experimental results that will be presented in the next section. The 130nm thick metal film is ignored in both cases for ease of simulation and this is not expected to contribute significant error. An unstructured mesh with a conjugate gradient solver is used and in case of transient simulation, the initial temperature is 273K. The heat flux in the serpentine portion of the resistor is different in both cases to attain a temperature of 373K.

3.2.2 Power consumption

Figure 3-3(a) and (b) shows a slice of the temperature profile in transverse cross sectional surfaces of both the devices. The volumetric heat generation rate to attain a maximum temperature of ~373K was 8.5×10^{11} W/m^3 in the case of the anchored device. This translates to 102mW. The same quantities for the released device were 3.5×10^{10} W/m^3 and 4.5mW. This shows an order of magnitude reduction in power consumption which is advantageous for portable applications.

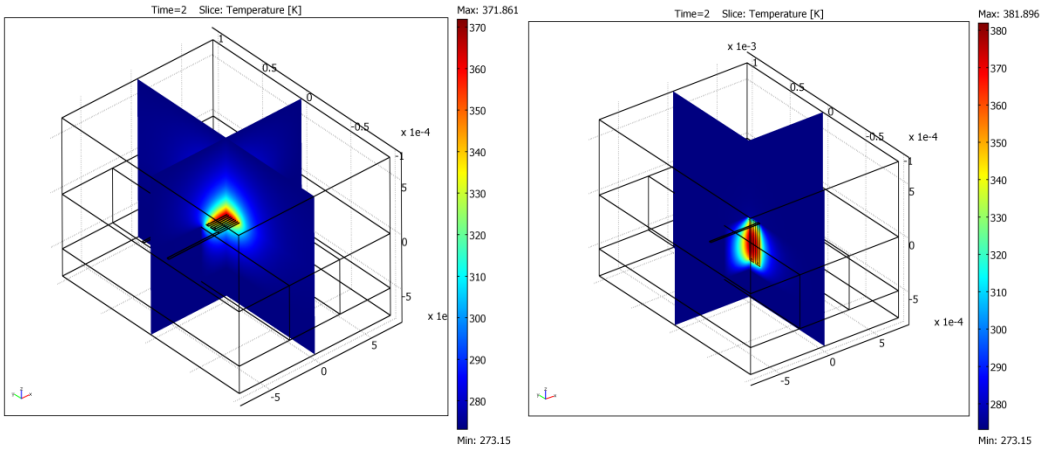

(a) (b)

Figure 3-3: Steady state temperature profiles along cross section of (a) non-suspended and (b) released devices

3.2.3 Warm-up time

A transient simulation of the device with the same heat source, provided details on the warm-up time defined as the time to heat up to 63% of its steady state temperature i.e. 336K. The preceding temperature profile shows that most of the drop in temperature is in the glass substrate, for the anchored device. The temperature profile does not penetrate to the depth of the channel. However, the suspended resistor forces the drop in the fluid within the cavity, in the case of the released device. A 2 second long transient simulation was performed for the anchored and released devices respectively. The rise in temperature at the center of the heater is plotted for both cases in Figure 3-4. The time taken for 90% rise in temperature is 150ms and 10ms respectively. An order of magnitude lower thermal time constant in the case of released devices contributes to increased sensitivity and faster system boot-up time.

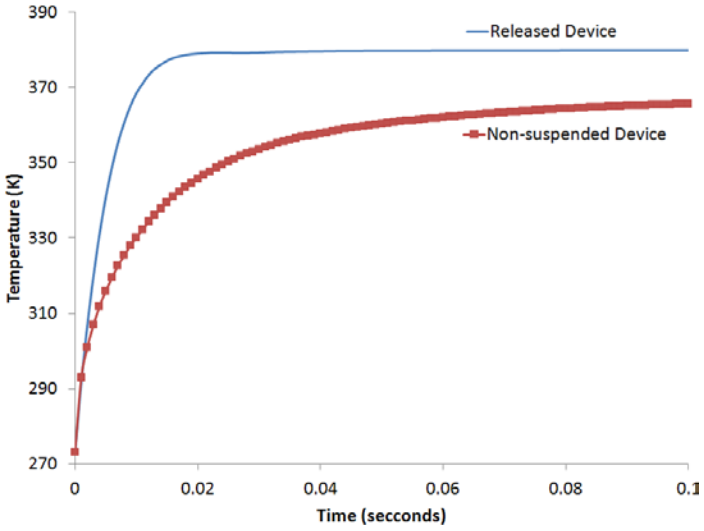

Figure 3-4: A plot of simulated temperature of the heater versus time for non-suspended and released device

A straightforward hand calculation for the suspended device approximated as a single lump can be calculated as follows.

$$\tau = \frac{\rho c V}{h A_{eff}} = \frac{2200*730*(2\mu m*A)}{324*(2A)} = 4.9ms \qquad \textbf{3-2}$$

Where '*A*' is the surface area of the resistor and the wetted surface area is twice the surface area of the resistor. The resistors are 2μm thick. *'h'*, the heat transfer co-efficient at the resistor-fluid interface, can be averaged as the ratio of the applied heat flux density at the surface of the resistor and the resultant temperature difference between the resistor and channel sidewall (ambient).

$$h = \frac{Q}{T_{diff}} = \frac{3.5*10^{10}*{}^{V}/_{A}}{108K} = 324 \qquad \textbf{3-3}$$

3.3 Fabrication

The device consists of a silicon substrate hosting the separation microfluidic channel and a Borofloat wafer hosting the TCD which are separately processed and finally bonded together. The process flow is summarized in Figure 3-5.

A 700μm thick Borofloat wafer is blanket deposited with a 650nm thick sacrificial PECVD oxide. AZ5214 was spun coated and patterned in image reversal mode to define the anchor. A 200nm thick sacrificial silicon was e-beam evaporated and lifted off on the patterned AZ5214. Another 1.5μm thick "structural" PECVD oxide was then blanket deposited. Following this, a 60nm/70nm thick Cr/Ni metal stack was evaporated and lifted off using the mask of the resistor. A 1.2μm thick AZ5214, patterned in image reversal mode, on the metallic resistor served as the mask for further processing. The wafer was diced prior to the releasing step. The releasing step consisted of an initial 5 minute wet etch of the structural oxide in Buffered Oxide Etch (BOE), revealing the sacrificial silicon. The device was then mounted on a handle wafer and the sacrificial silicon etched away using the SSLDE process [52]. This was performed in an Alcatel AMS100 i-Speeder DRIE, with 0.1mbar chamber pressure, 1500W coil power, no substrate bias at 20°C, platen height of 200mm, and a SF_6 flow rate of 300sccm. The chemistry of SF_6 enables high lateral etch-rates of up to 15μm/min. In the absence of the sacrificial PECVD oxide, the Borofloat surface is exposed to the aggressive SF6 plasma, while the resistors are being under etched and thus, rendered unsuitable for anodic bonding. Upon release, the device is raised to 400°C on a hot plate in atmosphere. This step anneals the thin metal film and causes further curling, giving the active element of the resistors a coil shape as shown in Figure 3-6. The coil has a cross sectional diameter of 168μm giving it sufficient coverage over the entire fluidic channel cross-section which is 400μm wide and 250μm deep. The interconnects and bond pads are anchored to the substrate. The photoresist was then ashed in an oxygen plasma.

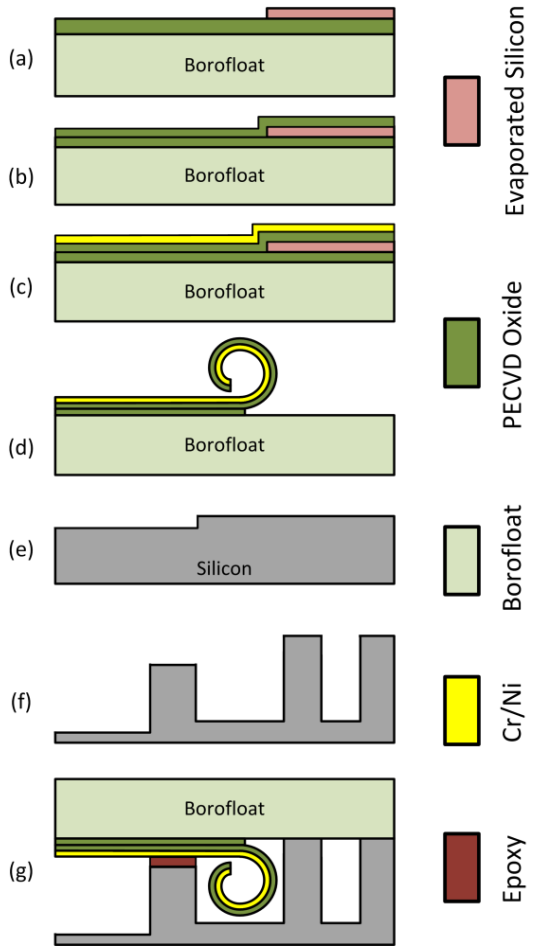

Figure 3-5: (a) through (d) show the fabrication of released coiled metal resistors by sacrificial etch of silicon. (e) and (f) show the two-step anisotropic etch in silicon for the feedthroughs and microfluidic channel, respectively. (g) shows the bonded structure followed by sealing of the shallow etch for feedthroughs with epoxy. The photoresist used as a mask to protect the metal while under-etching has been avoided in the diagram, for simplicity.

The separation column was fabricated on a 500μm thick single-side polished silicon wafer. First, the wafer was spin coated with S1813. The photoresist was then patterned and etched to a shallow depth of 2-3μm. This shallow etch prevents contact between the metal interconnects on the Borofloat wafer and the walls of the separation column in silicon, upon bonding. The photoresist was stripped and the wafer spun coated with AZ9260. The 8μm-thick photoresist was patterned with a mask for subsequent deep etching of the channels. Alcatel DRIE was employed in an anisotropic process, resulting in 250μm-deep channels for the separation column (Figure 3-6). Finally, the photoresist was stripped off, and the silicon wafer also diced into individual devices.

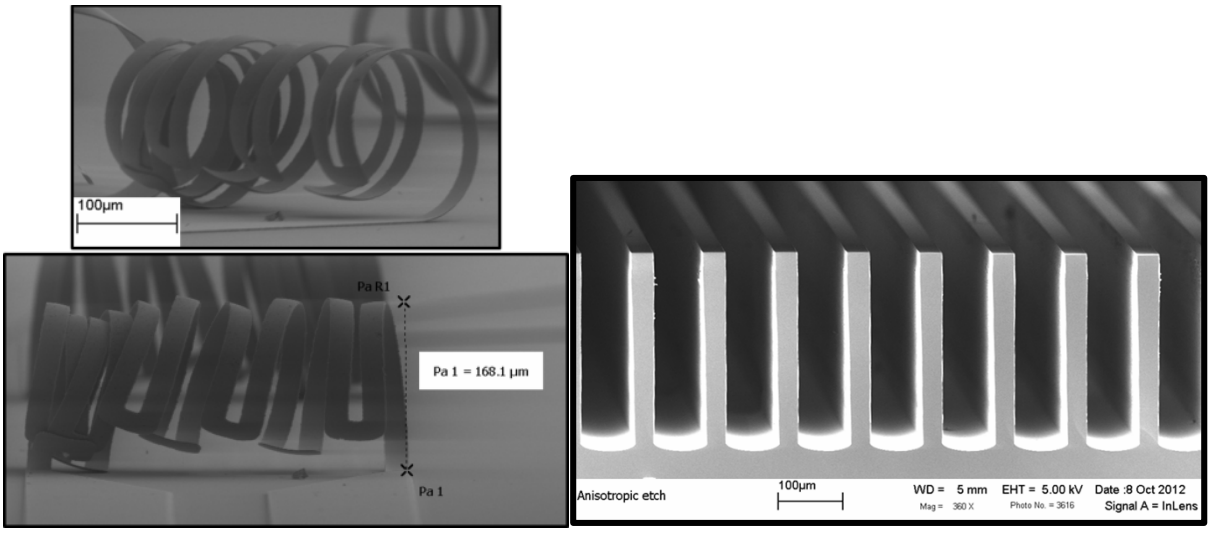

(a) (b)

Figure 3-6: SEM images of (a) released coil with side view (on top) and the front view (bottom) and (b) anisotropic etch of the microfluidic channels for separation column

The diced detector on Borofloat and the diced separation column on silicon were aligned and brought into contact using a pick and place bonder followed by anodic bonding. The inset in Figure 3-7 shows the alignment of the resistors in the fluidic channel, while seeing through the Borofloat wafer. The coiled structures are mostly out-of-focus due the out-of-plane bending. They align into the fluidic channel etched in silicon, which acts as a recess.

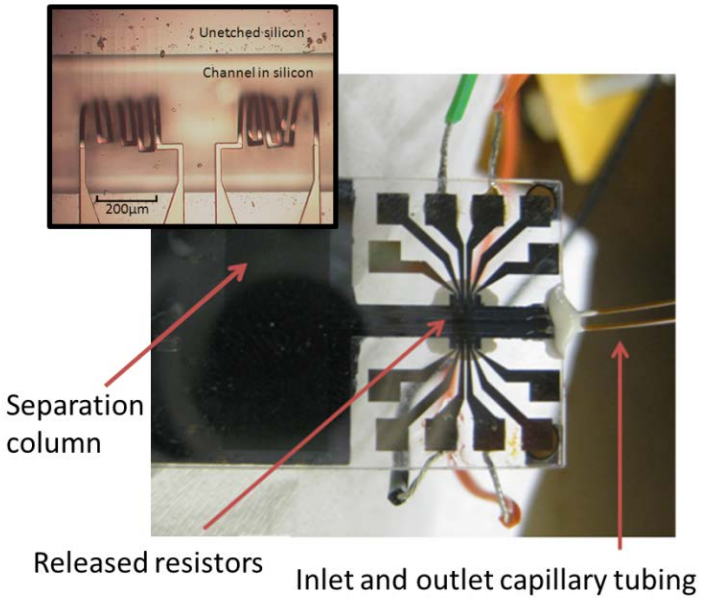

Figure 3-7: Optical image of the packaged device with a close-up of the released resistors in the channel (inset)

Capillary tubes were fixed to the inlet and outlet ports of the device. The device was then static coated with polydimethylsiloxane [53]. This was achieved by filling the channel with a solution of polydimethylsiloxane (OV1) in pentane at 40psi followed by drawing vacuum at one end with the other end sealed with wax. Vaporization of pentane leaves behind a thin film of polydimethylsiloxane, which serves as the stationary phase. It should be noted that the flow of the viscous solution through the resistors did not cause the released structures to detach, at the point of anchor. This is a current point of investigation to understand the limit of fluidic flow, which will cause the resistors to detach. An optical image of the packaged device is shown in Figure 3-7.

3.4 Experimental results

3.4.1 TCD operation

A 1m-long, 100µm-wide separation column was fabricated with the released resistors and packaged as shown in Figure 3-7. A current of 10mA was sourced into a Wheatstone bridge with the two resistors in each of its arms. The differential voltage was fed into an Agilent 34401A and recorded through LabVIEW. The inlet of the device was connected to the inlet of a HP5890 while the outlet was connected to the FID in the HP5890, for verification purposes. The injector inlet of the HP5890 was maintained at 11psi of helium@280°C while the oven itself was held at 65°C. The device was tested by injecting a 0.2µl sample from a mixture of 20µl each of n-nonane, n-decane, n-undecane and n-dodecane diluted in 200µl of n-octane. The response from the TCD is shown in Figure 3-8. The suspended nature of the resistors resulted in a reduction in power by a factor of four. Additionally, our non-suspended TCD could barely detect 5000ppm of pentane in octane while we could readily achieve 500ppm sensitivity with our new released resistors.

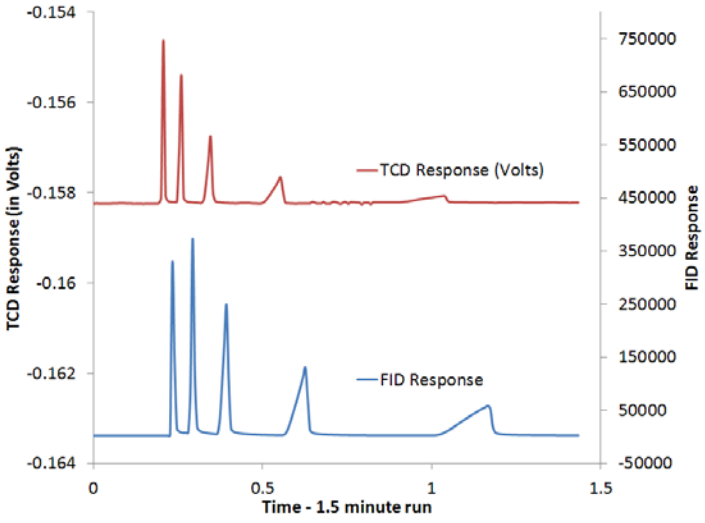

Figure 3-8: Comparison of the TCD and FID response to a mixture of n-hexane, n-octane, n-nonane, n-decane and n-undecane

3.4.2 Power consumption and warm-up time

The anchored and released devices were placed in an HP5890 and the resistor *vs* temperature profile characterized. Power was then applied to the resistors with the oven at 35°C to obtain a resistance *vs* power graph. This was then translated into a heater temperature *vs* power applied graph, shown in Figure 3-9. The measurements also indicate an order of magnitude difference in the power consumption to maintain the resistors at 100°C.

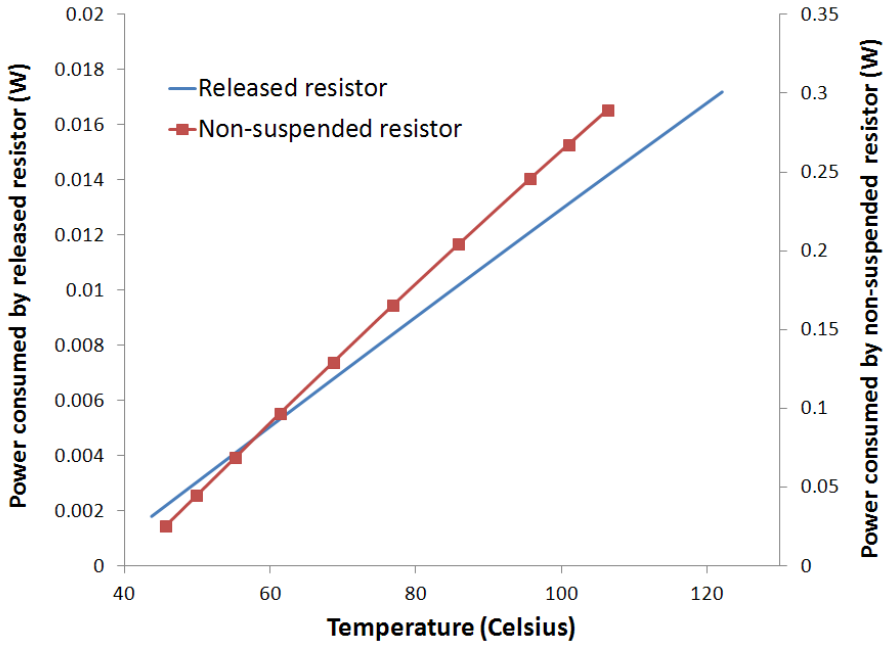

Figure 3-9: Measured power consumption values of the released and non-suspended resistor as a function of resistor temperature

The warm-up time, defined as the time constant corresponding to a 63% rise in temperature of the resistor was measured by recording the current when the source was turned ON. Dividing the current into the applied voltage gives the resistance of the heater, which is translated to its temperature. It should be noted that the voltage source output has a rise time during which, the calculated resistance (by dividing the measured current into the steady state applied voltage value) is invalid. This indeterminate time is 6ms long and the minimum measurement limitation in our setup. The indeterminate data points at 45°C correspond to this rise time of the output of the voltage source. For both cases, the voltage was selected to provide a final temperature of 100°C. Figure 3-10 shows the rise in temperature for the released and non-suspended resistors.

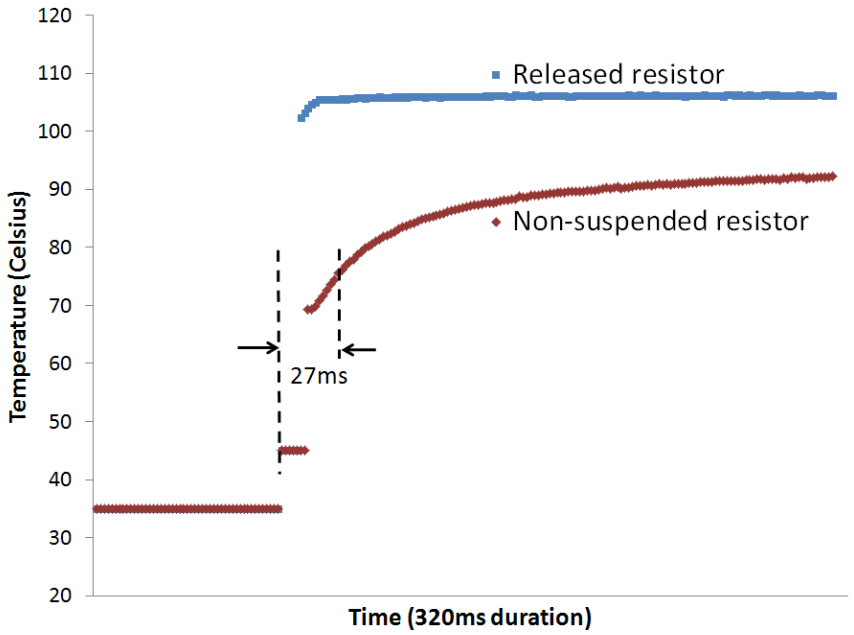

Figure 3-10: Transient temperature plot of released and non-suspended resistor at the instant when voltage is turned ON

It should be noted that the reduction in power consumed and the improvement in warm-up time, achieved by the released device, is on the lines of the predictions made in Section III. The simulated values do not match the experimental measurements since it does not include distributed Joules heating of the resistor, to keep the analysis computationally simple [54].

3.5 Inference

This chapter presented an unique technique to fabricate resistor coils, as tall as 170µm, on glass and employed it in a TCD. There are multiple advantages to this technique. First, it offered high thermal isolation similar to bulk-etched metal films. Second, despite minimal anchoring, they were robust to liquid flow. Third, the processing on glass did not render it unfit for anodic bonding and hence, the silicon can be processed with independently and with flexibility. The resistors were characterized by an order of magnitude reduced power consumption (13mW) and warm-up time (sub-6ms) when compared with non-suspended resistors. In the future, the simulations will be custom solved to include potential equation and accurately resemble the model and its heat flux pathways. The simulations can help in the study of the effect of the anchors. This integration technique will pave the way for greater flexibility in separation column design, such as utilizing nanoparticle stationary phases, and multicapillary and semipacked columns to realize high performance monolithically integrated µGC devices.

REFERENCES

[1] F. Bruner, *Gas chromatographic environmental analysis: principles, techniques, instrumentation*: Wiley-VCH, 1993.

[2] R. W. Cernosek, *et al.*, "Micro-analytical systems for national security applications," in *Proc. SPIE-Micro (MEMS) and Nanotechnologies for Space Applications*, Orlando (Kissimmee), FL, USA 2006, p. 622306.

[3] W. W. Christie, *Gas chromatography and lipids* vol. 39: Oily Press Ayr, 1989.

[4] G. Monti, *et al.*, "Monitoring Food Quality by Microfluidic Electrophoresis, Gas Chromatography, and Mass Spectrometry Techniques: Effects of Aquaculture on the Sea Bass (Dicentrarchus labrax)," *Anal. Chem.*, vol. 77, no. 8, pp. 2587-2594, 2005.

[5] D. Nielsen, *Practical handbook of environmental site characterization and ground-water monitoring*: CRC press, 2006.

[6] S. C. Terry, *et al.*, "A gas chromatographic air analyzer fabricated on a silicon wafer," *Electron Devices, IEEE Transactions on*, vol. 26, no. 12, pp. 1880-1886, 1979.

[7] K. Word, "GC/TCD Analysis of A Natural Gas Sample on A Single HP-PLOT Q Column."

[8] "490 Micro GC Solution Datasheet," A. Technologies, Ed., SI-02239 ed, 2012.

[9] A. De Mello, "On-chip chromatography: the last twenty years," *Lab on a Chip*, vol. 2, no. 3, p. 48N, 2002.

[10] J. A. Dziuban, *et al.*, "Portable gas chromatograph with integrated components," *Sensors and Actuators A: Physical*, vol. 115, no. 2–3, pp. 318-330, 2004.

[11] K. Hanseup, *et al.*, "A Micropump-Driven High-Speed MEMS Gas Chromatography System," in *Solid-State Sensors, Actuators and Microsystems Conference, 2007. TRANSDUCERS 2007. International*, 2007, pp. 1505-1508.

[12] P. R. Lewis, *et al.*, "Recent advancements in the gas-phase MicroChemLab," *Sensors Journal, IEEE*, vol. 6, no. 3, pp. 784-795, 2006.

[13] C.-J. Lu, *et al.*, "First-generation hybrid MEMS gas chromatograph," *Lab on a Chip*, vol. 5, no. 10, pp. 1123-1131, 2005.

[14] J. J. Whiting, *et al.*, "High-speed two-dimensional gas chromatography using microfabricated GC columns combined with nanoelectromechanical mass sensors," in *TRANSDUCERS*, 2009, pp. 1666-1669.

[15] M. Agah, *et al.*, "High-Speed MEMS-Based Gas Chromatography," *J. Microelectromech. Syst.*, vol. 15, no. 5, pp. 1371-1378, 2006.

[16] M. Agah, *et al.*, "Thermal behavior of high-performance temperature programmed microfabricated gas chromatography columns," in *Proc. Int. Solid-State Sens., Actuators Microsyst. Conf., Transducers*, 2003, pp. 1339-1342 vol.2.

[17] J. A. Potkay, *et al.*, "A Low-Power Pressure- and Temperature-Programmable Micro Gas Chromatography Column," *J. Microelectromech. Syst.*, vol. 16, no. 5, pp. 1071-1079, 2007.

[18] K. T. M. Beach, *et al.*, "A low-mass high-speed GC separation column with built-in fluidic chip-to-chip interconnects," in *Micro Electro Mechanical Systems (MEMS), 2011 IEEE 24th International Conference on*, 2011, pp. 813-816.

[19] R. P. Manginell, *et al.*, "Mass-Sensitive Microfabricated Chemical Preconcentrator," *J. Microelectromech. Syst.*, vol. 17, no. 6, pp. 1396-1407, 2008.

[20] B. Kaanta, *et al.*, "Monolithic Micro Gas Chromatographic Separation Column and Detector," in *23rd IEEE International Conference on Micro Electro Mechanical Systems (MEMS '10)*, HongKong, China, 2010, pp. 907-910.

[21] R. Manginell, *et al.*, "A Monolithically-Integrated μGC Chemical Sensor System," *Sensors*, vol. 11, no. 7, pp. 6517-6532, 2011.

[22] D. Cruz, *et al.*, "Microfabricated thermal conductivity detector for the micro-ChemLab™," *Sens. Actuators B Chem*, vol. 121, no. 2, pp. 414-422, 2007.

[23] B. Kaanta, *et al.*, "High sensitivity micro-thermal conductivity detector for gas chromatography," in *22nd IEEE International Conference on Micro Electro Mechanical Systems (MEMS '09)*, Sorrento, Italy, 2009, pp. 264-267.

[24] M. Kimura, *et al.*, "Application of the air-bridge microheater to gas detection," *Sens. Actuators B Chem*, vol. 25, no. 1-3, pp. 857-860, 1995.

[25] U. Lehmann, "Micro machined gas chromatograph based on a plasma polymerised stationary phase," ed: Kluwer Academic Pub, 2000, p. 167.

[26] J. Lysko, *et al.*, "Silicon thermal conductivity detector (TCD) with the Pt resistors," in *Proc. SPIE 5124, Optoelectronic and Electronic Sensors*, 2003, p. 258.

[27] S. Sorge, *et al.*, "Fully integrated thermal conductivity sensor for gas chromatography without dead volume," *Sens. Actuators A Phy*, vol. 63, no. 3, pp. 191-195, 1997.

[28] B. Kaanta, *et al.*, "A monolithically fabricated gas chromatography separation column with an integrated high sensitivity thermal conductivity detector," *J. Micromech. Microeng*, vol. 20, no. 5, p. 055016, 2010.

[29] G. E. Spangler, "Relationships for modeling the performance of rectangular gas chromatographic columns," *Journal of Microcolumn Separations*, vol. 13, no. 7, pp. 285-292, 2001.

[30] S. Narayanan, *et al.*, "Two-Port Static Coated Micro Gas Chromatography Column With an Embedded Thermal Conductivity Detector," *Sensors Journal, IEEE*, vol. 12, no. 6, pp. 1893-1900, 2012.

[31] M. Gajda, *et al.*, "Applications of thermal silicon sensors on membranes," *Sens. Actuators A Phy*, vol. 49, no. 1-2, pp. 1-9, 1995.

[32] B. Alfeeli, *et al.*, "MEMS-Based Selective Preconcentration of Trace Level Breath Analytes," *IEEE Sensors J.*, vol. 9, no. 9, 2009.

[33] B. Byunghoon, *et al.*, "A Fully-Integrated MEMS Preconcentrator for Rapid Gas Sampling," in *Solid-State Sensors, Actuators and Microsystems Conference, 2007. TRANSDUCERS 2007. International*, 2007, pp. 1497-1500.

[34] M. Agah, *et al.*, "Low-Mass PECVD Oxynitride Gas Chromatographic Columns," *J. Microelectromech. Syst.*, vol. 16, no. 4, pp. 853-860, 2007.
[35] S. Ali, *et al.*, "MEMS-based semi-packed gas chromatography columns," *Sens. Actuators B Chem*, vol. 141, no. 1, pp. 309-315, 2009.
[36] A. Bhushan, *et al.*, "Fabrication and Preliminary Results for LiGA Fabricated Nickel Micro Gas Chromatograph Columns," *J. Microelectromech. Syst.*, vol. 16, no. 2, pp. 383-393, 2007.
[37] G. Lambertus, *et al.*, "Design, Fabrication, and Evaluation of Microfabricated Columns for Gas Chromatography," *Anal. Chem.*, vol. 76, no. 9, pp. 2629-2637, May 2004.
[38] J. A. Potkay, *et al.*, "A high-performance microfabricated gas chromatography column," in *Micro Electro Mechanical Systems, 2003. MEMS-03 Kyoto. IEEE The Sixteenth Annual International Conference on*, 2003, pp. 395-398.
[39] A. Radadia, *et al.*, "New Column Designs for MicroGC," 2007, pp. 2011-2014.
[40] H. Shakeel, *et al.*, "First reconfigurable MEMS separation columns for micro gas chromatography," in *Micro Electro Mechanical Systems (MEMS), 2012 IEEE 25th International Conference on*, 2012, pp. 823-826.
[41] S. Bedair, *et al.*, "CMOS MEMS oscillator for gas chemical detection," in *Proceedings of IEEE Sensors*, 2004, pp. 955-958.
[42] A. Gutierrez, "New Thermal Conductivity Microsensor to measure the methane number of natural gas," in *23rd World Gas Conference*, Amsterdam, 2006.
[43] W. J. Kuipers, *et al.*, "A planar micro-flame ionization detector with an integrated guard electrode," *J. Micromech. Microeng*, vol. 18, no. 6, p. 064015, 2008.
[44] S. J. Martin, *et al.*, "Gas sensing with acoustic devices," in *Ultrasonics Symposium, 1996. Proceedings., 1996 IEEE*, 1996, pp. 423-434 vol.1.
[45] M. Moorman, *et al.*, "Microcombustor array and micro-flame ionization detector for hydrocarbon detection," in *Proc. SPIE—MEMS Components and Applications for Industry, Automobiles, Aerospace, and Communication II*,, San Jose, CA, USA, 2003, pp. 40-50.
[46] Y. Sun, *et al.*, "Rapid tandem-column micro-gas chromatography based on optofluidic ring resonators with multi-point on-column detection," *The Analyst*, vol. 135, no. 1, pp. 165-171, 2010.
[47] Q. Zhong, *et al.*, "Characterization of a high-performance portable GC with a chemiresistor array detector," *The Analyst*, vol. 134, no. 2, pp. 283-293, 2009.
[48] K. Chen, *et al.*, "Thermal analysis and simulation of the microchannel flow in miniature thermal conductivity detectors," *Sens. Actuators A Phy*, vol. 79, no. 3, pp. 211-218, Feb. 2000.
[49] Y. Huang, *et al.*, "The effects of forced convection on the power dissipation of constant-temperature thermal conductivity sensors," *Journal of heat transfer*, vol. 119, p. 30, 1997.
[50] R. Pecsar, *et al.*, "Performance of a reduced volume thermal conductivity detector," *Anal. Chem.*, vol. 45, no. 13, pp. 2191-2198, 1973.
[51] Y. Wu, *et al.*, "Fabrication and characterization of thermal conductivity detectors (TCDs) of different flow channel and heater designs," *Sens. Actuators A Phy*, vol. 100, no. 1, pp. 37-45, 2002.
[52] S. Frederico, *et al.*, "Silicon sacrificial layer dry etching (SSLDE) for free-standing RF MEMS architectures," in *Micro Electro Mechanical Systems, 2003. MEMS-03 Kyoto. IEEE The Sixteenth Annual International Conference on*, 2003, pp. 570-573.
[53] S. Reidy, *et al.*, "High-Performance, Static-Coated Silicon Microfabricated Columns for Gas Chromatography," *Anal. Chem.*, vol. 78, no. 8, pp. 2623-2630, 2006.
[54] F. Rastrello, *et al.*, "Measurements, FEM simulation and spice modeling of a Thermal Conductivity Detector," in *Instrumentation and Measurement Technology Conference (I2MTC), 2011 IEEE*, 2011, pp. 1-5.

4

Hybrid Integration of a Preconcentrator with an Integrated Column

Muhammad Akbar, Shree Narayanan, and Masoud Agah

Volatile organic compounds (VOCs) are emitted by a wide variety of products including solid and liquids [1]. Prolonged exposure to VOCs can cause serious health effects including liver, kidney, and nervous system diseases and can even cause cancer [2-7]. Similar effects have been reported for various aquatic organisms [8-10]. Different analytical techniques for their detection have been reported in the literature [11-13]. Microscale gas chromatography (μGC) provides a reliable solution for onsite analysis of complex VOCs with reduced size and low power consumption [14, 15]. μGC systems usually consist of an injector/preconcentrator, a separation column and a detector all developed using micro electromechanical systems (MEMS) technology [13, 16-21]. μTPC (thermal preconcentrator) is one of the important components which allow the trace level detection of VOCs by accumulating them over a period of time. The trapped VOCs are then released in the form of a concentrated plug through thermal desorption process. The separation column is coated with a stationary phase to separate the VOCs into individual components for final detection by the detector. Several reports have been published for applications of μGC system related to homeland security, biomedical diagnostic and real-time environmental analysis [22-24].

On the other hand, the detection of VOCs in an aqueous matrix has not received adequate attention among the μGC community due to incompatibility of the system with an aqueous matrix [25]. Water is found to saturate the adsorbent in μTPC by capturing available adsorption sites and also damages most common polymer based stationary phases, resulting in changes in retention time, selectivity and column bleeding. Extinguishing the most widely used flame ionization detector (FID) and a decrease in the sensitivity of electron capture detectors (ECD) has also been reported [26, 27]. The United States Environmental Protection Agency

(EPA) has specified a list of water organic compounds (WOCs) with their maximum contamination level (MCL). Above a specific concentration usually in ppb their presence in aqueous medium poses a serious threat to human and aquatic life as shown in Table 1.

Contaminants	Potential health effect	Contamination sources	Amount recovered (ng)	Recovery	Log (K_{ow})
Toluene	Nervous system, liver problems	Petroleum factories	5.7	23%	2.75
PCE	Liver problems, increased risk of cancer	Discharge from factories and dry cleaners	5.4	18%	2.57
Chlorobenzene	Liver and kidney problems	Discharge from chemical and agricultural chemical factories	9	25%	2.86
Ethylbenzene	Liver and kidney problems	Petroleum refineries	18.7	38%	3.14

Table 4-1: List of water organic compounds with their originating sources and potential health risks

Current methods for the identification of WOCs rely on removing them from an aqueous sample prior to analysis using bench-top GC systems. These methods include solid-phase micro-extraction (SPME), purge and trap, and hollow fiber membranes. They cannot be used for on-site monitoring of aqueous sample and rely on transporting the sample to the laboratory. Currently, commercially available FROG-4000TM from Defiant Technologies and Water Analysis Surety Prototype (WASP) from Sandia National Laboratories are capable of performing field analysis of water contamination. Nevertheless, the system is large, expensive, requires a trained technician and relies on conventional purge and trap mechanism. Thus, there still remains a demand for the development of a light weight, less power hungry, inexpensive independent systems capable of extracting and detecting WOCs from aqueous media.

Previously, our group has followed the direct injection method for monitoring water contamination. This approach requires additional time for removing the trapped water contents from the μTPC adsorbent (dry purge time) [28]. This chapter describes fluidic integration of μGC components with our newly developed μPE chip for analyzing WOCs. The results indicate that this hybrid integrated system successfully extracted and separated four WOCs at 500 ppb concentration. This is the first realization of an easily deployable microsystem for on-site water monitoring.

4.1 Method description

Figure 4-1 shows a block diagram explaining the proposed μGC experimental setup including the μPE (micro-purge extractor) for extraction of WOCs from the aqueous sample. The μPE device contains two inlets, one for aqueous sample to be analyzed and one for a pure inert gas to purge the WOCs. The distribution network for aqueous sample entrance provided at the top of the chip is used to uniformly spread the sample inside the chip. Similarly, the multiple inlets for purging gas are intended to enhance the interaction between two phases (air and water) inside the chip and to facilitate the removal of WOCs from the streaming water. The chip also contains two outlets; one is used as water waste and one for directing the purged WOCs to the trap (μTPC). The outlet for directing WOCs to the μTPC is provided at the top corner of the chip to prevent water from entering into the μTPC chip. The setup is operated in two phases namely; 1) extraction phase and 2) analysis phase. During the extraction phase, two microfabricated chips (μPE and μTPC) are connected in a tandem configuration using a valve. With the vial connected to sample inlet, aqueous solution is introduced into the μPE chip using purified nitrogen. High purity nitrogen gas is supplied through the air inlet of the μPE chip trapping WOCs on the adsorbent surface in the μTPC chip. The analyzed mass is calculated from the sample concentration and the volume of water collected during the purged time. During the analysis phase, the μPE is taken offline and μTPC connected in series with the μGC column with embedded μTCD detector using a six port switching valve. Helium, used as a carrier gas, is supplied through GC inlet while the outlet of the column is connected to the FID of a commercial GC system for verification purposes. The sensor on the backside of the μTPC is used to monitor the temperature profile of the chip when heated. A voltage applied to the heater on the backside of the μTPC heats it up from room temperature to 150 °C. The desorbed WOCs are separated by the μGC column. A 40 mA current is sourced into a Wheatstone bridge with two resistors of μTCD in each of its arm. The differential voltage measured across the two resistors enables the detection of WOCs which is fed into a Keithley 2700 and recorded on a LabVIEW program.

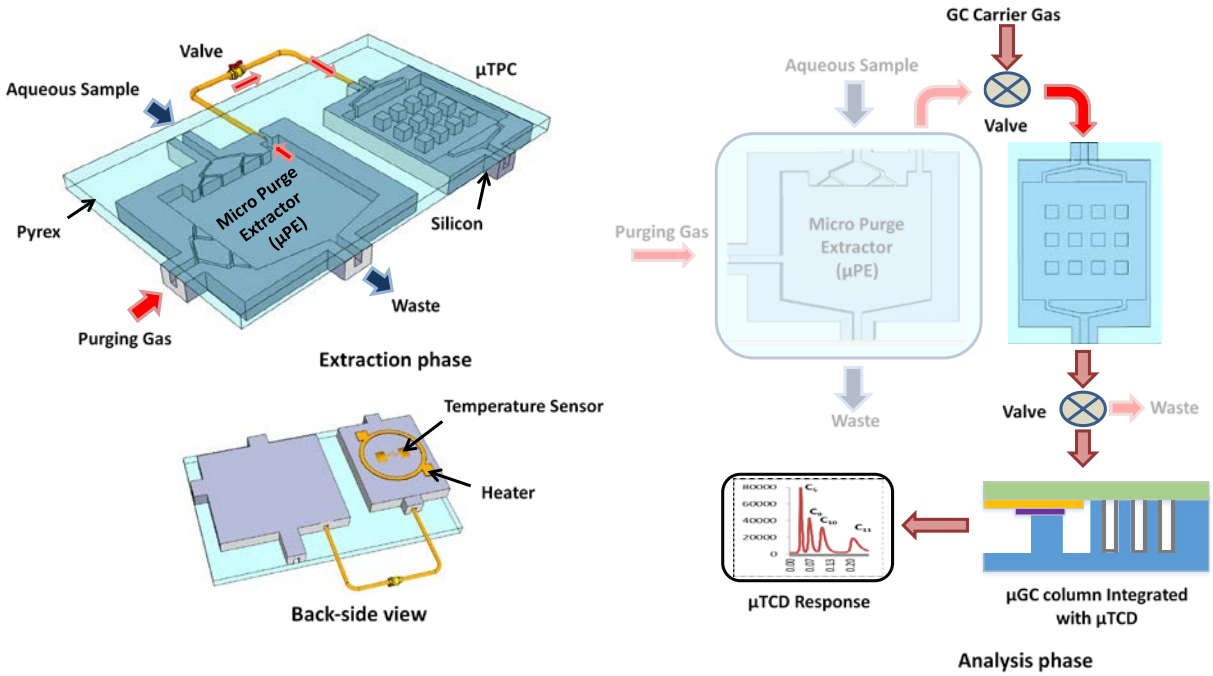

Figure 4-1: Conceptual diagram showing the topology for the extraction and analysis.

4.2 Materials and instruments

Reagent grade WOCs listed in Table 1, solvents, and Tenax TA (80/100 mesh) used in this work were purchased from Sigma-Aldrich (St. Louis, MO) in >99% purity. Silicon wafers (4 in. dia., 500 µm thick, n-type, single side polished) and Borofloat wafers (4 in. dia., 700 µm thick, double side polished) were purchased from University Wafers and Coresix Precision Glass (Williamsburg, VA), respectively. Fused capillary tubes (200 µm outer dia., 100 µm inner dia.,) were purchased from Polymicro Technologies (Phoenix, AZ). All adsorption/desorption tests were performed on Agilent HP7890 GC system, Agilent Technologies Inc. (Palo Alto, CA).

4.3 Fabrication process

Figure 4-2 summarizes the fabrication process for all the three MEMS components. We have previously reported the fabrication, characterization, and operation of the µTPC and the column integrated with µTCD [12, 16-21]. Herein, we briefly discuss the fabrication of these two components in addition to the fabrication of our newly developed microfabricated purge extractor.

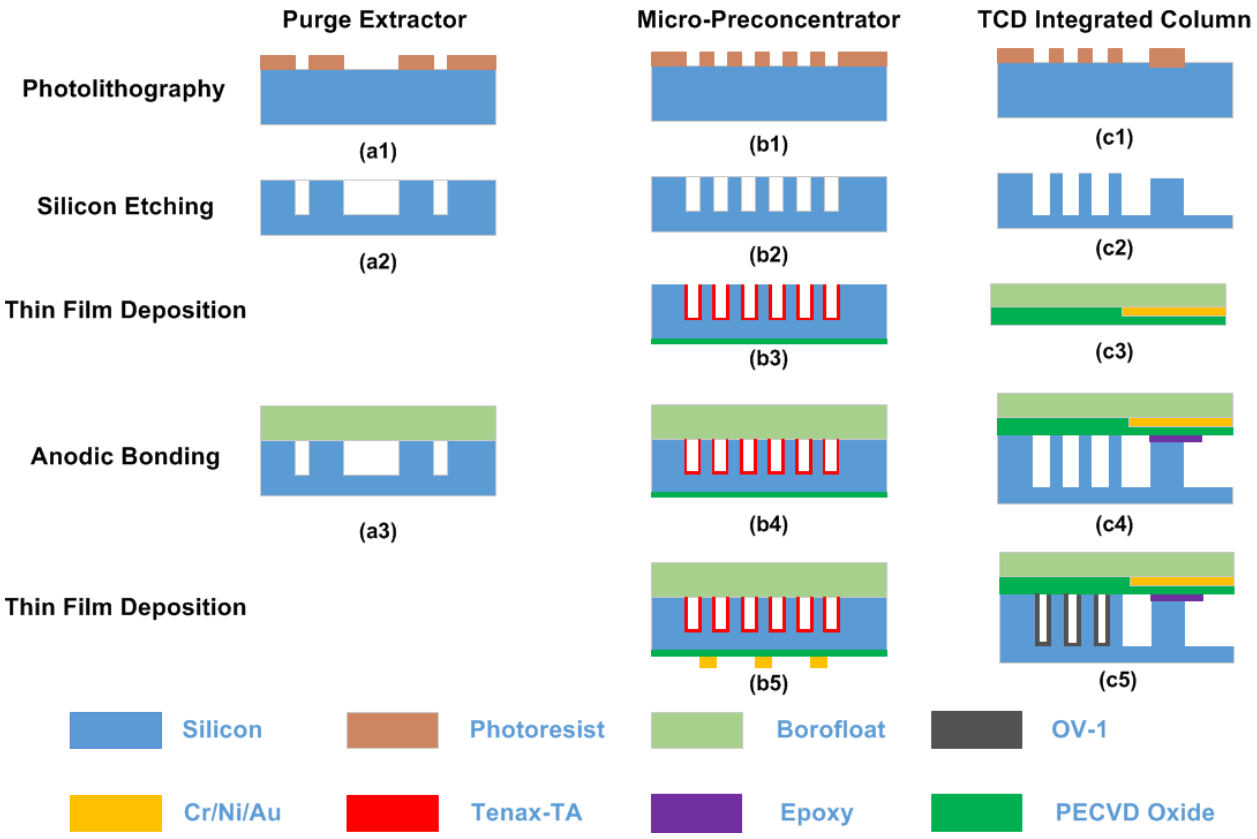

Figure 4-2: Fabrication procedure for µPE, µTPC and µGC column with µTCD detector. The left column shows MEMS processes performed for fabricating these chips.

4.3.1 µTPC and µPE chip

The fabrication of µTPC was performed on a standard 4" wafer using MEMS processing technology. First, photolithography was performed to pattern micro-posts/fluidic ports. The wafer was then subjected to deep reactive ion etching (DRIE, Alcatel) to achieve a depth of ~250 µm. After stripping the photoresist off the front-side, a 500nm thick oxide layer was deposited on the backside and the wafer diced into individual chips. The chip was then filled with Tenax TA solution (10 mg/ml in dichloromethane) and allowed to evaporate to deposit a thin film (~200 nm) of the polymer adsorbent on the cavity surfaces. It is worth mentioning that Tenax TA is categorized as a hydrophobic adsorbent having low affinity for water and is suitable for the extraction of WOCs from water samples. The chip was then capped with a borofloat wafer by anodic bonding. Following bonding, the chips were loaded onto the platen of an e-beam evaporator (PVD-250, Kurt Lesker) with the backside facing the crucible. The chips were masked by a stainless steel shadow mask patterned with the features defining the heater and sensor. Following this, 40nm/100nm/25nm of Cr/Ni/Au was deposited to get nominal resistances of 15 ohm and 250 ohm for the heater and sensor, respectively. Finally, the devices were unloaded; the shadow masks removed off and fused capillary tubes epoxied into the inlet/outlet ports. The

fabrication process of the μPE chip followed that of our μTPC but without the adsorbent coating and backside oxide/metal deposition.

4.3.2 μGC column with embedded TCD

A two-step anisotropic etching of silicon was performed for hosting the feedthroughs and microfluidic channel by spin coating the wafer with S1813. A shallow depth of 2–3 μm was achieved which prevented a contact between the metal interconnects on the Borofloat wafer and the walls of the separation column in silicon upon bonding. A 12-μm-thick AZ9260 photoresist was patterned with a mask for subsequent deep etching of the channels resulting in 250-μm-deep channels for the separation. Then, TCD resistors were fabricated on a glass substrate by utilizing a lift-off process of a 40nm/100nm/25nm Cr/Ni/Au stack in the e-beam evaporator. After aligned anodic bonding of the diced detector on glass and the diced separation column on silicon, capillary tubes were epoxied into the inlet/outlet ports. The chip was static coated with polydimethylsiloxane by filling it with a solution of 10mg/ml polydimethylsiloxane OV-1in pentane, followed by carefully sealing one end with wax and pulling a vacuum at the open end. This procedure left a thin layer of poly-dimethylsiloxane OV-1 coating (~250 nm) on the walls of the column channel. An SEM image of the Tenax TA and OV-1 coating is shown in Figure 4-3. The optical image of all fabricated chips is shown in Figure 4-4.

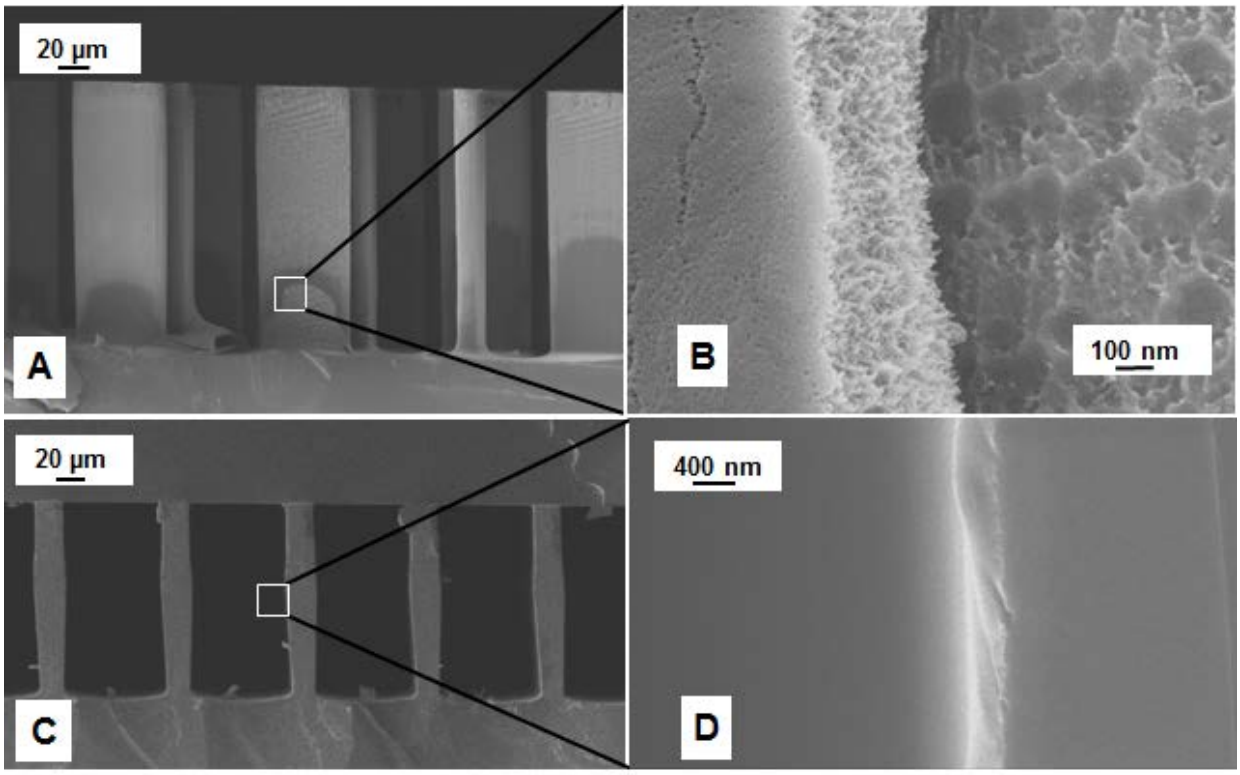

Figure 4-3: (A and B) SEM images showing Tenax TA coating on sidewall of micro-posts inside μTPC chip, (C and D) polydimethylsiloxane coating on the interior wall of the column channel.

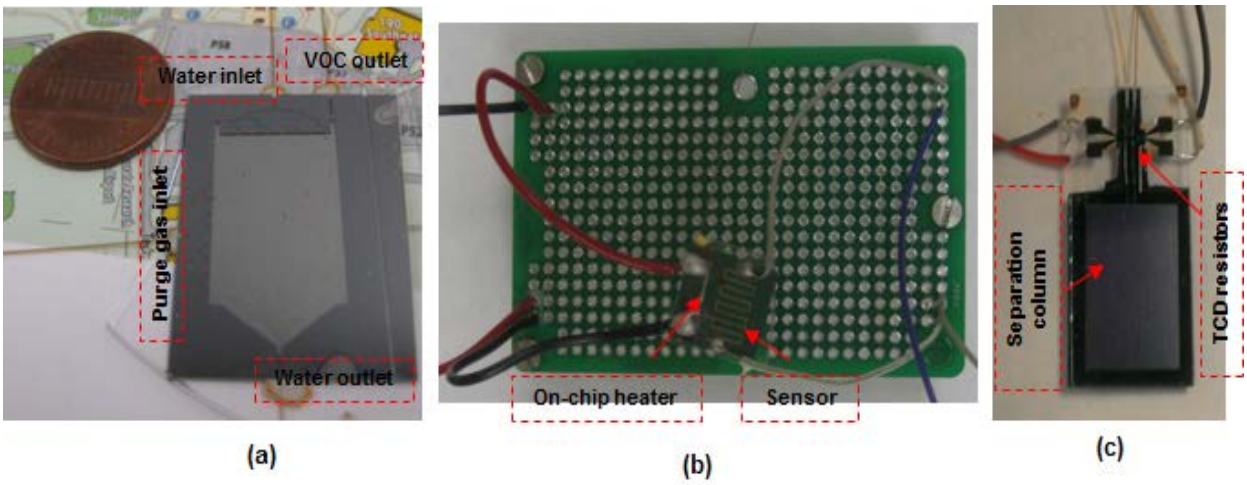

Figure 4-4: Optical image of fabricated (a) µPE (b) µTPC and (c) µGC chip with embedded resistors utilized as thermal conductivity detector for aqueous analysis.

4.4 Aqueous sample preparation

To avoid changing the concentration of WOCs, a 24 ml cylindrical vial was filled completely with deionized (DI) water leaving no headspace. Both 1 ppm and 500 ppb solutions (v/v) were prepared in two steps. First, 1000 ppm (v/v) solution was made by adding 24 µL of each WOC to 24 ml of DI water. Second, the solution was further diluted 1:24 and 1:12 with DI water to achieve concentrations of 1 ppm and 500 ppb, respectively. The solution was analyzed immediately to avoid compromising the sample integrity. Before processing any sample, all parts of the equipment in contact with the sample were demonstrated to be interference free. This was accomplished through a blank run.

4.5 Results and discussion

Before evaluating the performance of the whole integrated purge and trap µGC system, the heating and sensing elements of the microfabricated preconcentrator, separation column, and the detector were calibrated and the separation performance of the column was evaluated. For accurately measuring the temperature reached during the desorption process, an on-chip heater was calibrated by placing the µTPC in a commercial GC oven and then the resistance was measured for each given temperature. Next, a 12 V DC voltage was applied to the heater and the sensor resistance was measured until the resistance representing the desired temperature value was reached. The sensor resistance varied with applied voltage due to ohmic heating. The final temperature of 150 °C was attained within 7 s representing a ramp rate of 20 °C per second. This condition maintained constant during the desorption process of the WOCs trapped on the Tenax TA polymer coating of the µTPC.

The efficiency of the coated column was evaluated with µTCD switched to the ON condition by applying an 8.3 V DC voltage . This voltage corresponds to a temperature of 95°C.

This was measured with helium flowing at the operating pressure of 12 psi, similar to the method we have previously reported [29]. The metric commonly used for column performance is height equivalent to a theoretical plate (HETP),

$$\mathrm{HETP} = \frac{\mathrm{L}}{\mathrm{N}} \qquad \textbf{4-1}$$

where L is the length of column and N is the number of theoretical plates in the column. N is calculated experimentally from peak retention time (t_r) and peak width at half height ($w_{1/2}$).

$$\mathrm{N} = 5.54 \left[\frac{\mathrm{t_r}}{\mathrm{w_{1/2}}}\right]^2 \qquad \textbf{4-2}$$

The plate number was calculated over a range of column pressures with constant split injection ratio of 150:1 using chlorobenzene diluted to 2% (v/v) in hexane. The maximum plate number (optimum condition) observed was about 6200 for a 2 m long column at 12 psi (flow rate 0.62 ml/min). The column was operated at this optimum flow condition for further investigations.

Further, we tested the separation and identification of the four WOCs using the column and its μTCD. A 0.1 μl volume of sample containing the WOCs diluted to 2% (v/v) in hexane was injected into the μGC column. The chip was installed in the GC oven with its inlet and outlet connected to the injector and the GC flame ionization detector (FID), respectively. FID was used to verify the chromatogram generated by the μTCD. WOCs were successfully separated and detected by the chip within 1.5 min. Next, a calibration curve showing the output of the μTCD as a function of the injected WOC concentration was obtained. For that purpose, five samples (0.5%, 10%, 20%, 30%, and 40% (v/v) in hexane) for each WOC were prepared and tested. A 0.1 μl of each sample was injected three times in succession using the GC autosampler module with the split ratio maintained at 150:1. By using the density, mass for each WOC was calculated taking split injection ratio into account. The injected mass varied from about 3 ng to 23 ng for toluene, 5.4 ng to 43 ng for PCE, 3.7 ng to 29.3 ng for chlorobenzene and 3 ng to 23 ng for ethylbenzene. A calibration curve showing the average peak area under the μTCD signal obtained for three injections is shown in Figure 4-5. Results obtained indicate a unique response of the μTCD for each WOC with relative standard deviation (RSD) less than 10% for all cases. The coefficient of determination (R^2) was greater than 0.99 in all cases.

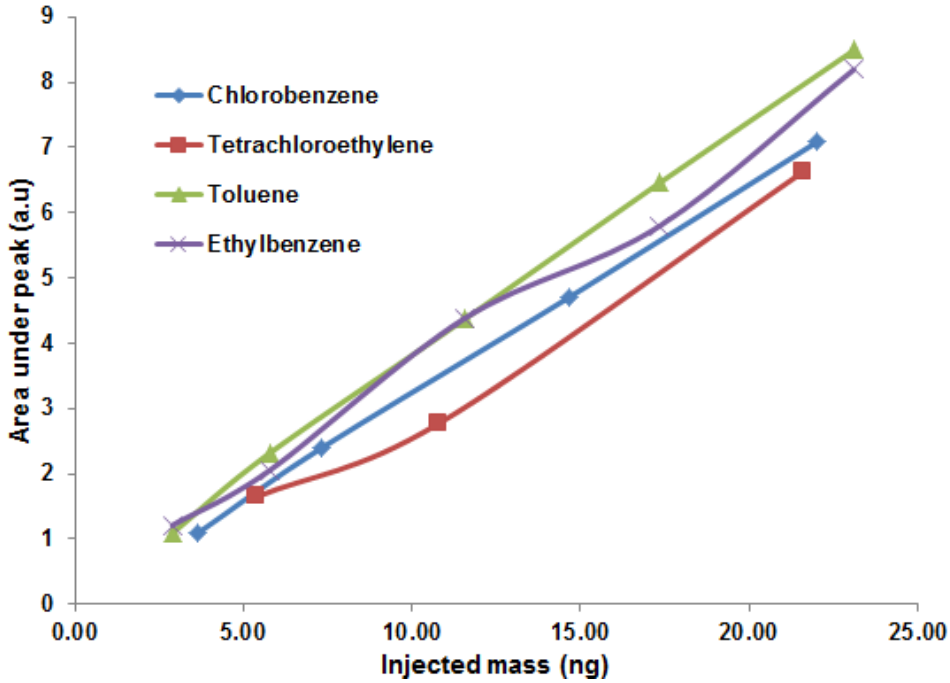

Figure 4-5: Calibration curve showing response of μTCD for five different concentrations of WOCs in this study. The relative standard deviation is < 10% for all cases. Peak assignments: 1. toluene, 2. tetrachloroethylene, 3. chlorobenzene, 4. ethylbenzene.

Following calibration and performance evaluation of the μGC unit, the μPE was put in place. The ability of the complete system comprising μPE and μTPC chip, separation column, and the thermal conductivity gas detector (μTCD) to continuously monitor WOCs in aqueous sample was realized experimentally by the method explained earlier. Aqueous solution was introduced into the μPE chip using purified nitrogen at 10 psi. High purity nitrogen gas was supplied through the air inlet of the μPE chip trapping WOCs on the adsorbent surface with a flow rate maintained at 0.4 ml/min through μTPC chip. The extraction period was varied for three discrete periods of 7, 14 and 21 min. The set of chromatograms in Figure 4-6 was generated using 500 ppb and 1 ppm aqueous samples for two different extraction periods. The initial negative dip is due to the sample mixture passing over the reference detector. After this stage, the signal detector experiences carrier gas and hence is constant. This results in a negative voltage output as explained before [21]. As the sample mixture moves through the column, it is separated over time. When the individual components pass over the sample detector, the reference detector experiences the carrier gas and hence results in positive peaks corresponding to each eluted compound. The second peak is due to trace moisture extracted from the purge chip and is not seen on the FID signal which is insensitive to trace water content. The increase in peak heights for all WOCs with the increase in extraction time was observed which clearly indicated the validation of the proposed approach. It is also evident that rapid chromatographic separation and detection of all four WOCs within 1.5 min is achieved at room temperature.

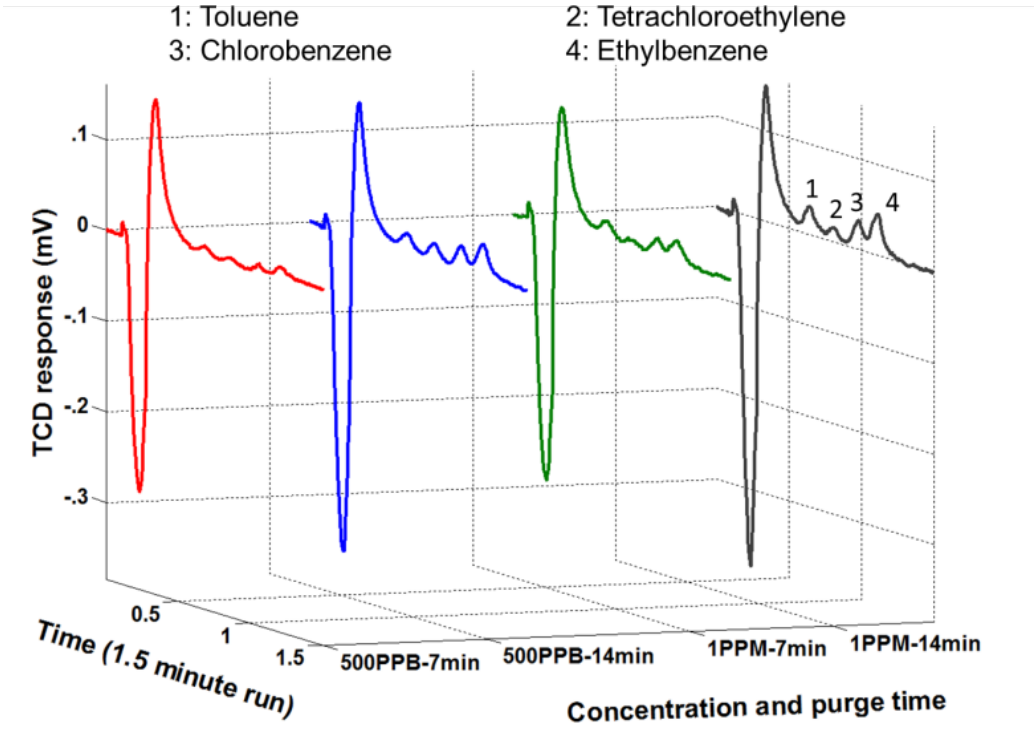

Figure 4-6: Set of chromatogram indicating increase in µTCD response, with increase in purge time and concentration of WOCs

The method precision was evaluated by three repetitive analyses for each test. After each analysis, the µTCP was heated to 150 °C (conditioning step) to prevent carry-over from the previous runs, following which a blank run was performed to confirm the same. The change in detector response (area under the peak) with purge time was then monitored for a sample containing four WOCs at 1 ppm concentration. The experiment was repeated thrice for three different purging times and the average value was plotted for each WOC. Figure 4-7 shows that the peak area increases with purging time. The increase in peak area was attributed to the increase in the quantity of nitrogen (inert gas used) that bubbled through the aqueous sample, and consequently, more quantity of WOC moved from the liquid to the vapor phase. Additionally, in streaming mode more fresh sample entered the µPE chip replacing the old one, thereby increasing the amount of WOC purged over time.

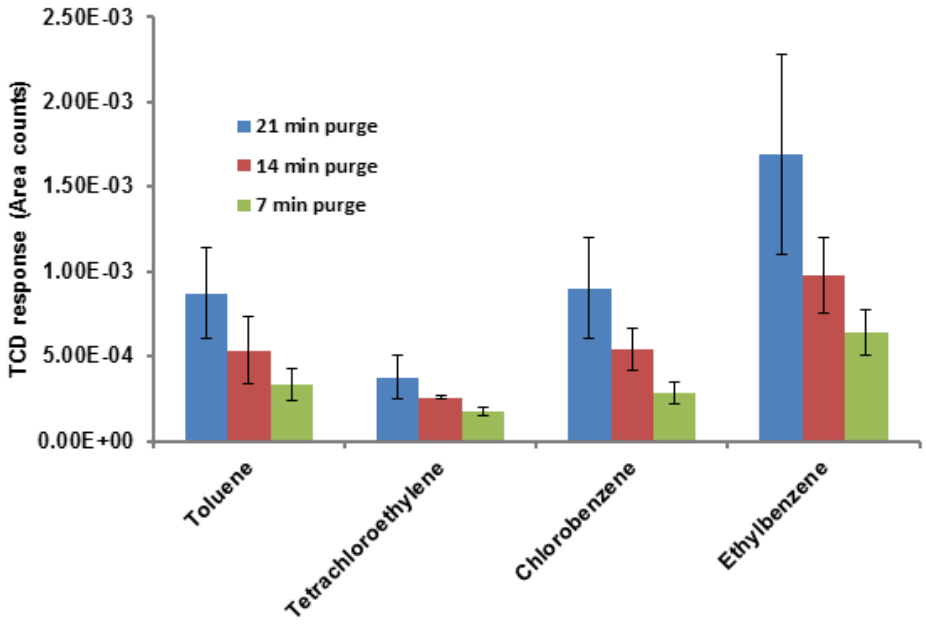

Figure 4-7: Graph showing the μTCD response variation with increasing purge time for a sample containing four WOCs at 1 ppm concentration.

Results in Figure 4-7 indicate that ethylbenzene and chlorobenzene are purged easily from the aqueous sample as compared to PCE and toluene. This is due to their relatively high partition coefficient (K_{ow}) value, which is defined as the ratio of concentration of a compound in a hydrophobic solvent (usually octanol) to its concentration in water at equilibrium. In other words, it is a measure of hydrophobicity and depends on size, polarity and hydrogen bond strength of a compound. Hydrophilic compounds (with low partition coefficient) are held by very strong dipole-dipole interaction and/or hydrogen bonds in water and thus could not be easily purged from the sample. Increasing the temperature of the sample should increase the purged amount by supplying enough thermal energy to the molecule to break the dipole-dipole interaction [30]. The sample analyzed during the purge time was collected to determine the percent recovery of each compound. Assuming that the trap is able to capture the entire purged amount, percent recovery is defined as the ratio of the amount that is collected for chromatographic analysis relative to the amount that was originally present in the aqueous sample. Table 4-1 summarized the percent recovery for each compound at 1 ppm concentration. The percent recoveries are lower than those reported in literature. This can be attributed to the fact that commercial purge and trap systems use high purging gas flow rates (normally 40 ml/min) and also use traps consisting of a short length micro-bore tubing packed with granular form of adsorbent material. Such traps at the cost of high pressure drops and high power consumptions can provide higher adsorption capacity. It is notable that low recoveries have also been reported previously by Sandia National Laboratories in their bench-top system due to the flow limitations in their setup [31]. Nevertheless, the purpose of this work was to integrate all μGC components to automate the sampling of water and extract and identify WOCs in real

world situation. Modification in design parameters and thermal manipulation for optimization of μPE chip performance will be described in a separate report.

4.6 Inference

The first micro-scale version of a purging device for the extraction of WOCs from aqueous sample has been described. The potential application of the chip for on-site monitoring of aqueous sample when equipped with all necessary μGC components has also been discussed. We have first characterized the performance of the μGC column with μTCD turned ON and explored the optimum conditions for the μGC column. Next, we have obtained a calibration curve indicating the change in μTCD response to different amount of individual WOCs (in the absence of the μPE and μTPC). We have shown that fixed volume samples of water spiked with known concentrations of the WOCs can be extracted using the μPE chip and subsequently trapped on the μTPC. We have finally determined the percentage recovery of each compound thereby successfully demonstrating the ability of the complete system in analyzing WOCs in an aqueous sample.

We expect to enhance the recovery of analytes by modifying the design of the μPE chip and integrating temperature programming ability on this chip. In future work, in addition to the overall chip size, the design parameters including the location of the inlets and outlets, the configuration of the fluidic ports (distributed versus single) and their widths, and the inclusion of pillars and their associated shapes and arrangements will be thoroughly studied to improve the recovery of WOCs. Other parameters including the mode of operation (streaming solution versus steady solution), flow rate of sample to purging gas in streaming mode and temperature manipulation for purging high boiling point organic compounds (semi-VOCs) as external controllable parameters on recovery of WOCs will also be considered.

REFERENCES

[1] U. S. EPA, "Draft Guidance for Evaluating the Vapor Intrusion to Indoor Air Pathway from Groundwater and Soils," *Report No. EPA/540/1–89/2002, U.S. EPA, Washington, DC, 2002*.

[2] ATSDR, "Toxicological Profile for n-Nitrosodimethylamine," ed. Washington DC: Agency for Toxic Substances and Disease Registry, 2012.

[3] D. Pobel, *et al.*, "Nitrosamine, Nitrate and Nitrite in Relation to Gastric Cancer: A Case-Control Study in Marseille, France," *European Journal of Epidemiology*, vol. 11, no. 1, pp. 67-73, 1995.

[4] P. A. Jones, *et al.*, "Interpretation of the in Vitro Proliferation Response of MCF-7 Cells to Potential Oestrogens and Non-Oestrogenic Substances," *Toxicol. in Vitro*, vol. 12, no. 4, pp. 373-382, 1998.

[5] T. Nishihara, *et al.*, "Estrogenic Activities of 517 Chemicals by Yeast Two-Hybrid Assay," *Journal of health science (Tokyo, Japan)*, vol. 46, no. 4, pp. 282-298, 2000.

[6] K. S. Betts, "Brain Drain? PBDEs Alter Development of Human Brain Cells," *Environ Health Perspective*, vol. 118, p. A173, 2010.

[7] P. Burkhardt-Holm, *et al.*, "Nonylphenol Affects the Granulation Pattern of Epidermal Mucous Cells in Rainbow Trout, Oncorhynchus mykiss," *Ecotoxicol. Environ. Saf.*, vol. 46, no. 1, pp. 34-40, 2000.

[8] H. Ishibashi, *et al.*, "Reproductive effects and bioconcentration of 4-nonylphenol in medaka fish (Oryzias latipes)," *Chemosphere*, vol. 65, no. 6, pp. 1019-1026, 11// 2006.

[9] M. F. Kirby, *et al.*, "Ethoxyresorufin-O-deethylase (EROD) and vitellogenin (VTG) in flounder (Platichthys flesus): System interaction, crosstalk and implications for monitoring," *Aquatic Toxicology*, vol. 81, no. 3, pp. 233-244, 3/10/ 2007.
[10] F. Lahnsteiner, *et al.*, "The effect of 4-nonylphenol on semen quality, viability of gametes, fertilization success, and embryo and larvae survival in rainbow trout (Oncorhynchus mykiss)," *Aquatic Toxicology*, vol. 71, no. 4, pp. 297-306, 3/4/ 2005.
[11] J. J. Johnston, *et al.*, "Determination of White Phosphorus Residues in Ducks: An Atomic Emission Detection/Compound-Independent Calibration-Based Method of Generating Residue Data for Risk Assessment and Environmental Monitoring," *Environmental Science & Technology*, vol. 34, no. 9, pp. 1856-1861, 2000.
[12] B. Alfeeli, *et al.*, "Characterization of poly(2,6-diphenyl-p-phenylene oxide) films as adsorbent for microfabricated preconcentrators," *Microchemical Journal*, vol. 98, no. 2, pp. 240-245, 2011.
[13] C.-J. Lu, *et al.*, "First-generation hybrid MEMS gas chromatograph," *Lab on a Chip*, vol. 5, no. 10, pp. 1123-1131, 2005.
[14] J. H. Seo, *et al.*, "Fabry-Perot cavity sensor-based optofluidic gas chromatography using a microfabricated passive preconcentrator/injector," *Lab on a Chip*, vol. 13, no. 5, pp. 851-859, 2013.
[15] W. R. Collin, *et al.*, "Microfabricated Gas Chromatograph for Rapid, Trace-Level Determinations of Gas-Phase Explosive Marker Compounds," *Analytical Chemistry*, 2013.
[16] M. Akbar, *et al.*, "A Microfabricated Propofol Trap for Breath-Based Anesthesia Depth Monitoring," *Microelectromechanical Systems, Journal of*, vol. 22, no. 2, pp. 443-451, 2013.
[17] M. Akbar, *et al.*, "Improved performance of micro-fabricated preconcentrators using silica nanoparticles as a surface template," *Journal of Chromatography A*, vol. 1322, no. 0, pp. 1-7, 2013.
[18] M. Akbar, *et al.*, "A MEMS enabled integrated microgc platform for on-site monitoring of water organic compounds," *Solid-State Sensors, Actuators and Microsystems (TRANSDUCERS & EUROSENSORS XXVII), 2013 Transducers & Eurosensors XXVII: The 17th Inte*, pp. 2759-2762, 2013.
[19] H. Shakeel, *et al.*, "Self-Patterned Gold-Electroplated Multicapillary Gas Separation Columns With MPG Stationary Phases," *Journal of Microelectromechanical Systems*, vol. 22, no. 1, pp. 62-70, 2013.
[20] D. Wang, *et al.*, "Highly Stable Surface Functionalization of Microgas Chromatography Columns Using Layer-by-Layer Self-Assembly of Silica Nanoparticles," *Analytical Chemistry*, vol. 85, no. 17, pp. 8135-8141, 2013/09/03 2013.
[21] S. Narayanan, *et al.*, "Two-Port Static Coated Micro Gas Chromatography Column With an Embedded Thermal Conductivity Detector," *IEEE Sensors Journal*, vol. 12, no. 6, pp. 1893-1900, 2012.
[22] J. H. Seo, *et al.*, "Microfabricated passive vapor preconcentrator/injector designed for microscale gas chromatography," *Lab on a Chip*, vol. 12, no. 4, pp. 717-724, 2012.
[23] S. K. Kim, *et al.*, "Microfabricated Gas Chromatograph for the Selective Determination of Trichloroethylene Vapor at Sub-Parts-Per-Billion Concentrations in Complex Mixtures," *Anal. Chem.*, vol. 83, no. 18, pp. 7198-7206, 2011/09/15 2011.
[24] J. H. Seo, *et al.*, "Effect of Thermal Desorption Kinetics on Vapor Injection Peak Irregularities by a Microscale Gas Chromatography Preconcentrator," *Analytical Chemistry*, vol. 84, no. 15, pp. 6336-6340, 2012/08/07 2012.
[25] R. K. Eberhardt, "Water injection in GC-how wet can you get,," vol. 5, pp. 30-32, 2001.
[26] K. Grob, *et al.*, "Trace analysis of halocarbons in water; Direct aqueous injection with electron capture detection," *Journal of High Resolution Chromatography*, vol. 6, pp. 11-15, 1983.
[27] R. B. Ulrich, *et al.*, "Effect of vacuum on the performance of the flame ionization detector used for vacuum-outlet gas chromatography," *Journal of Microcolumn Separation*, vol. 12, pp. 226-235, 2000.
[28] B. Alfeeli, *et al.*, "Micro Preconcentrator for Handheld Monitoring of Water Quality," in *14th International Conference on Miniaturized Systems for Chemistry and Life Sciences* Groningen, The Netherland, 2010, pp. 1721-1723.
[29] S. Narayanan, *et al.*, "Fabrication and Characterization of a Suspended TCD Integrated With a Gas Separation Column," *Journal of Microelectromechanical Systems*, vol. 22, no. 5, pp. 1166-1173, 2013.
[30] C. W. Lee, *et al.*, "Determination of methyl tert-butyl ether and tert-butyl alcohol in human urine by high-temperature purge-and-trap gas chromatography-mass spectrometry," *Journal of analytical toxicology*, vol. 22, no. 1, pp. 1-5, 1998.
[31] C. D. Mowry, *et al.*, "Research into the variables affecting purge and trap collection for a portable field trihalomethane testing unit," SAND2006-2447 United States10.2172/883140Tue Feb 05 05:15:13 EST 2008SNLEnglish, 2006.

5

Matrix GC: Multi-dimensional Analysis/Detection using Integrated Columns

Shree Narayanan, Apoorva Garg, and Masoud Agah

Separating a mixture of gases and detecting them, as approached in gas chromatography, is an enormous challenge when facing an unknown mixture. Even when restricted to the class of organic compounds the sheer number of possible compounds (>10 million by most accounts) that need to be analyzed is impractical for a separation column with finite plate height. The plate height or plate number is a measure of the efficiency of a column and is given by the equation

$$N = 5.54 * \left(\frac{t_r}{w_h}\right)^2 \qquad \textbf{5-1}$$

where, t_r and w_h are retention time and peak width at half height, respectively. The non-zero peak width of practically observed peaks results in merging of compounds with similar retention indices – coelution. A measure of the resolution between two closely spaced peaks is given by

$$R = \frac{t_{r2} - t_{r1}}{(w_2 + w_1)/2} \qquad \textbf{5-2}$$

Where, t_{r1} and t_{r2}, and w_1 and w_2 are the retention times and peak-widths-at-base, respectively, for the two peaks. For a given resolution threshold, the number of peaks that can be accommodated in a chromatographic run duration is finite. This peak capacity limits the number of compounds that can be identified.

The crux of the problem lies in avoiding co-elution. Lengthening the column to increase the plate number and improve the resolution between the co-eluting compounds is possible but impractical. A more practical solution for a one-column approach is to modify the stationary phase. Application specific stationary phase blends can achieve separation of the co-eluting peaks at the same length. However, this method does not improve the peak capacity of the column. An alternative to improve the peak capacity while avoiding co-elution is that of temperature

programming. In particular cases, temperature programming can reverse order of elution and improve separation. Yet, the improvement in peak capacity is limited by the usage of a single column (coating).

A more powerful technique utilizes multiple columns, each coated with stationary phase of different selectivity [1]. In the simplest of configurations, two columns of different coatings are connected in series and provide a response similar to the application specific blend discussed earlier. This is referred to as multichromatography [2, 3] and results in shifting of retention times without improvement in the peak capacity. Most prior multichromatography experiments suffered from the lack of an inline detector on the first column. The presence of a FID at the junction of the two columns measures column hold-up times. or measures only a portion of the eluent, as in stop-flow tandem chromatography [4]. The complete separation power of two columns – Multidimensional GC – can be realized when each peak eluting out of the first column is individually run through an uncorrelated chromatographic separation on the second column through an interface [5]. When a specific section or slice of the first column is run through the second column, the method is referred to as "heart-cut". On the other hand, comprehensive-GC results when this slicing is performed repeatedly on the elution from the first column. Multi-dimensional GC is thus the technique of enhancing peak capacity of the system as the product of the individual columns, albeit, at the expense of increased complexity of the system. A number of interfaces exist – thermal, cryogenic, stop-flow tandem, flow routing [6-12].

There are limitations in implementing this idealized description of comprehensive-GC since components separated should not combine in a later column. For example, when adsorbent/thermal modulation is employed to refocus the elutant from the first column into the second column, the second column is typically short, has a thin stationary phase coating, and higher flow rates so as to enable a quick separation before the next modulated peak is injected into the second column. This results in significant amount of data acquired every run, requiring data handling and visualization techniques [13]. The peak capacity of the second column is kept smaller when compared to the first column and limits the extent to which a 2-D comprehensive GC can be extended. Sophisticated architectures employing multiple secondary columns or tertiary columns have been demonstrated [14-16]. As such, multi-dimensional GC, despite its introduction in the early 1990s, has been restricted to few laboratories that can afford the technical expertise required for operating such systems.

Herein, we offer an alternative approach to the analysis of a complex and multitudinous mixture, taking advantage of the benefits of miniaturization. In 1979, Terry et. al. proposed the first microfabricated gas chromatographic analyzer [17]. The separation column was a microfluidic channel in silicon and capped with a glass. A separately fabricated TCD was mounted on the backside. The sub-optimal coating and contemporary etching technology constraints limited its performance. Over the years, technological innovations such as deep-reactive ion etching have enabled narrow and deep anisotropic channels that offer a high plate

efficiency [18]. Similarly, microfabricated channels are coated reliably well with stationary phase using static coating methods [19]. Previously, we have demonstrated the ability to monolithically integrate an in-line micro thermal conductivity detector with a micro separation column, hereafter referred to as an integrated column [20, 21]. Its unique embedded approach avoids the need for a reference channel and instead, places the reference resistor close to the inlet which sees the carrier gas, while the outlet sees the elutants. Such 2-port integration offers great flexibility to be integrated in a matrix. Using off-the-shelf components, multiple integrated columns are connected in a matrix. The multiplicity of detectors and orthogonality of phases increases the dimensionality and offers increased peak capacities.

5.1 Theory

5.1.1 Wrap-around effect in matrix GC

The uniqueness of this architecture lies in the usage of robust in-line μTCDs. In a similar technique called multichromatography, an end-of-the-line detector such as an FID monitors the response of a coupled column. The columns have different phase selectivities to separate apart a target set of peaks which would otherwise not resolve sufficiently when either column is used alone. However, it was pointed out that such a technique does not offer increase in peak capacity [22, 23]. Peak capacity, is the number of peaks that can fit into a chromatogram. It is a valid tool to compare various configurations under the assumption that peaks array themselves along the time axis. Even though multichromatography offers shift in retention times, peaks separated in first column can merge in the second column. This effect – wrap-around effect – is characteristic of multidimensional systems that use a single end-of-the-line detector. In Figure 5-1, a detector at the end of Column 2 cannot distinguish the presence of A and B in the mixture. One workaround is to introduce an interface at the junction. The interface modulates the junction pressure between the two columns and separates the peaks further [24]. Expertise in pulse width and timing optimization is required to minimize loss of sample through the vent line. On the other hand, the presence of a detector on each column identifies the presence of A and B which is the focus in matrix GC, thus increasing the peak capacity of the system.

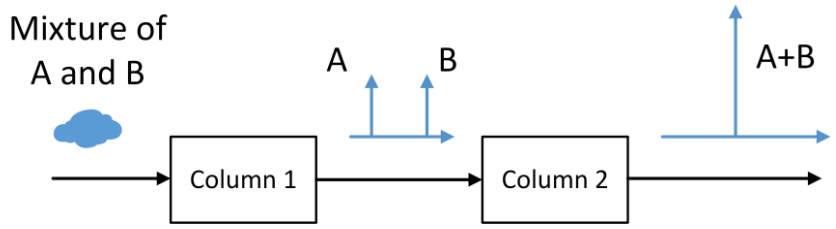

Figure 5-1: A coupled column configuration with two components separated by the first column but re-merged by the second column. Presence of an in-line detector on each column helps identify both and increases peak capacity.

5.1.2 Effect of architecture on peak capacity

As described earlier, increasing length of a single column offers insignificant increase in the peak capacity. The practical alternative is to employ multiple columns with different stationary phase coatings. If the response of the phases does not correlate, they are said to be orthogonal and the peak capacity is either additive or multiplicative, depending on the architecture.

Consider a single integrated column of peak capacity, n_1. Changing its phase only shifts the retention times but the peak capacity remains the same. Connecting a differently coated integrated column, of peak capacity n_2, in parallel realizes a total peak capacity of $n_1 + n_2$. On the other hand, if two integrated columns are connected in series, the peak capacity would be the sum of n_1 peaks from the first detector and $2n_2$ peaks from the second detector i.e. $n_1 + 2n_2$. The factor two is due to the fact that the last peak from the first column results in another n_2 set of peaks on the second detector. This difference in series and parallel configurations, in the time domain, can be understood from the following situation (Figure 5-2). For a mixture of three compounds A, B and C, where column 1 cannot differentiate between A and B, and column 2 cannot differentiate between B and C, a series connection is effective in separating all three. The tradeoff is the increased separation time in the series configuration.

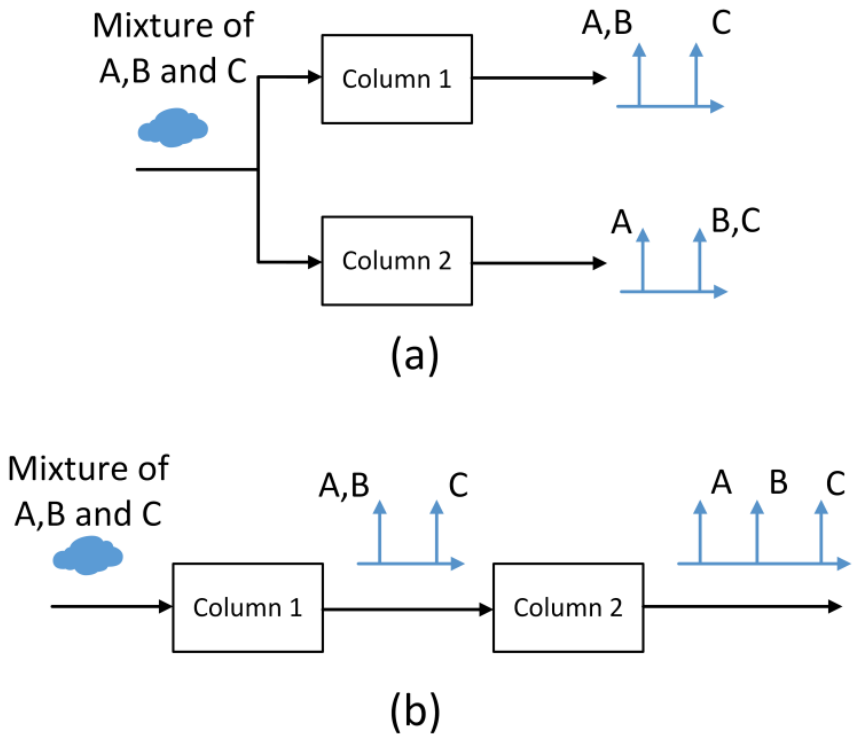

Figure 5-2: Separation of a mixture of three components – A, B and C – on two columns with different selectivity. (a) shows a series connection capable of separating the three in a longer time whereas (b) is a parallel connection that cannot distinguish B, from either A or C.

5.1.3 Effect of temperature on peak capacity

The retention index (or retention time) of a compound is a thermodynamic property that is exponentially dependent on the column temperature. Increasing column temperature reduces the retention time and increases peak capacity and worsens resolution.

$$\log K = A + \frac{B}{T_c} \qquad \textbf{5-3}$$

However, peaks that elute late and tend to be spaced apart farther elute earlier and without loss of resolution. This effect is exploited in matrix GC by operating identical arms in parallel, but at different temperatures. In time domain, this is equivalent to focusing different arms on different set of compounds or temperature tuning.

5.2 Fabrication

Fabrication of the integrated device follows the process flow, using standard techniques, shown in Figure 5-3. It consists of a silicon and a glass die, hosting the microfluidic channel and TCD resistor elements, bonded together. A 4" 700 μm Borofloat 33 wafer (Schott, NY) was spun coated with photoresist and patterned for liftoff. A 40 nm/100 nm/25 nm stack of chromium/nickel/gold was deposited by e-beam evaporation in a PVD-250 physical vapor deposition tool (Kurt Lesker). The metal pattern for each column consists of two identical patterns, for differential measurement. Each consists of an active metal heater, an interconnect and bond pads for soldering. On the other hand, a 4" diameter p-type double-side polished test grade wafer (University Wafers, MA) was spun coated with photoresist and patterned with a mask that defines a 7μm shallow etch. This etch corresponds to interconnects on the metal pattern for the TCD. After stripping away the photoresist, the wafer was coated with thick photoresist, patterned to define the anisotropically deep etched regions for the microfluidic channel and the bond pad release. These correspond to the active metal heaters and the bond pads, on the glass, respectively. The deep etched wafers were then stripped of the photoresist and a 1μm thick oxide was deposited on its backside. After dicing the wafers, individual dies were aligned and bonded anodically. A 40 nm/100 nm/25 nm stack of chromium/nickel/gold was evaporated on the backside of the silicon side of the bonded die, to define the metal heaters and sensors used for column heating, employing shadow masks.

The fabricated dies were sealed in with capillary tubes using epoxy for the microfluidic connections. The strength of the separation column lies in the stationary phase. Three different phases – OV-1 (dimethyl silicone), OV-17 (phenyl methyl silicone) and OV-215 (trifluoropropyl methyl silicone) – with increasing order of polarities were chosen. To static coat the column, the column was first filled with hexamethyldisilazane (HMDS) and heated to 120°C on a hotplate. Following this, any remaining HMDS was purged out with nitrogen and the channel filled with a 5 mg/mL solution of the stationary phase. With one end sealed with wax, the other end of the column was pulled with a vacuum pump, to evaporate the solvent and leave behind a thin film of

the stationary phase on the walls of the microfluidic channel. It should be noted that each die consisted of two separation columns with a TCD embedded in each. Both the columns were externally connected, with a union, in series. Fabricating both columns on the same die provided for accurate temperature tracking, necessary for series connected TCDs.

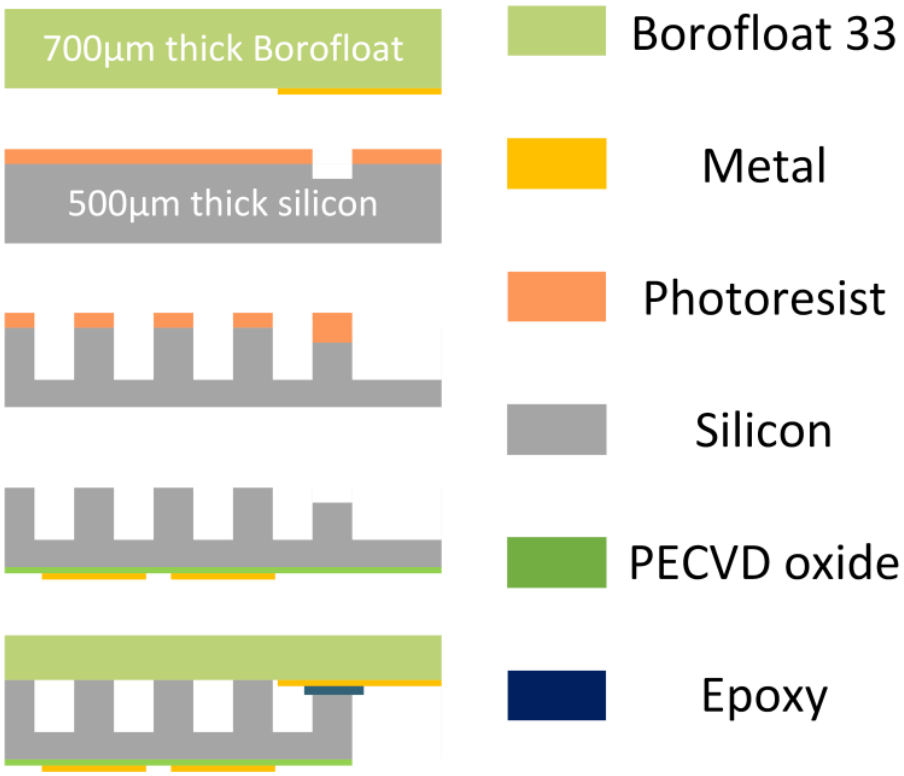

Figure 5-3: Process flow for the separation column with an integrated thermal conductivity detector

5.3 System description

Figure 5-4 shows the communication control to 1) control the heater on a PWM signal, 2) read the temperature off the column, 3) and read the TCD response from each column. The latter two are digitized by 24-bit SPI-enabled ADCs (AD7793) on board the module. An Arduino ATMEGA performs the task of 1) receiving instructions from a C# graphical user interface (GUI) on a desktop (Figure 5-5), 2) translating the instructions into chip select signals for the ADC, 3) modulate the PWM output and maintain column temperature with feedback, 4) and transferring module related data to C# GUI for data visualization and recording. A PWM or pulse width modulated signal is an output of an on-chip peripheral included on modern day microcontrollers. The output of such a unit is a square wave signal whose duty cycle is defined by a software instruction. By relying on an independent timer to generate the signal, interrupt service routines are not necessary to toggle the square wave signal.

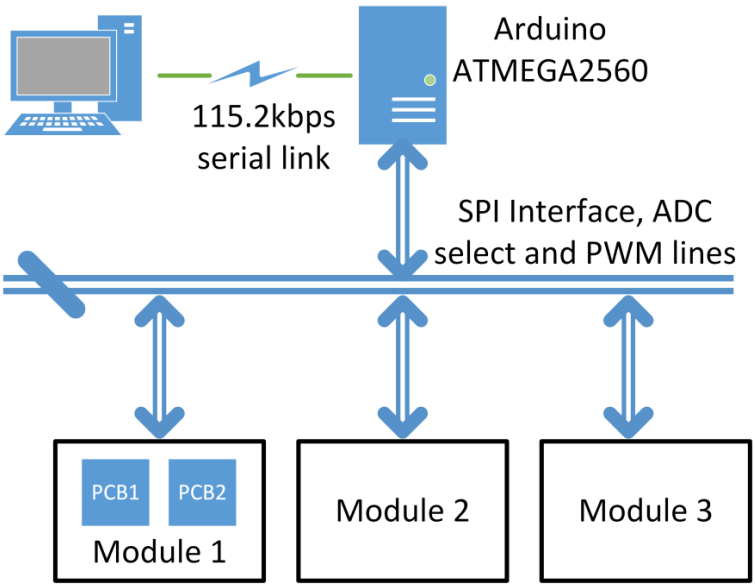

Figure 5-4: A system-level description of the interaction of the modules with the data acquisition setup

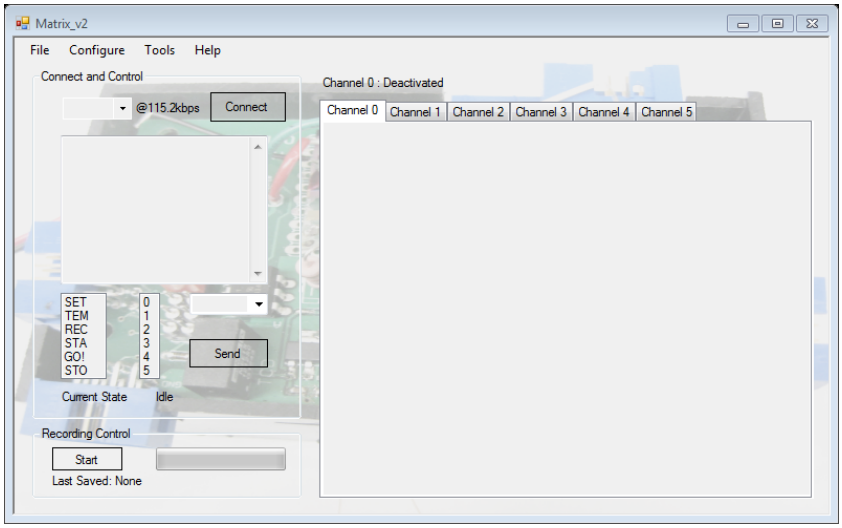

Figure 5-5: A screenshot of the desktop GUI to provide instructions to the Arduino and receive data

Each module contains logic to control a die consisting of two columns connected in series, as mentioned in previous section. The series connected in the three modules are connected in parallel such that the sample to be analyzed splits equally into all three modules. The modules do not interact with each other electrically. The schematic view of a PCB to control one of the columns is provided in Figure 5-6. Selector headers are provided for the PWM control bus and the chip select bus lines for both ADCs. An appropriately placed jumper on the header defines the exact channel on which the PCB responds. Instructions are given to the Arduino from the GUI, specify the channel on which the Arduino can expect a module. The PCBs are exactly identical except that the reference signal for the TCD at the output of the second column in the series connection is tapped from the reference signal of the first TCD, to prevent a

superimpose effect. The superimpose effect occurs when an elutant reaches the outlet of the second column while another elutant enters the second column after separation in the first column. This results in the superimposition of the corresponding positive and negative peaks and unpredictable output on the response of the second TCD. A snapshot of the module is shown in Figure 5-7. Detailed circuits are provided in Appendix B, at the end of this dissertation.

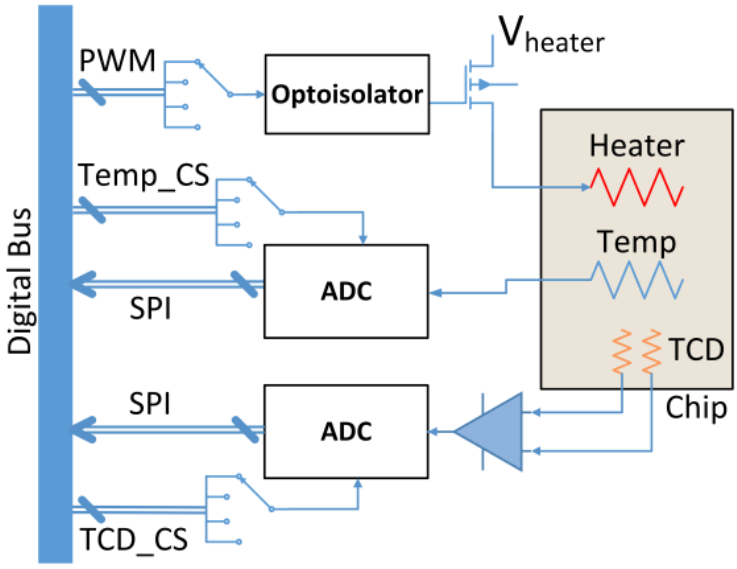

Figure 5-6: The logic for heating the column, reading off its temperature and detector response on the SPI bus. The selector switches (PWM, Temp_CS, TCD_CS) on each PCB provide for selecting the corresponding channel for that PCB by suitably shorting the header with jumpers, making it reconfigurable.

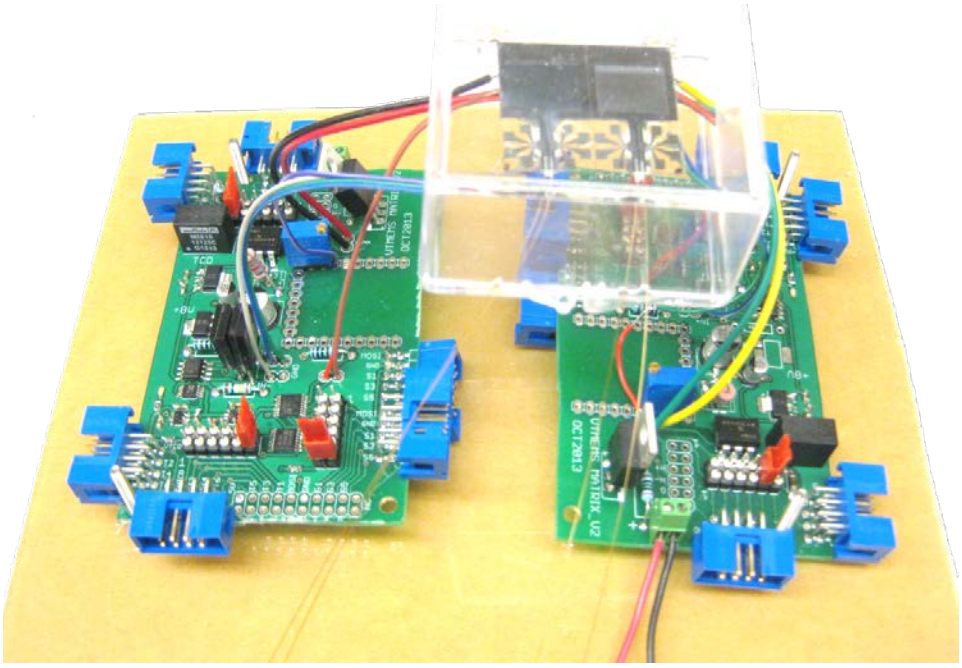

Figure 5-7: A snapshot of a module showing two PCBs and a die consisting two columns

5.4 Results and discussion

5.4.1 A coupled integrated-column setup

A die with an OV-1/OV-215 pair was tested for this purpose. Each column was fabricated 1 m-long, 260 µm-deep and 80 µm-wide. To begin, the dies were characterized for the intercept and slope of the resistance versus temperature graphs corresponding to the temperature sensor on the column backside. These values were input into the GUI against the corresponding unit settings. When suitably instructed, the Arduino scans the module with the provided intercept and slope values. The temperature thus calculated was handed over to the GUI and displayed. The inlet to the OV-1 column was connected to the injector on a HP5890 with helium as the carrier. A 0.1 µL sample of various compounds were injected in sequence into the injector. As the sample traveled through the OV-1 and OV-215 column, they are retained to different extents, due to the different stationary phase polarity. The two retention times, t_{r1} and t_{r2}, are plotted in Figure 5-8.

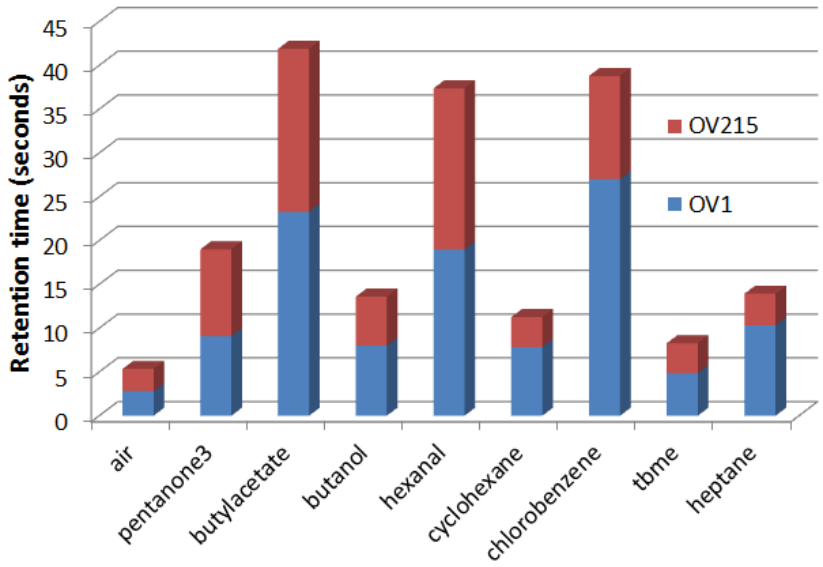

Figure 5-8: Retention times of 8 different compounds and air on a series connected OV-1 and OV-215 columns at 35°C

The reference-less µTCD design offers a negative peak corresponding to the injection into the column. The retention times are calculated against this negative peak. When two columns are in series, the retention time of the second column is calculated with respect to the negative-going injection peak from the first column. Butyl tert-methyl ether or TBME with a boiling point of 55°C and chlorobenzene with a boiling point of 131°C form the extreme ends of the boiling points in the sample under consideration. The retention time for air corresponds to the hold-up time and depends on the flow rate in the column. If t_{m1} and t_{m2} are the gas holdup times in both columns, relative retentivities, φ_1 and φ_2 can be defined for the individual columns as [25]

$$\varphi_1 = \frac{t_{m1}}{t_{m1} + t_{m2}} = 0.52 \quad and \quad \varphi_2 = 1 - \varphi_1 = 0.48 \qquad \textbf{5-4}$$

The slightly lower relative retentivity for the second column in spite of using two identical columns can be attributed to the extra length of capillary connecting the outlet of the first to the inlet of the second. This length of capillary tube gets counted in the hold-up time of the second column. It should be noted that the 8 compounds elute out in under 45 seconds. For quicker analysis, a higher column temperature is preferred. Commonly referred to as temperature programming, a varying column temperature during runtime deteriorates the TCD response due to shifting baseline. However, the column can be operated at a higher isothermal temperature. Figure 5-9 lists the retention times for the same set of compounds at an elevated column temperature of 75°C.

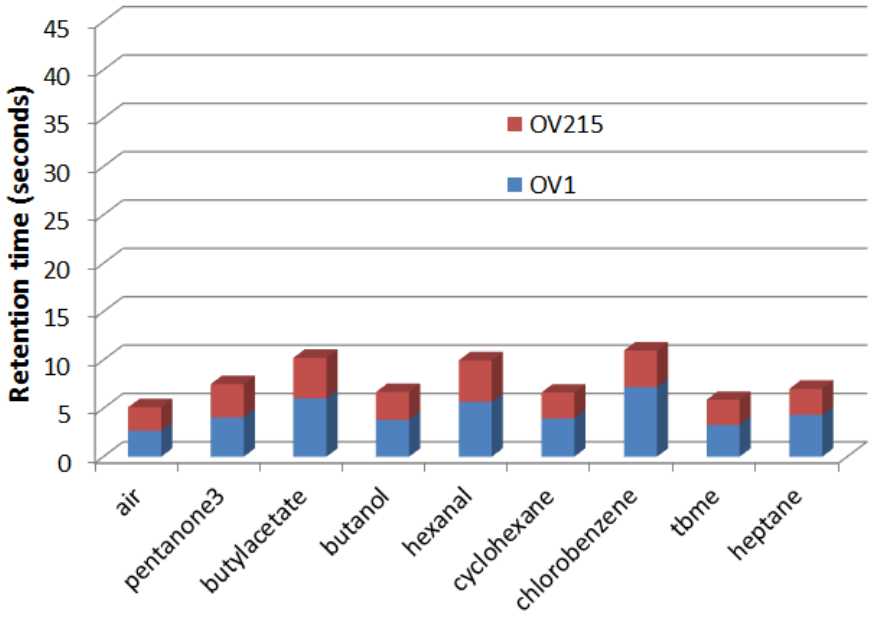

Figure 5-9: Retention times for the 8 compounds and the unretained peak of air is listed for both OV-1 and OV-215 columns, at an elevated temperature of 75°C.

5.4.2 Verifying qualitation through quantitation

Qualitative analysis refers to the identification of the analytes present in a mixture. In gas chromatography, this is achieved by comparing the retention times of the peaks in a chromatogram against a library of retention times of known set of compounds. On the other hand, quantitative analysis refers to determining the percentage compositions of the analytes in the mixture. Given, the inevitable presence of unknown compounds that can co-elute with any of the known compounds, it is preferable to be able to at least confirm the presence or absence of the unknown compounds. Series connected columns, in addition to the two-dimensional retention times, provide us with an additional means to detect the presence of an unknown co-eluting compound.

Figure 5-10 shows the TCD response of two series connected integrated columns of OV-1 and OV-215. The negative peak is the injection marker, at the inlet of the OV-1 column. The analyte mixture of 3-pentanone and 1-butanol have the same retention time on the OV-1 column and co-elute with an area A_1. However, they are retained to different extents on the OV-215 column and elute at different instants with areas, A_2 and A_3. Since the same plug travels through both the series connected columns, their areas should be related by a proportionality factor ($\kappa=A_1/A_2$). This proportionality factor is expected to be a constant for a given compound. Injecting 3-pentanone and 1-butanol, individually, their corresponding proportionality factors were determined to be 1.3 and 1.2, respectively. The value is slightly greater than unity, due to the band-broadening and subsequent integration error.

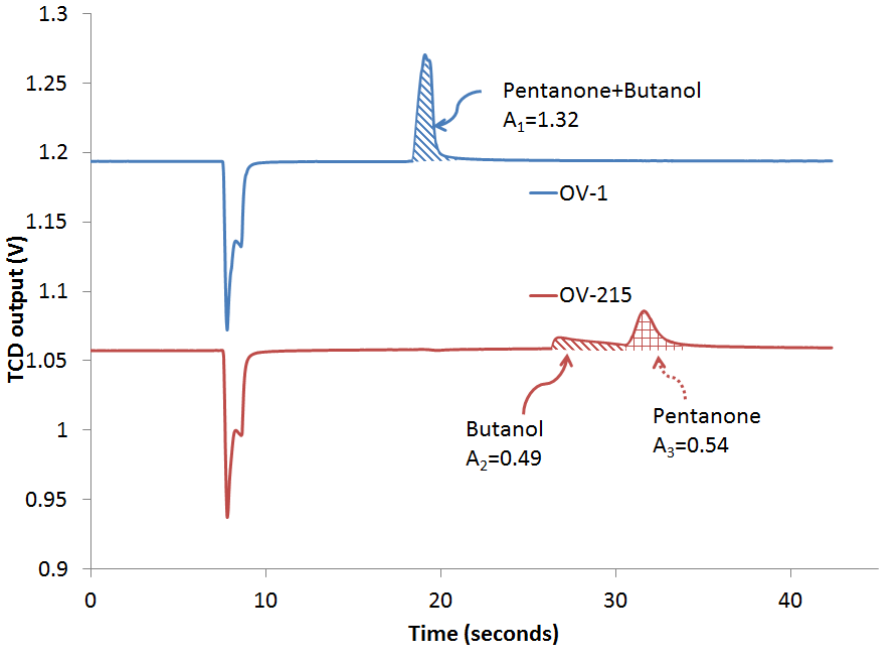

Figure 5-10: Plot shows the TCD response from a series coupled integrated column of OV-1 and OV-215. The single co-eluting peak of 3-pentanone and 1-butanol, at the end of OV-1, have an area of 1.32 A.U. Whereas, at the outlet of the OV-215 they are elute as two separate peaks with individual areas 0.49 and 0.54 A.U., respectively. $A_1 \approx 1.2*A_2+1.3*A_3$, as expected.

For three successive runs for the same mixture, the maximum error in the predicted value of A_1, based on the measured values for A_2 and A_3 and the previously determined κ for 3-pentanone and 1-butanol was 20%. This serves as an alternative approach to determine the possibility of an unknown compound having co-eluted in a known peak, by comparing the area of the corresponding peak in the series connected column.

5.4.3 Comparison with other multi-dimensional techniques

Multi-dimensional techniques such as multi-dimensional GC (MDGC) and comprehensive GC operate on a similar tiered structure with coupled columns. They rely on sequentially separating each peak in a succeeding tier using a fast and short column. At the end

of the final tier column, is a high-speed detector capable of resolving 100ms wide peaks. On the other hand, matrix GC has multiple low-speed detectors. Even in the case of correlation between the selectivities of any two elution trains, the redundancy strengthens the qualitation aspect when working with unknown samples.

The strength of matrix GC lies in its clean interface for the end user. The absence of run-time flow switching, timing optimization for optimal analysis etc. provides a less complicated tool which is, however, more powerful than a single column. The increase in the peak capacity was theorized earlier. There is no practical limit on cascading another column of a different stationary phase in series and the peak capacity of successive tiers does not decrease. Such a three-tier system will require larger operating pressure and increase analysis time. However, in the case of comprehensive GC, where peak capacities of different tiers multiply, each succeeding tier has significantly reduced peak capacities requiring even more stringently constrained detectors and powerful data acquisition methods. All this contributes to increasing the cost of the multidimensional system for the end user.

5.5 Inference

Looking forward, the various modules operated in parallel can add significantly to the separation efficiency. While the 75°C separation reduces resolution due to closely spaced peaks, it enables detection of compounds with higher boiling points (~200°C). Operating different modules at different temperatures can thus enable detection of the entire set, with each module focusing on a different set of boiling point ranges. The entire separation is performed in reduced time due to the parallel processing.

REFERENCES

[1] H. J. Cortes, *et al.*, "Comprehensive two dimensional gas chromatography review," *Journal of Separation Science*, vol. 32, no. 5-6, pp. 883-904, 2009.

[2] L. H. Wright, *et al.*, "Prediction of retention times in temperature-programmed multichromatography," *Journal of Chromatography A*, vol. 540, no. 0, pp. 311-322, 1991.

[3] F. Garay, "Application of a flow-tunable, serially coupled gas chromatographic capillary column system for the analysis of complex mixtures," *Chromatographia*, vol. 51, no. 1, pp. S108-S120, 2000/01/01 2000.

[4] J. V. Hinshaw, Jr., *et al.*, "Selectivity tuning of serially connected open-tubular (capillary) columns in gas chromatography. Part II. Implementation," *Chromatographia*, vol. 21, no. 12, pp. 669-680, 1986/12/01 1986.

[5] J. B. Phillips, *et al.*, "Comprehensive two-dimensional gas chromatography: a hyphenated method with strong coupling between the two dimensions," *Journal of Chromatography A*, vol. 856, no. 1–2, pp. 331-347, 1999.

[6] J. Harynuk, *et al.*, "Comprehensive two-dimensional gas chromatography in stop-flow mode," *Journal of Separation Science*, vol. 27, no. 5-6, pp. 431-441, 2004.

[7] T. Veriotti, *et al.*, "High-Speed Characterization and Analysis of Orange Oils with Tandem-Column Stop-Flow GC and Time-of-Flight MS," *Anal. Chem.*, vol. 74, no. 21, pp. 5635-5640, 2002/11/01 2002.

[8] J. J. Whiting, *et al.*, "High-speed two-dimensional gas chromatography using microfabricated GC columns combined with nanoelectromechanical mass sensors," in *TRANSDUCERS*, 2009, pp. 1666-1669.

[9] S.-J. Kim, *et al.*, "Microfabricated thermal modulator for comprehensive two-dimensional micro gas chromatography: design, thermal modeling, and preliminary testing," *Lab on a Chip*, vol. 10, no. 13, pp. 1647-1654, 2010.

[10] J. Liu, *et al.*, "Smart multi-channel two-dimensional micro-gas chromatography for rapid workplace hazardous volatile organic compounds measurement," *Lab on a Chip*, vol. 13, no. 5, pp. 818-825, 2013.

[11] P. Boeker, *et al.*, "Comprehensive Theory of the Deans' Switch As a Variable Flow Splitter: Fluid Mechanics, Mass Balance, and System Behavior," *Anal. Chem.*, vol. 85, no. 19, pp. 9021-9030, 2013/10/01 2013.
[12] G. Serrano, *et al.*, "Comprehensive Two-Dimensional Gas Chromatographic Separations with a Microfabricated Thermal Modulator," *Anal. Chem.*, vol. 84, no. 16, pp. 6973-6980, 2012/08/21 2012.
[13] M. Pursch, *et al.*, "Modulation techniques and applications in comprehensive two-dimensional gas chromatography (GC×GC)," *Analytical and Bioanalytical Chemistry*, vol. 373, no. 6, pp. 356-367, 2002/07/01 2002.
[14] E. B. Ledford, *et al.*, "GC3: Comprehensive Three-Dimensional Gas Chromatography," *Journal of High Resolution Chromatography*, vol. 23, no. 3, pp. 205-207, 2000.
[15] B.-X. Chen, *et al.*, "A multidimensional micro gas chromatograph employing a parallel separation multi-column chip and stop-flow [small mu]GC [times] [small mu]GCs configuration," *Lab on a Chip*, vol. 13, no. 7, pp. 1333-1341, 2013.
[16] D. Chen, *et al.*, "Smart Three-Dimensional Gas Chromatography," *Anal. Chem.*, vol. 85, no. 14, pp. 6871-6875, 2013/07/16 2013.
[17] S. C. Terry, *et al.*, "A gas chromatographic air analyzer fabricated on a silicon wafer," *Electron Devices, IEEE Transactions on*, vol. 26, no. 12, pp. 1880-1886, 1979.
[18] G. E. Spangler, "Relationships for modeling the performance of rectangular gas chromatographic columns," *Journal of Microcolumn Separations*, vol. 13, no. 7, pp. 285-292, 2001.
[19] S. Reidy, *et al.*, "High-Performance, Static-Coated Silicon Microfabricated Columns for Gas Chromatography," *Anal. Chem.*, vol. 78, no. 8, pp. 2623-2630, 2006.
[20] S. Narayanan, *et al.*, "Two-Port Static Coated Micro Gas Chromatography Column With an Embedded Thermal Conductivity Detector," *Sensors Journal, IEEE*, vol. 12, no. 6, pp. 1893-1900, 2012.
[21] S. Narayanan, *et al.*, "Fabrication and Characterization of a Suspended TCD Integrated With a Gas Separation Column," *J. Microelectromech. Syst.*, vol. 22, no. 5, pp. 1166-1173, 2013.
[22] J. C. Giddings, "Two-Dimensional Separations: Concept and Promise," *Anal. Chem.*, vol. 56, no. 12, pp. 1258A-1270A, 1984/10/01 1984.
[23] J. C. Giddings, "Concepts and comparisons in multidimensional separation," *Journal of High Resolution Chromatography*, vol. 10, no. 5, pp. 319-323, 1987.
[24] T. Veriotti, *et al.*, "A Tandem Column Ensemble with an Atmospheric Pressure Junction-Point Vent for High-Speed GC with Selective Control of Peak-Pair Separation," *Anal. Chem.*, vol. 73, no. 4, pp. 813-819, 2001/02/01 2001.
[25] J. V. Hinshaw, Jr., *et al.*, "Selectivity tuning of serially connected open-tubular (capillary) columns in gas chromatography. Part I: Fundamental relationships," *Chromatographia*, vol. 21, no. 10, pp. 561-572, 1986/10/01 1986.

6

A Prototype Micro-Discharge Ionization Detector for Gas Sensing

Shree Narayanan, Gary Rice, and Masoud Agah

Detectors for micro-gas chromatography (μGC) are as diverse as the applications using GC [1-10]. They are broadly classified as selective and universal detectors. Universal detectors typically monitor a bulk property of the carrier gas for changes in the presence of analytes such as thermal conductivity [11-13]. These detectors tend to be simple in construction. However, they are characterized by low sensitivity since bulk properties of the carrier gas can be significantly affected by external parameters such as temperature and flow rate in addition to the presence of analytes. This lack of sensitivity led to the development of selective detectors which respond to a specific property of analytes and are thus relatively insensitive to the carrier gas. Some examples are flame ionization detectors (FID), chemiresistors, flame photometric detectors (FPD), and electron capture detectors (ECD) [14-16]. The FID is the most widely used detector in conventional GCs because of the near universal detection of any organic compound, broad linear range in response, and absolute limits of detection in the pg range for hydrocarbons. However, the need to provide additional hydrogen and air gas supplies makes it less desirable for portable applications. Reduction in the flame size also decreases the ionization power and, subsequently, the efficiency of detecting higher molecular weight analytes [17]. Polymer-based absorptive sensors, in spite of their simple construction, have a very poor time response when compared to FID [18]. Fabry-Perot type optical sensors reach detection limits in the low picograms but are not suitable for a low-power environment since they require a laser, spectrometer/photodetectors, and beam splitter/collimator [19, 20]. As recent as 2012, peer researchers in micro-based systems have emphasized the need for an improved detector [21]. Such a detector should 1) have low detection limits, 2) consume very low power, 3) can be batch-fabricated easily, and 4) is preferably non-destructive and non-selective for analytes. Herein, we report on the initial

development of a micro-plasma based photoionization detector fabricated by a simple lift-off process that possesses all the favorable qualities identified above.

Gas detectors can be broadly categorized into two groups: concentration sensitive (CSD) and mass sensitive (MSD). CSDs are more pliable to miniaturization without loss of sensitivity compared to MSDs [22]. While this is true, it is also found that dependence on concentration makes a detector respond to the bulk (carrier gas), thereby causing higher background noise levels in CSDs. Therefore, MSDs can outperform CSDs with regard to Minimum Detectable Quantity (MDQ) when miniaturized.

Plasma-based micro-gas detectors, which are mass sensitive, were first introduced in 1999; Eijkel reported on a DC microplasma across Cr/Au thin film electrodes at reduced pressure [23]. Analyte molecules, when passed through this plasma, were fragmented and the resulting atomic emission lines observed with a spectrophotometer. Though this discharge was characterized by a 2 hour lifetime, the same group later developed an atmospheric pressure DC microplasma that operated reliably at 9mW for 24 hours without noticeable degradation [24]. Mitra proposed innovative electrode configurations that reduced the energy discharged in a pulsed plasma, and in the process was able to detect 50ppm of acetone vapor [25]. Both of these detectors relied on the fragmentation of molecules in a micro-plasma which is typically a high-voltage but low power phenomenon. However, the spectrometric detection mechanism is not suitable for miniaturization and can consume up to 10W of operational power [26]. Thus, an alternative sensing mechanism is required in a power-starved environment.

In 2008, Fu reported on the correlation between the current flowing through the plasma and the presence of an analyte [27]. Limits of detection in the tens or hundreds of picograms were demonstrated for different classes of compounds. This device was still susceptible to electrode fouling. The fragmentation of analytes also prevented further analysis. It should be noted that the complete fragmentation of analytes requires that the plasma covers the cross-section of the microfluidic channel. This is not possible if the electrodes are implemented as 1μm thin metal films in a 100-200μm deep channel, which are typical dimensions in batch-fabricated micromachined devices. Few related micromachined detectors for gas chromatography and their features are summarized in Table 6-1.

In 1994, Wentworth reported on the ability to non-destructively photoionize analytes using photons from a pulsed helium plasma [28, 29]. This helium discharge photoionization detector (HDPID) was an improvement over the radioactive electron capture detector (ECD) and a UV-Photoionization detector (UV-PID). The HDPID was assembled using conventionally machined components. We herein demonstrate the first photoionizing gas detector enabled using microfabrication techniques, hereafter referred to as the micro-discharge photoionization detector (μDPID). The following sections describe the fabrication, experimental setup and verification of this new microinstrument for gas detection.

Reference	Detector type	LOD	Fabrication complexity	Power consumption	Remarks
Fu [27]	Plasma emission/ current sensing	25-750pg	Simple but assembled	14.6mW	Portable but destructive on analytes
Mitra [25]	Plasma emission/ spectrometry	50ppm of acetone	Simple but assembled	6.9mA@93V =640mW	Pulsed discharge reduces power
Eijkel [24, 30]	Plasma emission/ spectrometry	1pg of hexane	Simple	9mW	Fouling of electrodes is a serious shortcoming
Reddy [19, 20]	Fabry-Perot optical sensor	sub-ng	Bottom-up assembly	N/A	Laser, photodetector, white light source etc. implies power hungry and bulky
Zimmerman, Kuipers [31, 32]	Flame Ionization detector	195pg of methane	Complex multi-wafer	N/A	Smaller flames reduce ionization and performance
Bae, Kim [33, 34]	Flame Ionization detector	780pg of hexane	Complex multi-wafer	N/A	Consumable hydrogen and oxygen and air supply limits μFID portability and lifetime
Narayanan [35]	Thermal conductivity detector	200ppm of octane	Multi-mask process	50mW	Universal but high power consumption, poor sensitivity

Table 6-1: A listing of detectors related to micro gas chromatography.

6.1 Experimental

6.1.1 Materials

Borosilicate glass wafers (Borofloat 33, Schott, NY) of 700μm thickness and 100mm diameter were used as substrate wafers for fabrication. The separation column was produced from 100mm <100> silicon wafers (Test grade, University Wafers) of 500μm thickness.

Multi-component mixtures of benzene, heptane, toluene and octane (Sigma Aldrich) were prepared by pipetting 100μl of each into an autosampler vial and the headspace above the liquid used as the source for sample injection. A 50-200ppm mixture of octane in air was prepared by pipetting 50μl of analytical grade octane in a custom-made 1L volumetric flask. The mouth of the flask was sealed with a 24/40 septa and left overnight for the octane to volatilize. To prepare a different dilution, the octane in the flask was cleared by removing the septa seal and running the flask through a cycle of nitrogen purge, oven heating at 80°C, and repurging with nitrogen. After letting the flask cool down to room temperature, octane corresponding to the desired dilution was pipetted out, the flask re-sealed and left to homogenize. Capillary tubing of 100μm I.D. and 200μm O.D. (Polymicro TSP100200) served as fluidic interconnects between the detector and the separation column. Sealing was achieved with a two-part epoxy (Epoxy 907, Miller Stephenson). Polydimethylsiloxane (OV-1, Ohio Valley, OH) was used as the stationary phase coating for the separation column.

6.1.2 Fabrication of the detector

To fabricate the microfluidic channels, a (bottom) Borofloat wafer was blanket deposited with 50nm/30nm chromium/gold by e-beam physical vapor deposition (PVD-250, Kurt Lesker). AZ9260 was spun-coated and lithographically patterned with the first mask that exposes an area corresponding to the feed through for the electrodes. After etching the chromium and gold layers, Borofloat was shallow etched to a depth of 10μm using a 10:1 HF/HCl mixture (Figure 6-1(a)). Following this, the mask was completely stripped off and a 50nm/30nm chromium/gold was blanket deposited once again. AZ9260 was spun-coated and patterned with a second mask to expose areas where Borofloat has to be deep etched, as shown in Figure 6-1(b). This area corresponds to the fluidic channel and bond pads. A 10:1 HF/HCl was utilized once again to etch to a depth of 250μm. The mask was then completely stripped off.

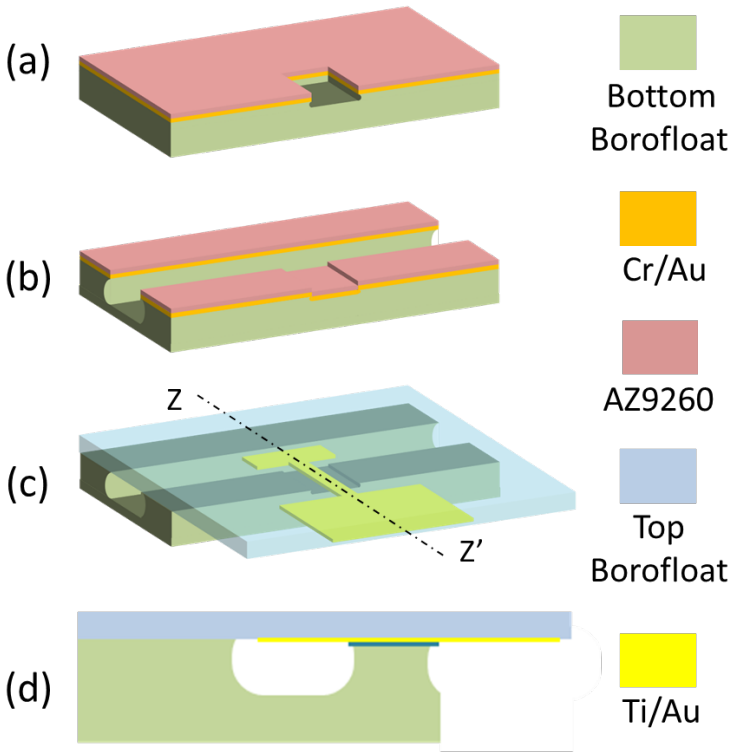

Figure 6-1: Process flow for the fabrication of the detector. The bottom substrate is successively (a) shallow etched and (b) deep etched with patterned Cr/Au/AZ9260 as the mask. (c) shows a top substrate containing patterned Ti/Au as electrodes epoxied to the bottom substrate. (d) cross section of the device along the ZZ' axis.

The top Borofloat wafer was spun-coated with AZ9260 and patterned. A 1μm/30nm titanium/gold stack was e-beam deposited and patterned by lift-off. Both the wafers were diced into individual devices and bonded together with epoxy (Figure 6-1(c)). Capillary tubing was slid

into the channel exits and epoxied in place. A picture of the completed assembly is shown in Figure 6-2.

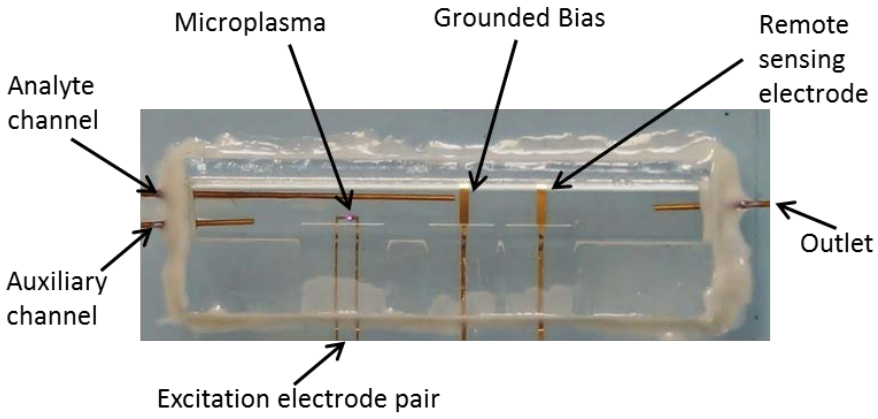

Figure 6-2: An optical image of the packaged detector. The microplasma is visible across the 20μm excitation electrode pair gap.

6.1.3 Fabrication of the separation column

The separation column was also fabricated using standard micromachining procedures as detailed in our previous publications [36]. The column consists of a serpentine microfluidic channel etched in silicon and capped with a borosilicate glass. The channels are anisotropically etched in an Alcatel DRIE AMS-100 by the Bosch process to a depth of 240μm. The width and length of the channel are designed to be 70μm and 2m, respectively. The silicon and glass wafers are anodically bonded for a good seal. The capillary tubes are sealed in place for the inlet and outlet fluidic interconnects using epoxy. The channel is then filled with a solution of 6mg ml^{-1} polydimethylsiloxane in pentane. With one end sealed with wax, a vacuum is pulled at the other end, causing pentane to evaporate and leave behind a coating of the stationary phase on the walls of the microfluidic channel.

6.1.4 Measurement setup

A diagram of the complete configuration for chromatographic testing and plasma diagnostics is depicted in Figure 6-3. An Agilent 5890 oven, set to an ambient temperature of 20°C and fitted with two electronic pressure control (EPC) inlets and an FID, was used to test the detector. Ultra high purity helium (UHP 300, Airgas) was used as the carrier gas. Industrial grade air (AIB 300, Airgas) and hydrogen generated by a hydrogen generator (Model 20H, Domnick Hunter) provided the FID gas supplies. One end of the MEMS-separation column was connected to Inlet A of the oven held at 14psi as shown in Figure 3. The split flow on this inlet was set to 100sccm to only allow 1/100 of the sample volume injected to reach the column. The other end of the column was connected to the analyte channel of the detector. The analyte channel bypassed the plasma which is fed by helium from Inlet B, held at 3psi, through the auxiliary channel. Both inlets and the FID were maintained at 280°C. A picoammeter (Model 480, Keithley) was used to

detect the signal from the remote electrode while a LabVIEW program recorded the measurement from the rear-terminal output viz. a Keithley 2700. A gas tight syringe (Model 1701, Hamilton) was used for making manual injections of samples during testing.

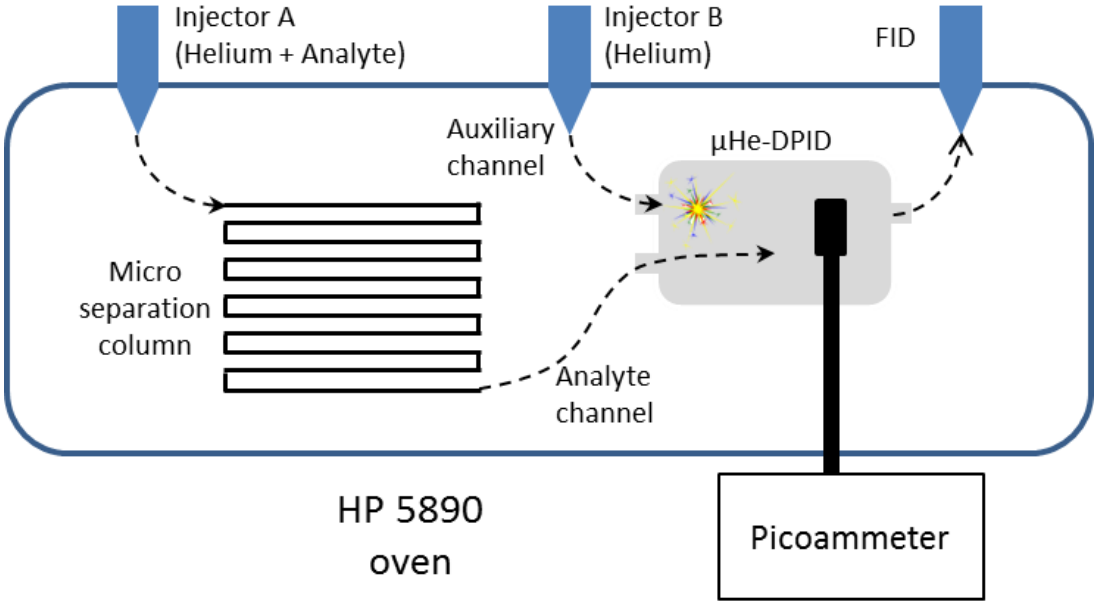

Figure 6-3: Setup of the detector within the HP5890. The high voltage source and the excitation electrodes are not shown.

6.2 Results and discussion

6.2.1 Plasma characterization

The plasma was first characterized by exposing an uncapped-device to ambient air. For IV-curve extraction, a 100MΩ resistor and a 10MΩ resistor were connected in series with the excitation electrodes exposed to air, and observed under a microscope. A high voltage power supply (PS-310, Stanford Research Systems) sources the "applied voltage" which is stepped up in increments. A Keithley 2700 DMM was used to measure the voltage across the 10MΩ resistor. The current through the plasma was deduced from the voltage across the 10MΩ resistor and plotted as shown in Figure 6-4. For 525V and lesser, the current measured was on the order of tens of nanoamperes. At 550V an unstable plasma was observed with the current changing anywhere between tens of nanoamperes and a microampere. Beyond 550 V, a stable plasma was sustained and the current increased with applied voltage.

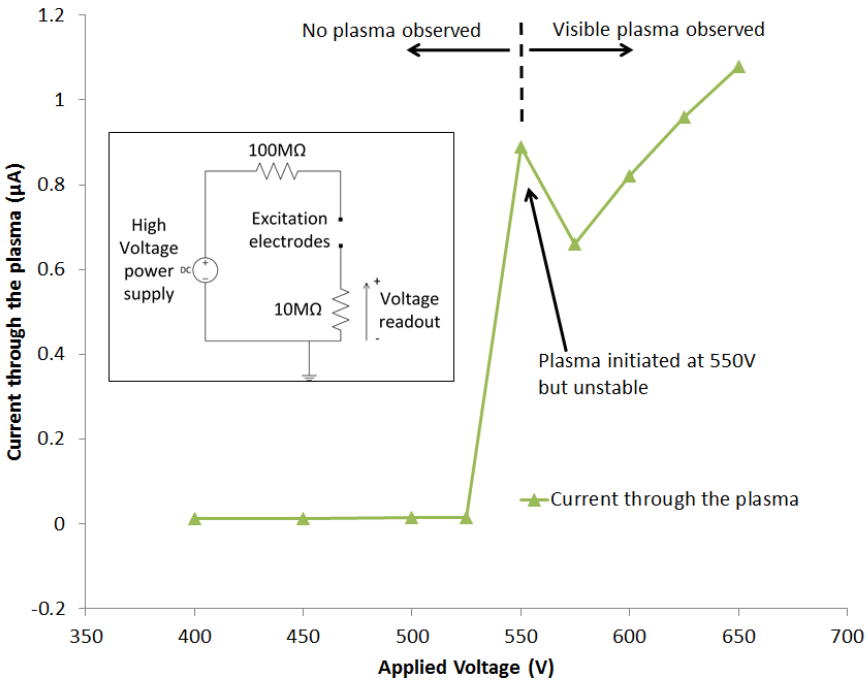

Figure 6-4: Current through the plasma as a function of the applied voltage

Paschen's law relates the breakdown voltage across a gap as a function of the product of distance (d) across the gap and the pressure (p).

$$V = \frac{apd}{\ln(pd)+b} \qquad \textbf{6-1}$$

Here, the empirically derived values for a and b are 4.36×10^{7} V/(atm.m) and 12.8, respectively. Correspondingly, for p = 1atm and d = $20\text{x}10^{-6}$m in air, the breakdown voltage is deduced to be 440V. It should be noted that this voltage is strongly dependent on the electrode material, substrate and pressure, thus the deviation in the measured breakdown voltage can be attributed to this variation. However, for an applied voltage of 575V and higher, the current is found to roughly increase linearly with the applied voltage. The dynamic resistance within this section is calculated to be 68.6MΩ.

The long term stability of the plasma was monitored by applying an excitation voltage of 600V and monitoring the readout voltage across the 10MΩ resistor. After 4 hours of operation, a 2-hour long measurement of the voltage was made as shown in Figure 6-5. The deviations are characteristic of variations in the ambient environment. The overall plot does not show a trend which would otherwise indicate a gradual deterioration of the excitation electrodes.

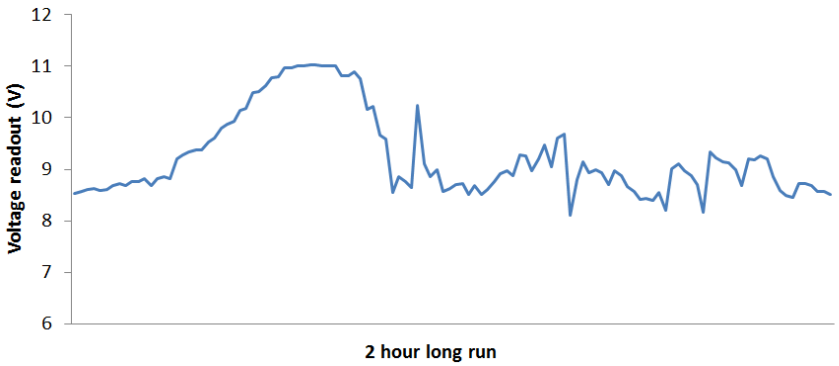

Figure 6-5: A plot of the voltage across the 10MΩ resistor for a 2-hour long duration.

The device was then capped and packaged as described in the fabrication section. The plasma was produced at 700V with a helium flow of 1sccm. The photon energy from the helium plasma is sufficiently energetic to ionize analytes as they exit the analytical channel. The power dissipation for the detector was determined to be 1.4mW with a current of 2.4μA. The higher operating current, compared to 1μA when the plasma is exposed to ambient conditions, is attributed to the flow of helium at 1sccm and the parasitics accompanying the epoxy seal around the feed throughs.

6.2.2 Mass dependence of the detector

With 700VDC applied across the 20μm electrode gap, various quantities of air were injected into the separation column using the setup shown in Figure 6-3, and the corresponding peak on the detector recorded. Air is not retained on the polydimethylsiloxane stationary phase and hence elutes in a few seconds. The corresponding peak is integrated to obtain a count which is plotted in Figure 6-6 against the amount injected. Apart from the universality of the detector, this plot shows a dependence on the injected quantity of sample which is characteristic of a mass sensitive detector (MSD).

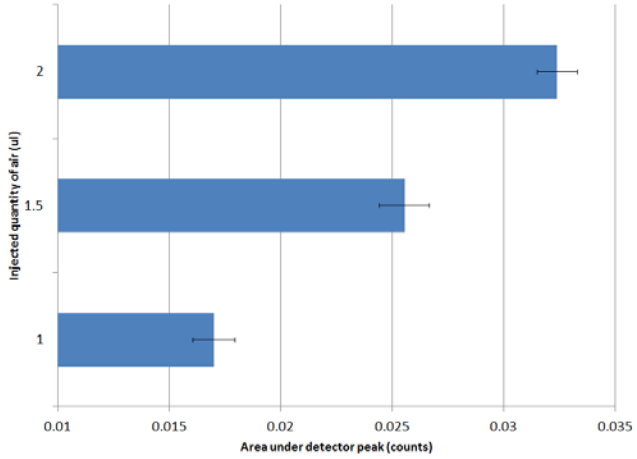

Figure 6-6: Variation in detector response with injected quantity of air

6.2.3 Effect of concentration

The detector response was also determined as a function of the concentration of octane in air at 50, 100, and 200ppm concentrations prepared as described in the Materials section. A 1µl sample volume was injected into the separation column with the split ratio set to 1/100 on the HP5890 injector and an oven temperature of 20°C. Comparisons of the signals obtained are shown in Figure 6-7. A 15-point moving average filter was used to smooth the high-frequency noise. The signal-to-noise-ratios (SNR) were calculated to be 3.4, 8.1 and 13.2 respectively. Thus, the demonstrated Limit of Detection (LOD) for this detector is approximately 50ppm for octane, which translates to an absolute mass of approximately 350pg.

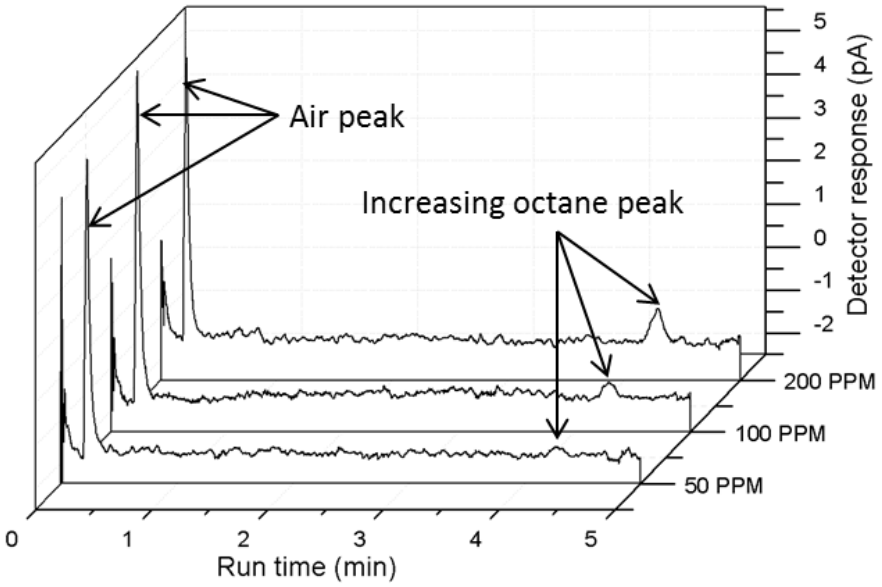

Figure 6-7: A comparative plot of 1µl injections of 50, 100 and 200ppm concentrations (volume/volume) of octane in air

6.2.4 Multi-component detection

A 1µl sample from a headspace mixture of benzene, heptane, toluene and octane, prepared as mentioned in the Materials section, was drawn into the syringe with an additional 1µl of ambient air, resulting in the injection of a 2µl volume into the separation column. Figure 6-8 is a chromatogram of the eluted components as detected by the µDPID and the FID. The outlet capillary tube that follows the µDPID and connects it to the FID introduces a delay, accounting for the increased retention times in the FID. The universality of the µDPID is exemplified in that air in the sample is detected. Aromatics and aliphatic compounds are also detected with a similar response to the FID. Aromatics, however, show a small hump in the tail, whose origin will be ascertained in future investigations.

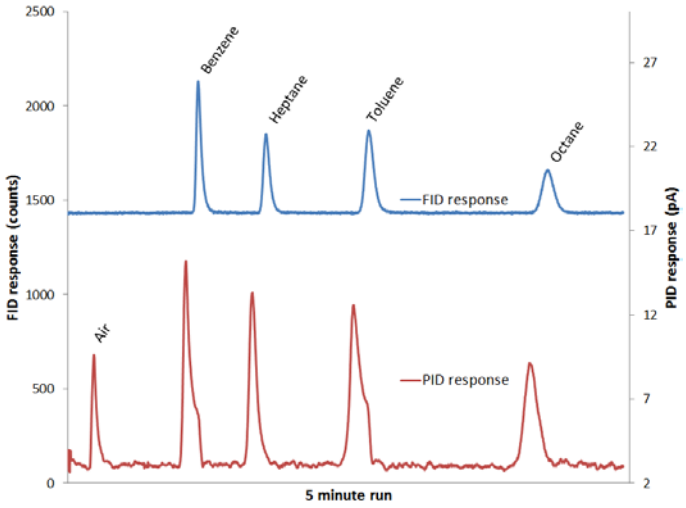

Figure 6-8: The chromatogram of a 2µl sample of 4-component mixture of benzene, heptane, toluene and octane in air. The PID response is similar to the FID response other than the initial peak for air.

6.3 Inference

A uniquely simple, rudimentary, yet sensitive miniaturized µDPID has been demonstrated as a promising detector for µGC systems. The encouraging LOD presented is expected to improve with modifications to the collector electrode design and orientation of the plasma relative to the analytical column. The absence of additional gases such as hydrogen or water electrolyzer units coupled with the universality and non-destructive nature are expected to make it a more suitable candidate for space exploration than ng-sensitive µFIDs [33]. Commercial off-the-shelf DC-DC converter and picoammeter measuring modules consuming 0.5W and 1W of operational power make it suitable for portable, low power applications. The lifetime of these devices is currently under study and could also be improved by utilizing sophisticated pulsing schemes and electrode structures [25].

REFERENCES

[1] G. Monti, *et al.*, "Monitoring Food Quality by Microfluidic Electrophoresis, Gas Chromatography, and Mass Spectrometry Techniques: Effects of Aquaculture on the Sea Bass (Dicentrarchus labrax)," *Anal. Chem.*, vol. 77, no. 8, pp. 2587-2594, 2005.

[2] D. Puente, *et al.*, "Thermal conductivity microsensor for determining the Methane Number of natural gas," *Sens. Actuators B Chem*, vol. 110, no. 2, pp. 181-189, 2005.

[3] R. W. Cernosek, *et al.*, "Micro-analytical systems for national security applications," in *Proc. SPIE-Micro (MEMS) and Nanotechnologies for Space Applications*, Orlando (Kissimmee), FL, USA 2006, p. 622306.

[4] D. Nielsen, *Practical handbook of environmental site characterization and ground-water monitoring*: CRC press, 2006.

[5] A. D. Radadia, *et al.*, "Micromachined GC Columns for Fast Separation of Organophosphonate and Organosulfur Compounds," *Anal. Chem.*, vol. 80, no. 11, pp. 4087-4094, 2008.

[6] B. Alfeeli, *et al.*, "MEMS-Based Selective Preconcentration of Trace Level Breath Analytes," *IEEE Sensors J.*, vol. 9, no. 9, 2009.

[7] M. Akbar, *et al.*, "A Microfabricated Propofol Trap for Breath-Based Anesthesia Depth Monitoring," *J. Microelectromech. Syst.*, vol. PP, no. 99, pp. 1-9, 2012.

[8] H. Shakeel, *et al.*, "First reconfigurable MEMS separation columns for micro gas chromatography," in *Micro Electro Mechanical Systems (MEMS), 2012 IEEE 25th International Conference on*, 2012, pp. 823-826.
[9] S. K. Kim, *et al.*, "Microfabricated Gas Chromatograph for the Selective Determination of Trichloroethylene Vapor at Sub-Parts-Per-Billion Concentrations in Complex Mixtures," *Anal. Chem.*, vol. 83, no. 18, pp. 7198-7206, 2011/09/15 2011.
[10] H. Shakeel, *et al.*, "Self-Patterned Gold-Electroplated Multicapillary Gas Separation Columns With MPG Stationary Phases," *J. Microelectromech. Syst.*, vol. 22, no. 1, pp. 62-70, Feb. 2013.
[11] S. Showalter, *et al.*, "Design and Testing of a Micro Thermal Conductivity Detector (TCD) System," SAND2003-0954, Sandia National Labs., Albuquerque, NM (US);2003.
[12] F. Rastrello, *et al.*, "Thermal Conductivity Detector for gas-chromatography: Acquisition system and experimental measurements," in *Instrumentation and Measurement Technology Conference (I2MTC), 2012 IEEE International*, 2012, pp. 1226-1230.
[13] R. Manginell, *et al.*, "A Monolithically-Integrated μGC Chemical Sensor System," *Sensors*, vol. 11, no. 7, pp. 6517-6532, 2011.
[14] S. Zimmermann, *et al.*, "Micro flame ionization detector and micro flame spectrometer," *Sensors & Actuators: B. Chemical*, vol. 63, no. 3, pp. 159-166, 2000.
[15] M. Moorman, *et al.*, "Microcombustor array and micro-flame ionization detector for hydrocarbon detection," in *Proc. SPIE—MEMS Components and Applications for Industry, Automobiles, Aerospace, and Communication II,*, San Jose, CA, USA, 2003, pp. 40-50.
[16] Q.-Y. Cai, *et al.*, "Dual-Chemiresistor GC Detector Employing Monolayer-Protected Metal Nanocluster Interfaces," *Anal. Chem.*, vol. 74, no. 14, pp. 3533-3539, 2002/07/01 2002.
[17] W. Kuipers, *et al.*, "Sensitivity of a planar micro-flame ionization detector," *Talanta*, vol. 82, no. 5, pp. 1674-1679, 2010.
[18] C.-J. Lu, *et al.*, "First-generation hybrid MEMS gas chromatograph," *Lab on a Chip*, vol. 5, no. 10, pp. 1123-1131, 2005.
[19] K. Reddy, *et al.*, "On-chip Fabry–Pérot interferometric sensors for micro-gas chromatography detection," *Sens. Actuators B Chem*, vol. 159, no. 1, pp. 60-65, 2011.
[20] K. Reddy, *et al.*, "Rapid, sensitive, and multiplexed on-chip optical sensors for micro-gas chromatography," *Lab on a Chip*, vol. 12, no. 5, pp. 901-905, 2012.
[21] J. Liu, *et al.*, "Adaptive Two-Dimensional Microgas Chromatography," *Anal. Chem.*, vol. 84, no. 9, pp. 4214-4220, 2012/05/01 2012.
[22] R. Pecsar, *et al.*, "Performance of a reduced volume thermal conductivity detector," *Anal. Chem.*, vol. 45, no. 13, pp. 2191-2198, 1973.
[23] J. C. T. Eijkel, *et al.*, "A Molecular Emission Detector on a Chip Employing a Direct Current Microplasma," *Anal. Chem.*, vol. 71, no. 14, pp. 2600-2606, 1999/07/01 1999.
[24] J. C. T. Eijkel, *et al.*, "A dc Microplasma on a Chip Employed as an Optical Emission Detector for Gas Chromatography," *Anal. Chem.*, vol. 72, no. 11, pp. 2547-2552, 2000.
[25] B. Mitra, *et al.*, "The Detection of Chemical Vapors in Air Using Optical Emission Spectroscopy of Pulsed Microdischarges From Two- and Three- Electrode Microstructures," *Sensors Journal, IEEE*, vol. 8, no. 8, pp. 1445-1454, 2008.
[26] LDetek, Inc. (2012, 04/29/2013). PlasmaDetek: Plasma Emission Detector System for Gas Chromatograph. Available: http://www.ldetek.com/uploads/images/products/pdf/PlasmaDetek.pdf
[27] Y.-M. Fu, *et al.*, "Characteristic responses of an atmospheric pressure DC micro-plasma detector for gas chromatography to organic functional groups," *Microchemical Journal*, vol. 89, no. 1, pp. 7-12, 2008.
[28] D. S. Forsyth, "Pulsed discharge detector: theory and applications," *Journal of Chromatography A*, vol. 1050, no. 1, pp. 63-68, 2004.
[29] W. E. Wentworth, *et al.*, "Pulsed discharge helium ionization detector universal detector for inorganic and organic compounds at the low picogram level," *Journal of Chromatography A*, vol. 688, no. 1–2, pp. 135-152, 1994.
[30] J. C. T. Eijkel, *et al.*, "An atmospheric pressure dc glow discharge on a microchip and its application as a molecular emission detector," *J. Anal. At. Spectrom.*, vol. 15, no. 3, pp. 297-300, 2000.
[31] S. Zimmermann, *et al.*, "Miniaturized flame ionization detector for gas chromatography," *Sensors and Actuators B: Chemical*, vol. 83, no. 1–3, pp. 285-289, 2002.
[32] W. Kuipers, *et al.*, "Characterization of a microelectromechanical systems-based counter-current flame ionization detector," *Journal of Chromatography A*, vol. 1218, no. 14, pp. 1891-1898, 2011.
[33] B. Bae, *et al.*, "Development of a portable gas analyzer using a micro-Gas Chromatograph/Flame Ionization Detector (micro-GC/FID) for NASA's environmental missions," presented at the 42nd International Conference on Environmental Systems, San Diego, California, 2012.
[34] J. Kim, *et al.*, "Development of a micro-flame ionization detector using a diffusion flame," *Sensors and Actuators B: Chemical*, vol. 168, no. 0, pp. 111-117, 2012.
[35] S. Narayanan, *et al.*, "Fabrication and Characterization of a Suspended TCD Integrated With a Gas Separation Column," *Microelectromechanical Systems, Journal of*, vol. PP, no. 99, pp. 1-1, 2013.
[36] S. Ali, *et al.*, "MEMS-based semi-packed gas chromatography columns," *Sens. Actuators B Chem*, vol. 141, no. 1, pp. 309-315, 2009.

7

Characterization of a Micro-Helium Discharge Detector for Gas Chromatography

Shree Narayanan, Gary Rice, and Masoud Agah

Micro gas chromatography (μGC) is based on developing miniaturized, portable systems capable of identifying the composition of a gas mixture by separation into its individual components. Such analyses are highly applicable for homeland security, space exploration, on-site or distributed environmental monitoring mechanisms, food assessment, etc [1-13]. In a typical μGC system, the sample mixture is first collected on an adsorbent bed referred to as the pre-concentrator. When thermally spiked, this device releases the adsorbed species in a sharp vaporized plug. This narrow plug enters a microfluidic channel, called the separation column, which is coated with a stationary phase film to chemically interact and retard the various analytes of the plug to different extents. The analytes are then separated in time and elute out of the column one-by-one into a detector. The movement of the gases through the entire system is facilitated by an inert carrier gas (mobile phase) such as helium or nitrogen.

Miniaturization offers unique advantages such as light-weight, low power consumption, less reagent usage and innovative architectures apart from lower cost when batch fabricated [14-23]. Stereotypical miniaturization utilizes components fabricated in silicon/glass. Common implementations involve etching a narrow bore microfluidic channel in silicon/glass wafers, with capillary dimensions similar to conventional GC columns, or fabricating posts within the silicon cavity and coating with an adsorbent material [24-27]. The primary incentive is the ability to conveniently pack a 1-2 m length tubing (cavity) into a 2 cm x 4 cm x 500 μm silicon die without having to wind equivalent length capillary tubing into a large coil. In addition, heating a silicon die with on-chip heaters is energetically far less taxing compared to heating capillary tubing with a convection oven.

The choices for detectors in the micro-world are numerous. While traditional GC systems are dominated by flame ionization detectors (FID), electron capture detectors (ECD) and flame photometric detectors (FPD), μGC offers the possibility of obtaining signals via other forms of reactive processes using sorptive sensors that transduce into electrical, acoustic or optical domains [28-34]. In general, any concentration-sensitive detector, such as the thermal conductivity detector (TCD), are more pliable to be reduced in size [35, 36]. It should be noted that while ionization detectors such as the FID provide robust performance and sensitivity, efforts to miniaturize them do not yield comparable detection levels since the hydrogen flame loses its ionizing potential when reduced in size [37, 38]. On the other hand, sorptive and thermal sensing detectors have inherent limitations since they are more temperature sensitive and hence their implementation and application has been inadequate as well. Mass spectrometry (MS), considered the gold standard in conventional analytical techniques, has also been subjected to miniaturization. A majority of these efforts has focused on reducing the size of a MS using techniques that are not found in silicon micromachining. This has resulted in dimensions slightly larger than that found in microGC and a power dissipation of on the order of tens of watts [39].

Commercially available μGC systems have adopted a hybrid approach wherein the detector is similar in style to conventional ultraviolet photoionization detectors (UV-PID). These systems offer excellent detection sensitivity, but are somewhat restricted by the photoionization energies available (< 11.7 eV with argon lamps). Micro-discharges or plasmas have also been utilized in gas detectors since 1991. Eijkel et. al. reported on a detector for μGC that fragmented the analytes in a DC microplasma to produce diatomic fragments from which emission was detected spectrophotometrically [40]. Improvements on this technique included an innovative electrode structure to generate pulsed plasma with drastically reduced power consumption [41, 42]. Spectrophotometric detection is an intensive operation that can consume power on the order of watts. An alternative is to monitor the current through the discharge itself as reported by Fu et. al [43]. However, a common concern with these designs is the fouling of the electrodes due to fragmentation of the analytes. Fragmentation also does not allow for the analytes to be subjected to further analysis.

We previously reported on a proof-of-concept micro-helium discharge detector [44] to address the need for a sensitive, low-power, easy-to-fabricate universal detector. This microdischarge utilizes high-energy photons and excited state helium metastable species to ionize the analytes and the resultant current monitored on a remote collector electrode. A limit of detection (LOD) of 350 pg for octane was demonstrated. A similarly designed device has been reported for conventional gas chromatography [45], with low-ppb detection for permanent gases and few watts of power consumption being salient features. Additional design parameters for our μHDID are considered here. Specifically, the effect of the He discharge voltage, distance of the bias electrode from the He discharge, collector electrode from bias electrode and the bias voltage are parametrically studied. The results were used to choose the best design to enhance the LOD.

7.1 Theory

The micro-helium discharge ionization detector (μHe-DID) is an ionization style detector that operates by counting the resultant current from ionization of the analytes without any molecular fragmentation. It utilizes a high voltage DC discharge in helium across a 20 μm gap as the source of high-energy photons and metastable excited helium atoms, which are thought to be the dominant species responsible for the ionization of analyte species. This is partly inspired by a pulsed discharge helium ionization detector that utilizes a pulsing technique to arc across an electrode pair to generate the excitation source [46]. However, an arc-mode plasma discharge is highly unstable, physically deteriorates the electrode, and is unsuitable for implementation on thin-film micromachined electrodes. At low gap dimensions of 10 μm, carrier transport within the discharge tends to be ballistic. This reduces the chance of collisions for an avalanche that can result in a destructive spark. Thus, a stable glow discharge can be sustained at higher pressures without arcing. Figure 7-1 is a schematic showing the concept and design parameters of the detector. Apart from the discharge electrode pair to produce the He micro-discharge, the device also consists of a bias electrode and a remote collector electrode downstream from the microplasma. Analytes contained in a helium carrier from the separation column are introduced into the detector at the bias electrode. The space between the bias and collector electrode defines the "volume of the collector" and dictates to some extent the level of signal response generated.

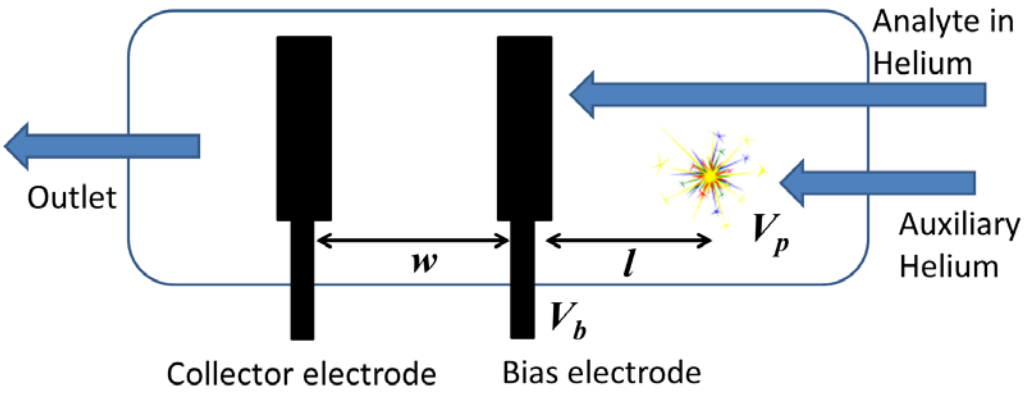

Figure 7-1: A schematic diagram showing the dual-inlet, single-outlet μHDID. The analytes from a micromachined separation column are introduced at the top of the bias electrode, bypassing the auxiliary channel fed helium microdischarge. Ionization of analytes in the region between the two electrodes results in the detector response at the collector electrode. The parameters of interest, namely *l*, *w*, V_p, and V_b are denoted.

When suitably excited, the He discharge results in the generation of a complex mix of positive and negatively charged ions, metastable He atoms, electrons, and photons. These omnidirectional energetic particles constitute what is called the ionizing flux. Some of these particles, such as metastable helium atoms and ions, flow downstream due to the microfluidic pressure. Thus, the ionizing flux at the bias electrode is a mix of positive and negatively charged particles as well as high energy photons and metastable He atoms. The high energy components

of this ionizing flux (normally considered to be photons with energies >10 eV and metastable He atoms with energies of 19.8 eV) are responsible for ionization of analyte species eluting from the GC column. The transmission of this flux through the detector volume decays exponentially due to absorption, and is given by

$$I_b = I_0 e^{-\alpha l} \qquad \textbf{7-1}$$

I_b, the flux observed at the bias electrode is related to the initial discharge emission I_0 by Beer-Lambert's law for photon flux transmission. α is the absorption coefficient of helium over the length of the detector *(l)* from the He discharge to the bias electrode. One can rationalize that l should be minimized to increase the flux density available at the bias electrode. On a similar note, the gap width w should be maximized to increase the total flux available within the collector volume for analyte species where the photon flux needs to be absorbed to the maximum extent within the collector volume. However, recombination processes with electrons within this volume can cause a portion of the generated carriers to be neutralized and hence not detected. The net effect of these factors determines the distance from the collector electrode in which a generated charge carrier will result in a favorable current. In the presence of a bias voltage, the effect of an electric field between closely spaced bias and collector electrodes can be advantageous in isolating the generated carriers within the collector volume more efficiently. The lifetime of metastable He species available for collisional energy transfer to analyte species will be a factor as well. A number of these considerations are considered in the following discussions.

7.2 Experimental

7.2.1 Materials and sample preparation

Borosilicate glass wafers (Borofloat 33, Schott, NY) of 700 μm thickness and 100 mm diameter were used as substrate wafers for fabrication of the microplasma devices. The separation columns were prepared from 100 mm <100> silicon wafers (Test grade, University Wafers, MA) of 500 μm thickness.

For the design characterization experiments, the headspace of a 1.8 mL autosampler vial filled with about 120 μL of reagent grade n-octane served as the source for constant vapor phase concentrations for gas-phase injections. For the limit-of-detection (LOD) experiments, 25 to 200 μL of analytical grade n-octane were pipetted into a custom-made 1 L volumetric flask. The mouth of the flask was sealed with a 24/40 septa and left overnight for the octane to volatilize. To prepare a different dilution, the octane in the flask was cleared by removing the septa seal and running the flask through a cycle of nitrogen purging, oven heating at 80°C, and repurging with nitrogen. After letting the flask cool down to room temperature, the volume of octane

corresponding to the desired concentration was pipetted into the flask which was then re-sealed and left to homogenize.

7.2.2 Fabrication

The detector was constructed from two Borofloat wafers. To fabricate the microfluidic channels, a (bottom) Borofloat wafer was blanket deposited with 50 nm/30 nm chromium/gold by e-beam physical vapor deposition (PVD-250, Kurt Lesker). Photoresist (AZ9260) was spun-coated and lithographically patterned with the first mask that exposes an area corresponding to the fluidic channels and bond pads. After etching the chromium and gold layers, the Borofloat was deep etched to a depth of 260 μm using a 10:1 HF/HCl mixture Figure 7-2(a). Following this, the mask was completely stripped off. The top Borofloat wafer was spun-coated with AZ9260 and patterned. A 1 μm/25 nm titanium/gold stack was e-beam deposited and patterned by lift-off. Both of the wafers were diced into individual devices and bonded together with epoxy (Figure 7-2 (d)). Capillary tubing of 100 μm I.D. and 200 μm O.D. (Polymicro TSP100200) were slid into the channel exits. Sealing was achieved with a two-part epoxy (Epoxy 907, Miller Stephenson, Danbury, CT). A picture of the completed assembly is shown in Figure 7-2 (ii). A 80 μm-wide, 240 μm-deep and 1 m-long micromachined separation column was fabricated using a standard process described elsewhere [44] for the octane separations. Polydimethylsiloxane (OV-1, Ohio Valley, OH) was used as the stationary phase to static coat the separation column [47].

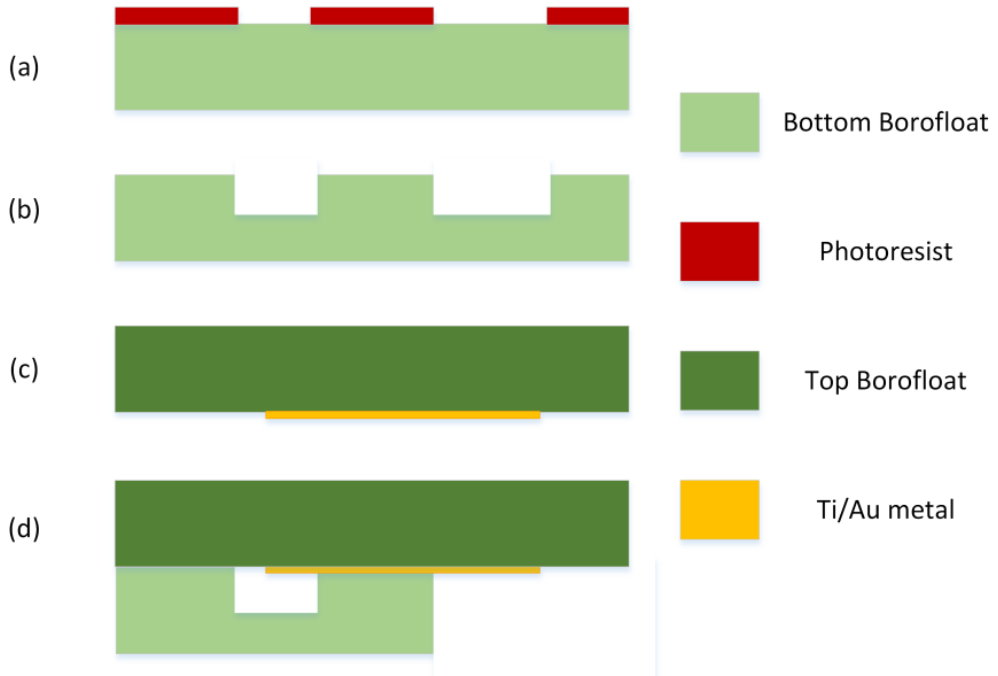

(i)

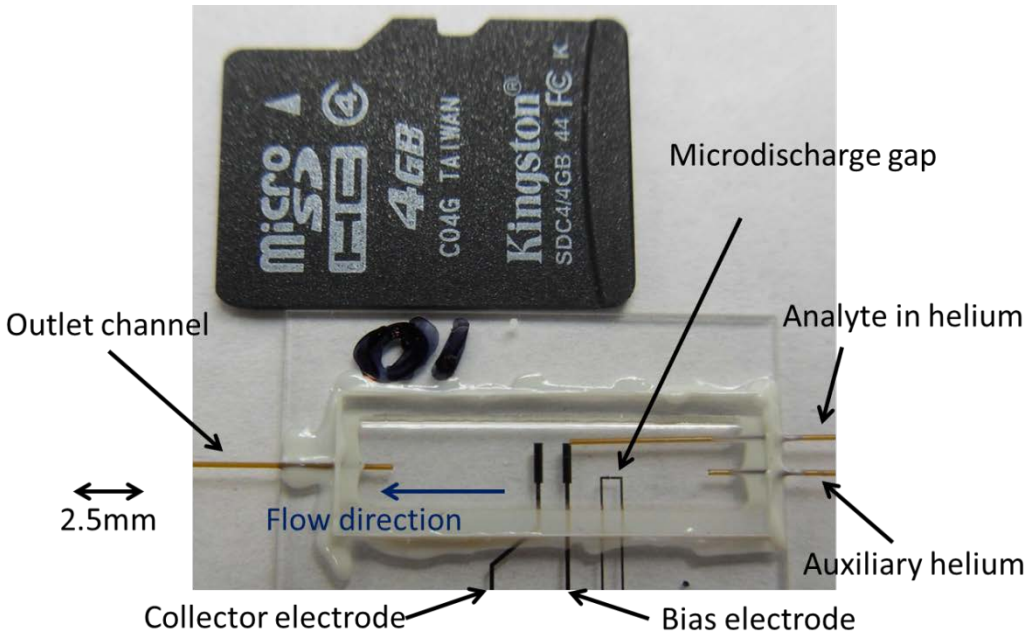

(ii)

Figure 7-2: (i) Top image shows the fabrication of the detector using Borofloat wafers. The top bottom wafer is patterned in (a), and wet etched and stripped in (b) to obtain the microfluidic channels. In (c) a lift-off on top wafer deposits the patterned metal structures for the electrodes. The wafers are diced and epoxy-bonded in (d). An optical image of the µHDID right next to a micro-SDcard is shown at the bottom in (ii).

A listing of the devices compared and their design parameters are provided in Table 7-1 and illustrated in Figure 7-1. Devices within design parameter sets 1-3 were fabricated with a fixed bias to collector-electrode distance *(w=2.5 mm)* but vary with the distance of the bias electrode from the He discharge *(l)*. Devices within design parameter sets 4- 6 have the bias electrode at a fixed distance from the He discharge *(l=1.5 mm)* but vary in the distance of the collector from the bias *(w)*. The third column provides the distance from the midpoint between the collector and bias electrodes to the He discharge. Its significance will be discussed in a later section.

Design #	Length *l* (mm)	Gap width *w* (mm)	Discharge to gap midpoint (*l*+*w*/2), (mm)
1	5	2.5	6.25
2	3	2.5	4.25
3	1.5	2.5	2.75
4	1.5	1	2
5	1.5	2	2.5
6	1.5	3	3

Table 7-1: Six different designs with values for the parameters *l* (distance between the He discharge and bias electrode) and *w* (distance between the bias and collector electrode). The distance from He discharge to the midpoint of the gap between the electrodes is calculated in the fourth column from the previous two. Multiple devices of the same design were tested in most cases.

7.2.3 Measurement Setup

A GC oven (Model 7890, Agilent, Santa Clara, CA), fitted with two electronic pressure control (EPC) inlets and an FID was used to test the detector. A G4513A autosampler was fixed to Inlet A of the GC when automated injections were required. The automated injection was configured for two sample priming events followed by drawing 1 µl from the 1.8 ml autosampler vials, all at a depth of 10 mm, to ensure consistent gas phase injections. A gas tight syringe (Catalog number 80000, Hamilton Syringe Company, Reno, NV) was used for making manual injections of samples during LOD testing. Ultra high purity helium (UHP 300, Airgas) was used as the carrier and auxiliary gases. Industrial grade air (AIB 300, Airgas) and hydrogen generated by a hydrogen generator (Model 20H, Domnick Hunter) provided the FID gas supplies. One end of the separation column was connected to Inlet A of the GC held at 14 psi. The split flow on this inlet was set to allow 1/150 of the sample volume injected to reach the column. The other end of the column was connected to the analyte channel of the detector. The analyte channel bypassed the He discharge, which was fed by a helium flow from Inlet B of the GC at 4 psi, resulting in a 0.22 mL/min flow rate through the auxiliary channel. Both inlets and the FID were maintained at 280°C whereas the µHDID was maintained at ambient temperature. A picoammeter (Model 480, Keithley, Cleveland, OH) was used to detect the signal from the remote electrode while a LabVIEW (National Instruments, Austin, TX) program recorded the measurement from the rear-terminal output viz. a digital multimeter (Model 2700, Keithley, Cleveland, OH). High voltage power supplies (PS310, Stanford Research Systems, Sunnyvale, CA) were used to provide the voltage necessary for the He discharge as well as the bias electrode voltage.

7.3 Results and discussion

7.3.1 Long duration operation

We have previously shown the onset of the He discharge from the current-voltage (IV) characteristics of a static 20 µm spark gap on thin film microelectrodes. A 550 V breakdown voltage was reported to initiate the He discharge in an unsealed environment beyond which a resistive current-voltage characteristic is observed. Here, however, the microgap electrodes are packaged and connected to the power supply. A 550 V DC potential was applied through a 50 MΩ resistor with the bias electrode grounded, and the current from the collector electrode recorded through the picoammeter. In order to study the empirical impacts of the signals generated over long time intervals, a 1 µL headspace of octane was injected from an autosampler every 1.5 hours over 24 hours of continuous operation and the response of the detector recorded. Figure 7-3 shows a stacked plot of the recordings with the earliest recording to the left. The raw data was smoothed with a 5-point moving average. The first peak corresponds to air, while the smaller peak that elutes at about 0.7 minutes corresponds to octane. The baseline for the detector decreases from its initial value by about 50% to stabilize within 4 hours (as shown in Figure 7-4). This “burn-in” period was noticed in the first few hours of every detector and could correspond

to the sputtering off of gold from the electrodes used to produce the discharge as well as removal of contaminant gases and compounds used in the fabrication process. Thereafter, the baseline was observed to be relatively stable and the detector's response (peak height minus baseline) considered reasonably constant for measurements.

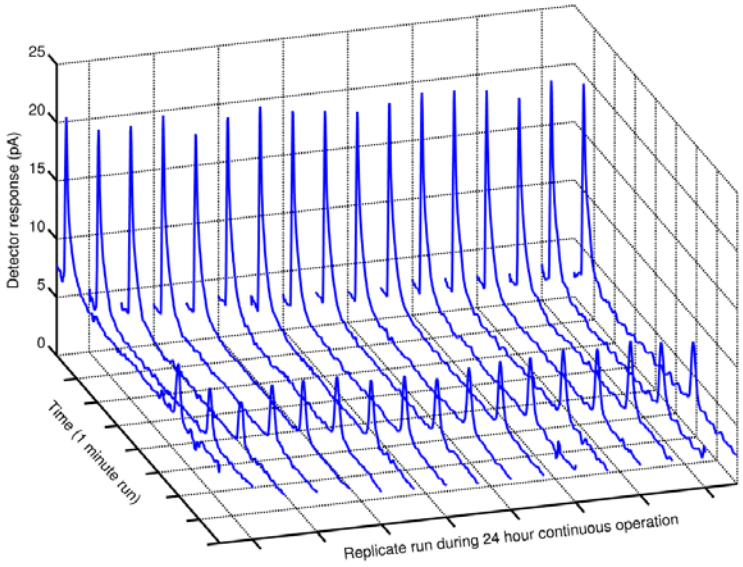

Figure 7-3: A series of chromatographic runs from injections of octane vapor in an autosampler vial headspace as detected by the μHDID. Chromatograms were taken regularly during a 24 hour continuous operation, with the earliest to the left. Each 5-point moving average shows two prominent peaks – a very early large peak due to air and a small late peak due to octane.

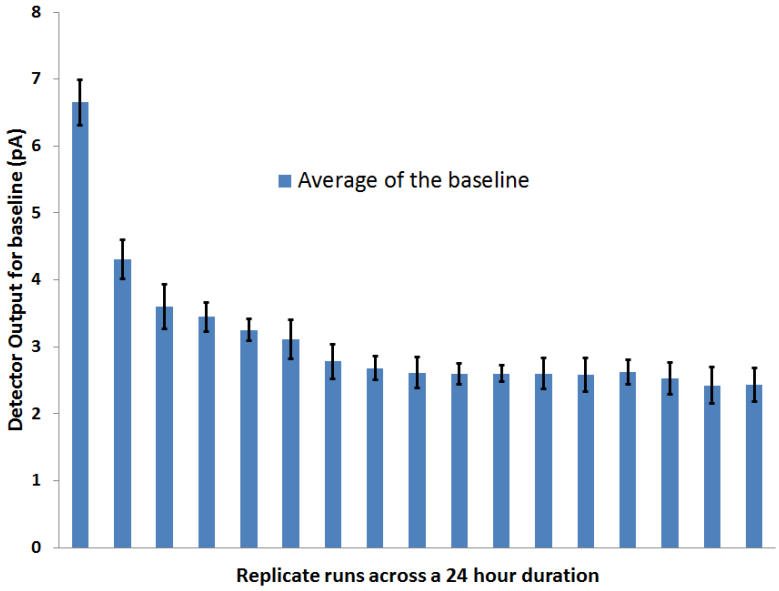

Figure 7-4: Plot of the average baseline obtained over a 24 hour period with the error bars indicating the variation in the baseline (noise) for each chromatographic run

7.3.2 Distance of the bias electrode from the discharge *(l)*

Multiple detectors of three different designs (Design 1, 2, and 3 in Table 1) were fabricated with a fixed distance between the bias and collector electrodes at 2.5 mm, and varying distances between the bias electrode and the He discharge. A total of 6 different detectors were tested. The response of the detectors to 1 µL injections of octane in the headspace of autosampler vials was measured with excitation voltages from 550 V to 700 V in increments of 50 V used to produce the He discharge, with the bias electrode grounded. The peak height corresponding to octane for the range of discharge voltages is plotted in Figure 7-5 for each device. Each data point is the average of triplicate runs. The positive slope on each line plot indicates that an increased voltage (V_p) predictably results in an enhanced response. This can be correlated to a larger current flux within the discharge gap which produces a larger ionizing flux. This would be reflected in an increase in the value of I_0 in Equation **7-1**. Deviations from monotonicity were matched to variations in the sample injected by the autosampler itself, as observed for signals obtained from the FID (data not shown here).

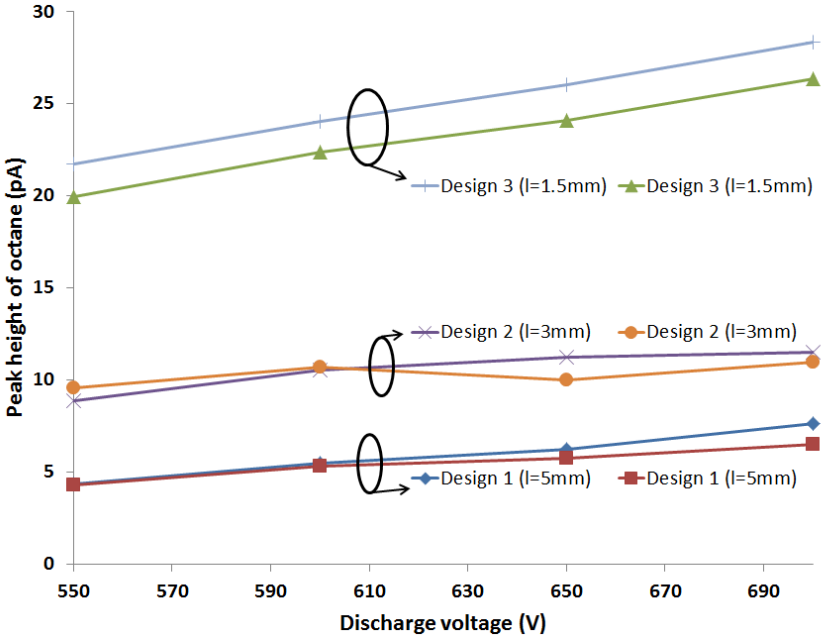

Figure 7-5: Variation in the detector response to octane headspace injection at different discharge voltages for six different devices. The devices are characterized by the distance from discharge to bias electrode (*l*) with a constant *w* = 2.5 mm. Each data point is the average of triplicate runs.

The octane signal was also observed to increase significantly in Figure 7-5 for smaller values of *l*. As the distance between the He discharge and the bias electrode is decreased, the flux observed at the bias electrode increases. This effect can be correlated to the exponential term in Equation 1, and correspondingly results in better analyte ionization. In addition, the number of high energy photons and metastable He atoms available for analyte ionization should be enhanced by reducing the distance between the discharge and the capillary outlet directly above

the bias electrode, effectively improving the density of the ionizing flux at the capillary outlet. Thus, it can be concluded that for a given w, the detector with the smallest value for *l* gives a better response. The extent to which *l* can be minimized is limited by the possibility of fragmentation of the analyte upon their introduction at the bias electrode and subsequent back-diffusion. This limitation has not been explored in this dissertation and is subject to further investigation.

7.3.3 Distance of the collector from the bias electrode *(w)*

Multiple detectors of three different designs (Design 4, 5, and 6) were fabricated and tested with the location of the bias electrode from the He discharge set at 1.5 mm. However, the distance of the collector electrode from the bias electrode was varied to understand the competing effects of ionization and recombination within the collector volume. Plots for the detector response for five different detectors over the same range of discharge voltages are shown in Figure 7-6. Each data point is the average of triplicate runs. In a manner similar to the distance between the bias electrode and He discharge, signals were observed to increase as the distance between the collector and bias electrodes decreased. The signal collected at the collector electrode relies on the ionization of analytes from the He discharge source to produce charged species with a sufficient lifetime to reach the collector electrode via the helium flow through the device. As this gap decreases, the time available for recombination effects, or neutralization of the charged species, decreases as well. Thus, for a given *l*, decreasing the width *w* is favorable.

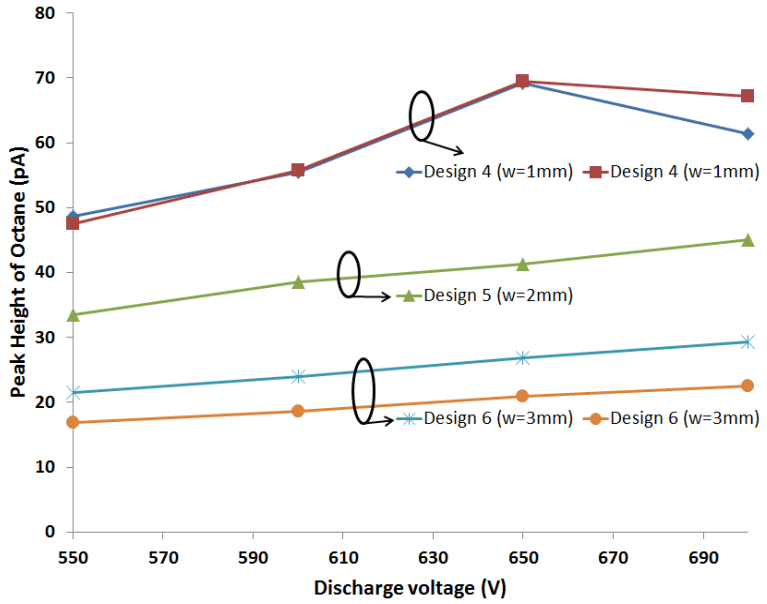

Figure 7-6: Variation in the detector response to octane headspace injection at different discharge voltages for five different devices with variations in the bias to collector electrode distance (w) with a constant *l* = 1.5 mm. Each data point is the average from triplicate runs.

The results from the previous two experiments can be combined to obtain a simple relation for the detector response R (peak height of the octane signal) in terms of the length *l* and width *w*,

$$R \propto V_p e^{-\alpha l}(1-\beta w) \qquad \textbf{7-2}$$

Here, α is the absorption coefficient from Beer-Lambert's law. β is an empirical coefficient to account for the improved collection as the collector is brought closer to the bias electrode and can be related to the presence of a first order recombination/decay length constant. Using the slopes generated from the data plotted in Figure 7-5 and Figure 7-6, the values of α and β were estimated to be 0.45 mm^{-1} and 0.23 mm^{-1}, respectively, at 550 V. The larger the value of α, the quicker the decay of the flux from the He discharge and hence, the closer the bias electrode has to be positioned to the He discharge. On the other hand, a lower value of β makes the design less sensitive to the width of the gap (*w*).

7.3.4 Bias voltage, V_b

The role of bias voltage in actively collecting charged species within the collector volume was examined by stepping the voltage from 0 to 100 V in increments of 25 V and measuring the detector response. Figure 7-7 also presents the effect of the electrode parameters on the detector response in the presence of a stepped bias voltage. A detector from each previously tested design was tested with the He discharge voltage (V_p) set to 550 V. Each data point is the average of two runs. One run was obtained while stepping the voltage up from 0 to 100 V and the other stepping down from 100 to 0 V.

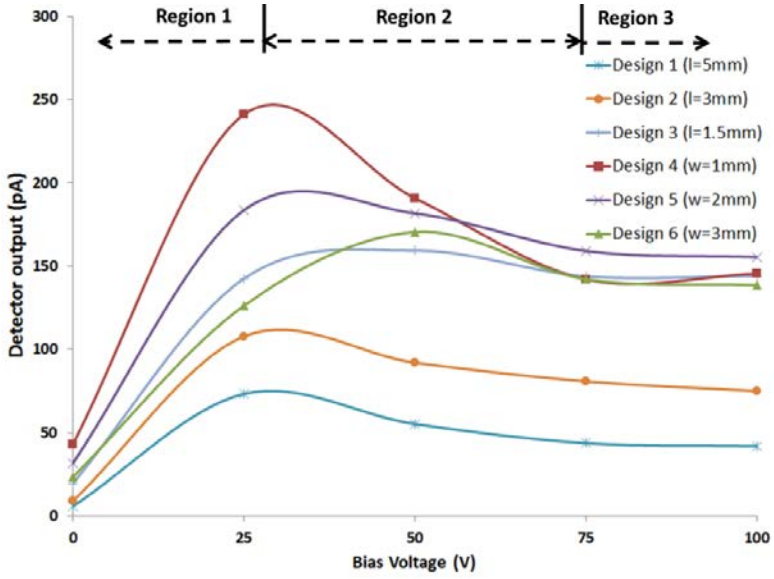

Figure 7-7: Response of the detector to octane headspace injections from stepped values of bias voltage from 0 to 100 V. Each data point is the average from two runs. A detector from each previously tested design was used for this analysis.

The plot in Figure 7-7 can be split in three distinct regions and the behavior of the detector hypothesized as follows. The analytes within the collector volume can be readily ionized by high energy photons and metastable He species from the ionizing flux. In Region 1, in the presence of a small positive bias, negatively charged species from the ionizing flux are collected at the bias electrode, which effectively reduces the possibility of recombination with the positive ions produced from the analytes. Similarly, the electrons created by the soft-ionization of the analytes within the collector volume are collected as well; in effect increasing the recombination time necessary for the ionized analytes. The resultant effect is signal amplification, as noted with the increase in detector output. The sensed current is thus a sum of the effect of the increase in the drift current owing to the removal of the negative species within the volume, and the secondary emission from the impinging flux on the bias. While the former depends on the proximity of the collector electrode to the bias electrode, the latter depends on the proximity of the bias electrode to the He discharge. The slope of the graph, in this region, can be related to the parameter (l+$w/2$), previously described as the distance of the midpoint of the gap from the He discharge, and tabulated in Table 1.

Beyond a certain voltage, the impact of the bias electrode on repelling positively charged species in the ionizing flux and the collection of high energy electrons reduces the ionization detected within the collector volume. This results in a decrease in detector response, as observed in Region 2 that eventually levels off into Region 3. If one assumes that a significant fraction of the ionization of analyte species is the result of metastable He atoms, then this implies that above a certain threshold voltage that energetic primary and secondary electrons responsible for the production of some of the metastable He population are depleted by the bias electrode. This would leave high energy photons produced in the ionizing flux as the primary means of analyte ionization, essentially resulting in a saturated signal since the photon population would be primarily dependent on the He discharge voltage and not the bias voltage. Since, the ionizing flux depends only on the proximity of the bias electrode to the He discharge, the saturated response increases with decreasing values of l but is not affected by w since removal of the electron population significantly reduces the detrimental impact of recombination with analyte ions. This is experimentally evident from the similar detector outputs observed in the saturated region (Region 3) for Designs 3-6 with the same value of l = 1.5 but varying in w. Measurements were taken with finer resolution in bias voltages between 0 and 50 V. While, the data fit the overall trend of the plot, a relation between the exact voltages of peak response could not be established due to measurement variations associated with such fine voltage resolution measurements.

7.3.5 Limit of detection (LOD)

A sensitivity test for the device with the best response (Design #4 in the bias voltage experiment) was performed using various dilutions of octane vapor in air. 1 μL samples from mixtures of 25, 50, 100 and 200 μL of octane in 1 L of air were drawn into a gas tight syringe and injected into Inlet A of the GC. The discharge voltage was set to 700 V and the bias to 25 V.

The power consumption was calculated to be 3.3 mW under these conditions. A calibration curve plotting octane peak area against the injected mass, in Figure 7-8 exhibited some deviation from linearity at the highest octane mass (950 pg). The worst case deviation in baseline noise from all 9 runs was 2.5 pA. Using a 3/1 signal to noise ratio as the criteria for the absolute limit of detection and plugging into the quadratic fit, an LOD of 60 pg for octane was obtained.

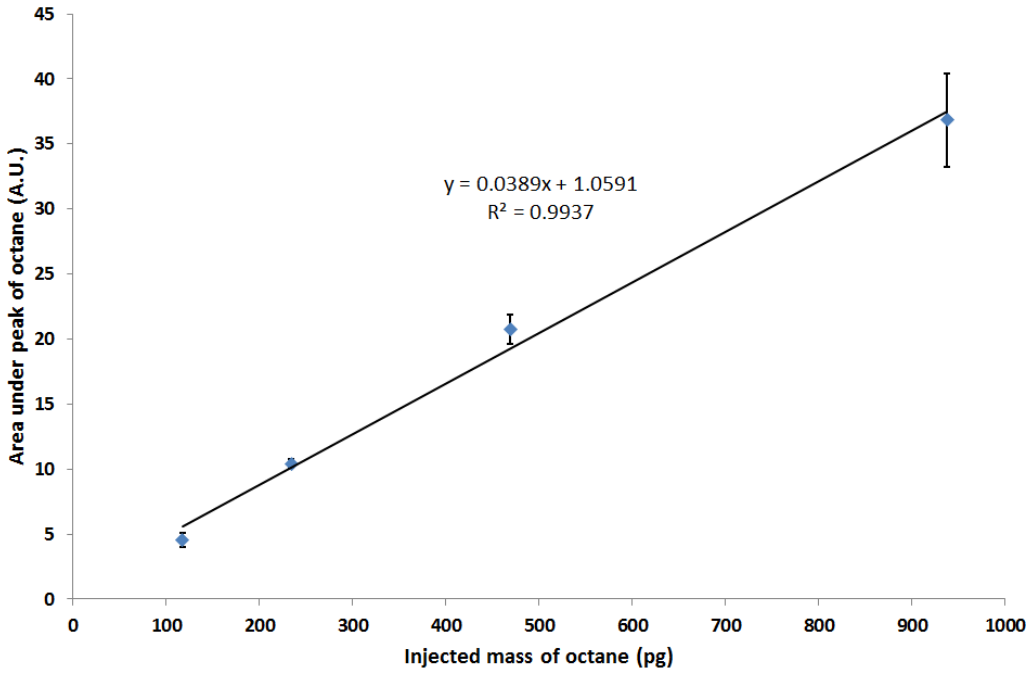

Figure 7-8: Response of the chip (Design 4) to various injected masses of octane, at a bias voltage of 25 V. Each data point is the average from three successive runs.

7.4 Inference

The effects from a number of parameters on the response of a miniaturized He discharge ionization detector for micro gas chromatography have been reported. A study of the signal-to-noise ratio would reveal more important operating constraints for optimal limits of detection. Detector response to other compound classes such as aromatics and halogenated species need to be investigated as well since ionization potentials can vary depending on the compound structures. In addition, the role of temperature and flow rate from both the analyte and auxiliary channels need to be better understood. Preliminary results indicate that column temperature has negligible effect on the detector response. Further research efforts will ultimately lead to the integration of the detector with the separation column for an integrated portable analysis system.

REFERENCES

[1] G. Monti, *et al.*, "Monitoring Food Quality by Microfluidic Electrophoresis, Gas Chromatography, and Mass Spectrometry Techniques: Effects of Aquaculture on the Sea Bass (Dicentrarchus labrax)," *Anal. Chem.*, vol. 77, no. 8, pp. 2587-2594, 2005.

[2] D. Puente, *et al.*, "Thermal conductivity microsensor for determining the Methane Number of natural gas," *Sens. Actuators B Chem*, vol. 110, no. 2, pp. 181-189, 2005.

[3] R. W. Cernosek, *et al.*, "Micro-analytical systems for national security applications," in *Proc. SPIE-Micro (MEMS) and Nanotechnologies for Space Applications*, Orlando (Kissimmee), FL, USA 2006, p. 622306.

[4] D. Nielsen, *Practical handbook of environmental site characterization and ground-water monitoring*: CRC press, 2006.

[5] A. D. Radadia, *et al.*, "Micromachined GC Columns for Fast Separation of Organophosphonate and Organosulfur Compounds," *Anal. Chem.*, vol. 80, no. 11, pp. 4087-4094, 2008.

[6] B. Alfeeli, *et al.*, "MEMS-Based Selective Preconcentration of Trace Level Breath Analytes," *IEEE Sensors J.*, vol. 9, no. 9, 2009.

[7] M. Akbar, *et al.*, "A Microfabricated Propofol Trap for Breath-Based Anesthesia Depth Monitoring," *J. Microelectromech. Syst.*, vol. PP, no. 99, pp. 1-9, 2012.

[8] H. Shakeel, *et al.*, "First reconfigurable MEMS separation columns for micro gas chromatography," in *Micro Electro Mechanical Systems (MEMS), 2012 IEEE 25th International Conference on*, 2012, pp. 823-826.

[9] S. K. Kim, *et al.*, "Microfabricated Gas Chromatograph for the Selective Determination of Trichloroethylene Vapor at Sub-Parts-Per-Billion Concentrations in Complex Mixtures," *Anal. Chem.*, vol. 83, no. 18, pp. 7198-7206, 2011/09/15 2011.

[10] I. Elmi, *et al.*, "A miniaturized gas-chromatographic system for the evaluation of fish freshness," in *Sensors, 2008 IEEE*, 2008, pp. 1084-1087.

[11] R. R. Reston, *et al.*, "Silicon-micromachined gas chromatography system used to separate and detect ammonia and nitrogen dioxide. I. Design, fabrication, and integration of the gas chromatography system," *J. Microelectromech. Syst.*, vol. 3, no. 4, pp. 134-146, 1994.

[12] D. Wang, *et al.*, "Highly Stable Surface Functionalization of Microgas Chromatography Columns Using Layer-by-Layer Self-Assembly of Silica Nanoparticles," *Analytical Chemistry, [online early access]*, Jul. 27 2013 2013.

[13] H. Shakeel, *et al.*, "Self-Patterned Gold-Electroplated Multicapillary Gas Separation Columns With MPG Stationary Phases," *J. Microelectromech. Syst.*, vol. 22, no. 1, pp. 62-70, Feb. 2013.

[14] S. C. Terry, *et al.*, "A gas chromatographic air analyzer fabricated on a silicon wafer," *Electron Devices, IEEE Transactions on*, vol. 26, no. 12, pp. 1880-1886, 1979.

[15] R. Manginell, *et al.*, "Monolithically-integrated MicroChemLab for gas-phase chemical analysis," in *Proceedings of the l-TAS 2003 Workshop (Squaw Valley, CA*, 2003, pp. 1247-1250.

[16] S. Showalter, *et al.*, "Design and Testing of a Micro Thermal Conductivity Detector (TCD) System," SAND2003-0954, Sandia National Labs., Albuquerque, NM (US);2003.

[17] R. Manginell, *et al.*, "Advancements in the Monolithically-Integrated MicroChemLab," in *Proceedings of the m-TAS 2004 Workshop*, Malmo, Sweden, 2004, pp. 61-63.

[18] G. Lambertus, *et al.*, "Stop-Flow Programmable Selectivity with a Dual-Column Ensemble of Microfabricated Etched Silicon Columns and Air as Carrier Gas," *Anal. Chem.*, vol. 77, no. 7, pp. 2078-2084, 2005/04/01 2005.

[19] S. Ali, *et al.*, "MEMS-based semi-packed gas chromatography columns," *Sens. Actuators B Chem*, vol. 141, no. 1, pp. 309-315, 2009.

[20] C.-J. Lu, *et al.*, "First-generation hybrid MEMS gas chromatograph," *Lab on a Chip*, vol. 5, no. 10, pp. 1123-1131, 2005.

[21] M. Agah, *et al.*, "Low-Mass PECVD Oxynitride Gas Chromatographic Columns," *J. Microelectromech. Syst.*, vol. 16, no. 4, pp. 853-860, 2007.

[22] J. J. Whiting, *et al.*, "High-speed two-dimensional gas chromatography using microfabricated GC columns combined with nanoelectromechanical mass sensors," in *TRANSDUCERS*, 2009, pp. 1666-1669.

[23] J. Liu, *et al.*, "Adaptive Two-Dimensional Microgas Chromatography," *Anal. Chem.*, vol. 84, no. 9, pp. 4214-4220, 2012/05/01 2012.

[24] B. Alfeeli, *et al.*, "MEMS-based multi-inlet/outlet preconcentrator coated by inkjet printing of polymer adsorbents," *Sens. Actuators B Chem*, vol. 133, no. 1, pp. 24-32, 2008.

[25] B. Byunghoon, *et al.*, "A Fully-Integrated MEMS Preconcentrator for Rapid Gas Sampling," in *Solid-State Sensors, Actuators and Microsystems Conference, 2007. TRANSDUCERS 2007. International*, 2007, pp. 1497-1500.

[26] R. P. Manginell, *et al.*, "Mass-Sensitive Microfabricated Chemical Preconcentrator," *J. Microelectromech. Syst.*, vol. 17, no. 6, pp. 1396-1407, 2008.

[27] C.-J. Lu, *et al.*, "A Dual-Adsorbent Preconcentrator for a Portable Indoor-VOC Microsensor System," *Anal. Chem.*, vol. 73, no. 14, pp. 3449-3457, 2001/07/01 2001.

[28] S. J. Martin, *et al.*, "Gas sensing with acoustic devices," in *Ultrasonics Symposium, 1996. Proceedings., 1996 IEEE*, 1996, pp. 423-434 vol.1.

[29] M. Kimura, *et al.*, "Application of the air-bridge microheater to gas detection," *Sens. Actuators B Chem*, vol. 25, no. 1-3, pp. 857-860, 1995.

[30] L. K. Wright, *et al.*, "A nanoparticle-coated chemiresistor array as a microscale gas chromatograph detector for explosive marker compounds: flow rate and temperature effects," *Analyst*, vol. 138, no. 22, pp. 6860-6868, 2013.

[31] I. Simon, *et al.*, "Micromachined metal oxide gas sensors: opportunities to improve sensor performance," *Sens. Actuators B Chem,* vol. 73, no. 1, pp. 1-26, 2001.
[32] Q.-Y. Cai, *et al.*, "Dual-Chemiresistor GC Detector Employing Monolayer-Protected Metal Nanocluster Interfaces," *Anal. Chem.*, vol. 74, no. 14, pp. 3533-3539, 2002/07/01 2002.
[33] S. Bedair, *et al.*, "CMOS MEMS oscillator for gas chemical detection," in *Proceedings of IEEE Sensors*, 2004, pp. 955-958.
[34] K. Reddy, *et al.*, "On-chip Fabry–Pérot interferometric sensors for micro-gas chromatography detection," *Sens. Actuators B Chem,* vol. 159, no. 1, pp. 60-65, 2011.
[35] R. Pecsar, *et al.*, "Performance of a reduced volume thermal conductivity detector," *Anal. Chem.*, vol. 45, no. 13, pp. 2191-2198, 1973.
[36] S. Sorge, *et al.*, "Fully integrated thermal conductivity sensor for gas chromatography without dead volume," *Sens. Actuators A Phy,* vol. 63, no. 3, pp. 191-195, 1997.
[37] W. Kuipers, *et al.*, "Sensitivity of a planar micro-flame ionization detector," *Talanta,* vol. 82, no. 5, pp. 1674-1679, 2010.
[38] M. Moorman, *et al.*, "Microcombustor array and micro-flame ionization detector for hydrocarbon detection," in *Proc. SPIE—MEMS Components and Applications for Industry, Automobiles, Aerospace, and Communication II,*, San Jose, CA, USA, 2003, pp. 40-50.
[39] Z. Ouyang, *et al.*, "Miniature Mass Spectrometers," *Annual Review of Analytical Chemistry*, vol. 2, no. 1, pp. 187-214, 2009.
[40] J. C. T. Eijkel, *et al.*, "A dc Microplasma on a Chip Employed as an Optical Emission Detector for Gas Chromatography," *Anal. Chem.*, vol. 72, no. 11, pp. 2547-2552, 2000.
[41] B. Mitra, *et al.*, "The micromachined flashFET: a low-power, three-terminal device for high speed detection of vapors at atmospheric pressure," in *Micro Electro Mechanical Systems, 2005. MEMS 2005. 18th IEEE International Conference on*, 2005, pp. 794-797.
[42] B. Mitra, *et al.*, "The Detection of Chemical Vapors in Air Using Optical Emission Spectroscopy of Pulsed Microdischarges From Two- and Three- Electrode Microstructures," *Sensors Journal, IEEE,* vol. 8, no. 8, pp. 1445-1454, 2008.
[43] Y.-M. Fu, *et al.*, "Characteristic responses of an atmospheric pressure DC micro-plasma detector for gas chromatography to organic functional groups," *Microchemical Journal,* vol. 89, no. 1, pp. 7-12, 2008.
[44] S. Narayanan, *et al.*, "A micro-discharge photoionization detector for micro-gas chromatography," *Microchim Acta,* pp. 1-7, 2013/12/21 2013.
[45] H. Miyahara, *et al.*, "Development and fundamental investigation of He plasma ionization detector (HPID) for gas chromatography using DC glow discharge," *Journal of Analytical Atomic Spectrometry,* vol. 29, no. 1, pp. 105-110, 2014.
[46] W. E. Wentworth, *et al.*, "Pulsed discharge photoionization detector: Application to analysis of chloro alkanes/alkenes," *Journal of High Resolution Chromatography,* vol. 19, no. 2, pp. 85-90, 1996.
[47] S. Narayanan, *et al.*, "Fabrication and Characterization of a Suspended TCD Integrated With a Gas Separation Column," *J. Microelectromech. Syst.*, vol. 22, no. 5, pp. 1166-1173, 2013.

8

Conclusion

8.1 Summary

Gas chromatography has a proven applicability in a multitude of domains for over a century. However, this is restricted to analysis of samples brought to lab from the field. For example, workers employed in laying out roads are regularly exposed to asphalt. The fumes from asphalt are a potential source of respiratory health concerns. The National Institute on Occupational Safety and Health (NIOSH) prescribes limits on occupational exposure to asphalt. A typical method employed in monitoring the exposure is to attach a "patch" onto a worker. At the end of the day, this patch is sampled for VOCs and analyzed in a lab using conventional GC-MS to evaluate the exposure. At the least, such a method can only provide information after the limit has been crossed. This is a classic example for application of an on-site handheld device. Such a device could warn workers of reaching their daily limits or worse, sudden peaking VOC concentrations.

Apart from health benefits, a handheld GC system will be a major asset in space exploration. Payload weight is a major factor when launching rovers that explore extra-terrestrial space, in search of signs for lifeform. Ongoing research is continuing into the development of chipscale technologies that perform gas mixture separation and analysis at NASA. Current deployments in the International Space station use compact forms of conventional separation and detection techniques. Miniaturized systems offer heavy incentives over such conventional techniques, provided they match the performance.

Keeping in mind such pressing needs, this research offers unique developments in miniaturized handheld GC systems and further improvements that will offer serious challenge to competing contemporaries.

8.2 Contributions

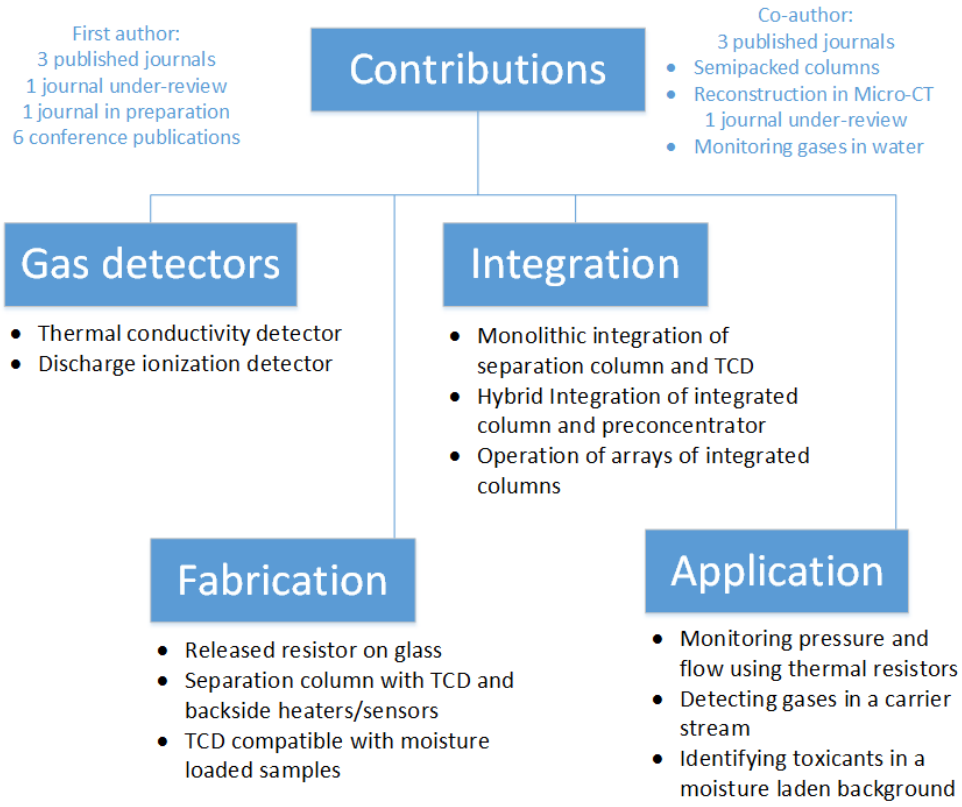

Figure 8-1: A breakdown of the contributions of this research towards fabrication, gas detectors, integration methodologies and application

8.2.1 Monolithic Integration of μTCD and resistor-on-glass

Starting with a well-known and easy to fabricate gas detector, the TCD, we have presented an unique embedded architecture with a separation column. Unlike cascading both, such an architecture saves on the silicon real-estate needed for a reference channel differential measurement. This reduces the number of fluidic ports from four to two. Integration also requires that the process flow of the μTCD and the μSC blend in. Hence, resistors for the μTCD were fabricated suspended in glass. Care was taken to not make the glass unfit for anodic bonding to silicon. This ensured that the silicon substrate could be independently processed for cutting-edge configurations such as semi-packed and multi-capillary columns. In addition the microfluidic channels can be coated with variety of nanostructured phases. This would have been impossible with μTCD resistors made on silicon.

Resistors-on-glass can find application much beyond μTCD. By making use of otherwise non-functional glass lid, they provide an ability to make resistive measurements in any previously realized glass-on-silicon device. This could mean pressure measurements in a silicon switch capped with glass or flow measurements in a silicon microfluidic channel.

8.2.2 Hybrid operation of micro-preconcentrator and the integrated device for water monitoring

The integrated device (of a μSC and a μTCD) has an inherent poor detection limit. This was improved by coupling a preconcentrator in front of the device. This hybrid integration, though fraught with thermal crosstalk, improved the detection limit. Analytes were detected at concentrations much below the TCD's inherent detection threshold. The application of such a configuration to monitoring volatile organic compounds in water was demonstrated. This required the modification of the process flow of the μTCD to include an insulating oxide layer on the metal filament. This prevented the interaction of moisture from water with an otherwise exposed filament.

8.2.3 Multi-dimensional analysis and separation in a matrix

A practical column is characterized by a finite plate number. Every analyte plug is associated with a band broadening that causes closely spaced plugs to merge. Identification of the individual component requires that the length of the column increase. Alternatively, the stationary phase is modified to effect an efficient separation. A much more viable alternative is to utilize multiple columns of differing selectivity. In contrast to existing multi-chromatography and multi-dimensional GC methods, we have explored an alternative matrix method. Taking advantage of miniaturization, an array of integrated devices (μSC and μTCD), coated differently, were operated in a matrix. This technique performs multi-dimensional analysis and detection to identify a complex mixture of wide boiling points in under 2 minutes.

8.2.4 Low-power and sensitive discharge ionization detector

μTCDs are characterized by inherent poor detection limit, whether fabricated in silicon or glass. The thermal dissipation on such resistive measurements limit the minimum operable column temperature when integrated on the same die. The power dissipation is relatively high when compared with other detectors and maybe a deal breaker in certain applications. As a suitable replacement, a photoionization detector has been developed that utilizes microplasma. Inspired by a conventional detector called the pulsed discharge helium photoionization detector, this μHe-DID operates on a 1.4mW DC plasma. It retains the μTCD characteristics of universality and non-destructive nature with regard to analytes. Thus, it promises not just VOC sensing but also environmental permanent gases such as in a traffic junction.

8.3 Future Improvements

This research has focused on placing two μSC-μTCD pairs on the same die, as shown in Chapter 5. The temperature of the entire die was held constant. The presence of a detector on each column does increase the capacity when compared to a single column. A further increase is obtained if flow or temperature tuning methods are employed. In this regard, the possibility of isolating the individual columns while being able to minimize the noise on the second PCB could

be of major concern. This can lead to fabricating multiple (greater than 2) columns on the same die. The fluidic connections of such a matrix can be terminated on a reconfigurable micro-valve manifold. Applying techniques of graph theory, one can determine the optimal matrix connection to efficiently separate the predicted composition of the sample mixture at the inlet.

The μHe-DID is the latest entry in the long list of detectors. Like the μTCD, it is a universal, non-destructive detector. However, the limit of detection has clocked a best of 60 pg consuming just 3.3 mW. The electrode placement has been studied and optimized for increased response. However, there are various aspects of this detector that need to be studied. For example, unlike a μTCD, a detector based on photoionization from a plasma is inherently less sensitive to ambient temperature since a plasma, in itself, is a very high temperature phenomenon. Similarily, the shape of the electrode and the flow rate are two important parameters that can reveal greater insights into the operation of the detector. A parallel investigation is required into the integration of the detector into a separation column on a silicon-glass architecture. Such a device should be expected to be leagues ahead of the μSC-μTCD combination investigated previously.

The preceding discussion should be a clear indicator that there is sufficient room for investigation and further improvement and contribution to the field of handheld micro gas chromatography.

Appendix A: List of publications

Shree Narayanan, Gary Rice, and Masoud Agah, "A micro-discharge photoionization detector for micro-gas chromatography," Microchimica Acta, December 2013.

Shree Narayanan, Gary Rice, and Masoud Agah, "A micro helium-discharge photoionization detector for gas sensing ," Sensors, 2013 IEEE, November 2013, Baltimore, MD, USA, pp. 1 - 4 .

B. Alfeeli, S. Narayanan, D. Moodie, P. Zellner, M. McMillan, D. Hirtenstein, G. Rice, and M. Agah, "Inter-channel Mixing Minimization in Semi-packed Micro Gas Chromatography Columns," IEEE Sensors, vol. 13, no. 11, November 2013, pp. 4312-4319.

Shree Narayanan and Masoud Agah, "Fabrication and Characterization of a Suspended TCD Integrated With a Gas Separation Column ," Journal of Microelectromechanical Systems, vol. 22, no. 5, October 2013, pp. 1166-1173.

Kriti Sen Sharma, Christian Holzner, Dragoş M Vasilescu, Xin Jin, Shree Narayanan, Masoud Agah, Eric A Hoffman, Hengyong Yu, and Ge Wang, "Scout-view assisted interior micro-CT," Physics in Medicine and Biology, vol. 58, no. 12, June 2013, pp. 4297-4314.

Kriti Sen Sharma, Xin Jin, Christian Holzner, Shree Narayanan, Baodong Liu, Dong Wang, Masoud Agah, Linbing Wang, Hengyong Yu, and Ge Wang, "Experimental studies on few-view reconstruction for high-resolution micro-CT," Journal of X-Ray Science and Technology, vol. 21, no. 1, March 2013, pp. 25-42.

Shree Narayanan and Masoud Agah, "A High-Performance TCD Monolithically Integrated with a Gas Separation Column," IEEE Sensors 2012, October 2012, Taipei, Taiwan, pp. 1412-1415.

Shree Narayanan and Masoud Agah, "A Micro Gas Chromatography Column with an Embedded Out-of-Plane Thermal Conductivity Detector," Solid-State Sensors, Actuators, and Microsystems Workshop (Hilton Head '12), June 2012, Hilton Head Island, SC, pp. 221-224.

Shree Narayanan, Bassam Alfeeli, Masoud Agah, "A 2-Port Static Coated Micro Gas Chromatography Column with an Embedded Thermal Conductivity Detector," IEEE Sensors Journal, vol. 12, no. 6, June 2012, pp. 1893-1900.

B. Alfeeli, S. Narayanan, M. McMillan, D. Hirtenstein, G. Rice, and M. Agah, "The Effect of Pillar Array in Semi-packed Micro Gas Chromatography," IEEE Sensors, October 2011, Limerick, Ireland, pp. 1097-1100.

S. Narayanan, B. Alfeeli, and M. Agah, "Thermostatted Micro Gas Chromatography Column with on-Chip Thermal Conductivity Detector for Elevated Temperature Separation," 2010 Ninth IEEE Sensors Conference (SENSORS 2010), November 2010, Waikoloa, HI, pp. 2504 - 2507.

S. Narayanan, B. Alfeeli, and M. Agah, "Micro Gas Chromatography Based Handheld Chemical Analyzers," 11th Mid-Atlantic Micro/Nano Alliance Symposium, October 2010, Laurel, MD.

S. Narayanan, B. Alfeeli, and M. Agah, "A Micro Gas Chromatography Chip with an Embedded Non-Cascaded Thermal Conductivity Detector," European Sensors, Actuators, and Microsystems Conference (EUROSENSORS XXIV), September 2010, Linz, Austria.

S. Narayanan, M. Nikkhah, J. S. Strobl and M. Agah, "Analysis of the Passivation Layer by Testing and Modeling a Cell-Impedance Micro-Sensor," Sensors and Actuators A, vol. 159, no. 2, May 2010, pp. 241-247.

M. Nikkhah, S. Narayanan, J. S. Strobl, and M. Agah, "Effect of Passivation Layer on Real Time Impedance Analysis of Mammalian Cells," 5th International Conference on Microtechnology in Medicine and Biology (MMB '09), March 2009, Quebec, Canada, pp. 140-141.

Appendix B: Circuits for Matrix GC

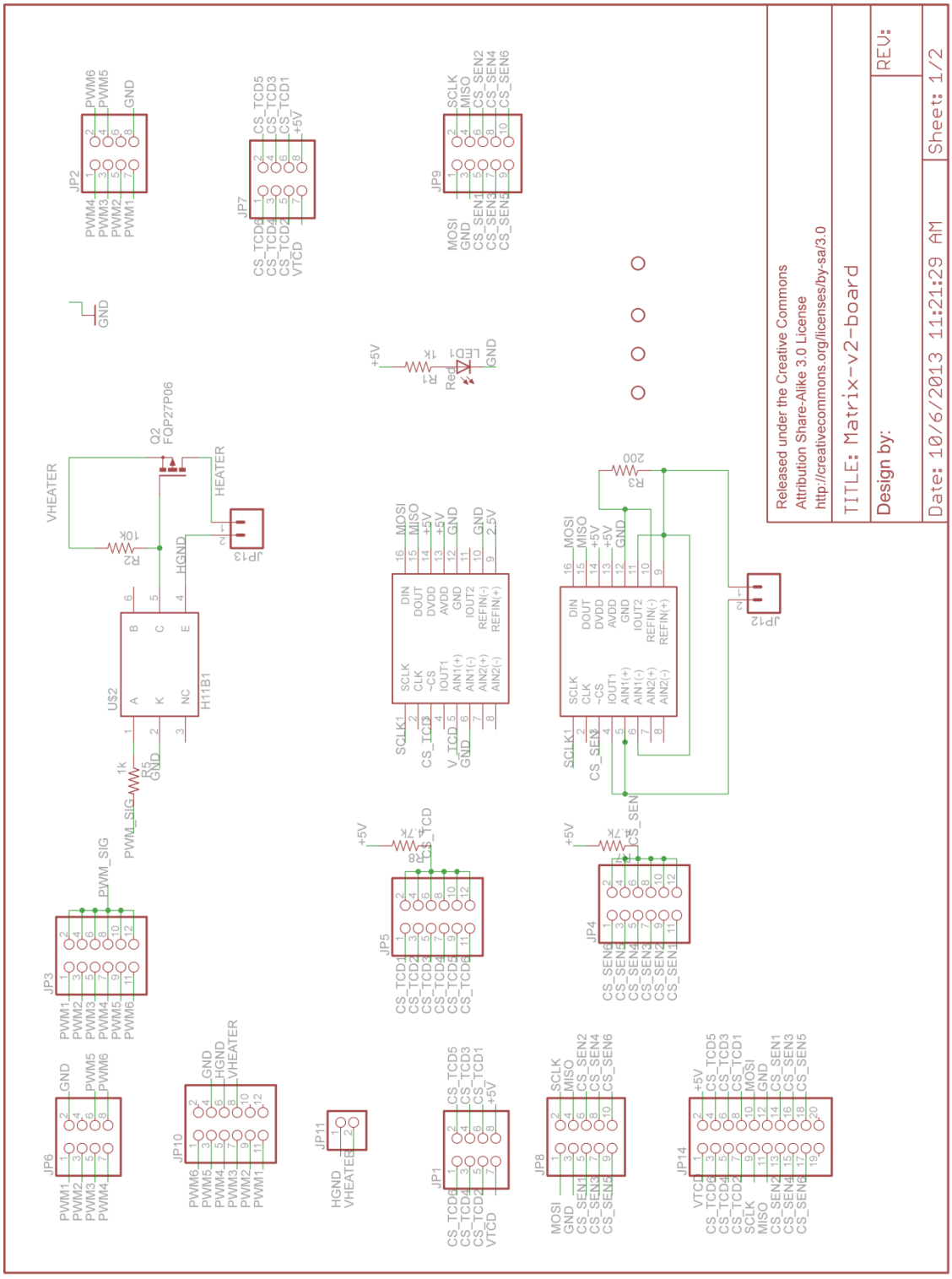

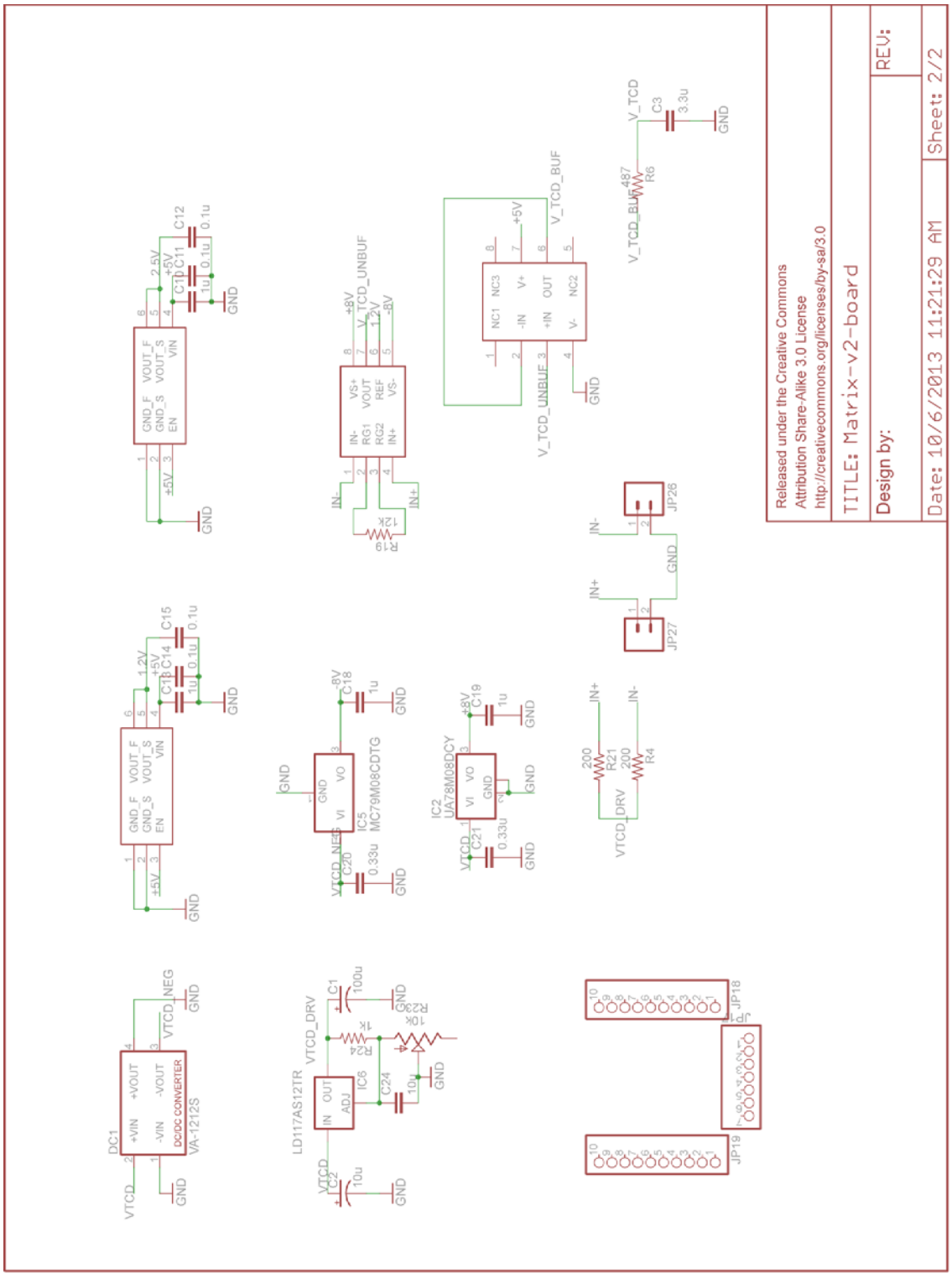
Released under the Creative Commons
Attribution Share-Alike 3.0 License
http://creativecommons.org/licenses/by-sa/3.0
TITLE: Matrix-v2-board
Design by:
REV:
Date: 10/6/2013 11:21:29 AM
Sheet: 2/2
DC1
DCDC CONVERTER
VA-1212S
+VIN
-VIN
+VOUT
-VOUT
VTCD
VTCD_NEG
GND
LD117AS12TR
IC6
VTCD_DRV
R24
1k
R23
10k
C24
10u
C1
100u
C2
IC5
MC79M08CDTG
VTCD_NEG
C20
0.33u
C18
1u
IC2
UA78M08DCY
C21
C19
R21
200
R4
DRV
IN+
IN-
JP18
JP19
JP26
JP27
IN_UNBUF
R19
12k
V_TCD_UNBUF
V_TCD_UNBUF_3
V_TCD_BUF
V_TCD_BUF_5
R6
487
V_TCD
C3
3.3u
GND
+5V
+8V
1.2V
2.5V
C10
C11
C12
C13
C14
C15
0.1u
1u